DOKUZ EYLÜL UNIVERSITY

GRADUATE SCHOOL OF NATURAL AND APPLIED SCIENCES

SOUND SOURCE CHARACTERIZATION OF VIBRATING BODIES BY THEORETICAL AND EXPERIMENTAL TECHNIQUES

by

Sinan ERTUNÇ

March, 2011

İZMİR

SOUND SOURCE CHARACTERIZATION OF VIBRATING BODIES BY THEORETICAL AND EXPERIMENTAL TECHNIQUES

A Thesis Submitted to the
Graduate School of Natural and Applied Sciences of Dokuz Eylül University
In Partial Fulfillment of the Requirements for the Degree of Master of Science
in Mechanical Engineering, Machine Theory and Dynamics Program

by

Sinan ERTUNÇ

March, 2011
İZMİR

M.Sc THESIS EXAMINATION RESULT FORM

We have read the thesis entitled **"SOUND SOURCE CHARACTERIZATION OF VIBRATING BODIES BY THEORETICAL AND EXPERIMENTAL TECHNIQUES"** completed by **SİNAN ERTUNÇ** under supervision of **PROF. DR. A. SAİDE SARIGÜL** and we certify that in our opinion it is fully adequate, in scope and in quality, as a thesis for the degree of Master of Science.

Prof. Dr. A. Saide SARIGÜL

Supervisor

Prof. Dr. Hira KARAGÜLLE

(Jury Member)

Prof. Dr. Ayşegül PALA

(Jury Member)

Prof.Dr. Mustafa SABUNCU
Director
Graduate School of Natural and Applied Sciences

ACKNOWLEDGMENTS

I would like to give my thanks to everyone who helped me in my thesis work. Foremost to my supervisor Prof. Dr. A. Saide SARIGÜL for her patience, excellent guidance, invaluable support and continuous encouragement throughout this study.

I would also like to thank Dr. Abdullah SEÇGİN for his tremendous help, critical suggestions and invaluable contributions to my master thesis.

I wish to express sincere thanks to a special person, Hande HAMAMCILAR for her love, moral support, sacrifice and understanding during the preparation of this thesis.

Finally, this work is dedicated to my family; my mother, my father, my sister, my brother-in-law and my niece. Their love, continuous and unconditional support inspired me.

Sinan ERTUNÇ

SOUND SOURCE CHARACTERIZATION OF VIBRATING BODIES BY THEORETICAL AND EXPERIMENTAL TECHNIQUES

ABSTRACT

Boundary element method (BEM) is a widely used technique which has been successfully applied for many structural and acoustic problems. Sound source characterization of vibrating bodies which is the main subject of this study has been accomplished by solving Helmholtz integral equation via BEM fed by surface velocity measurements. For these operations, an available in-house computer code which enables to perform acoustic analysis of vibrating bodies in full and half space has been rewritten in MatLAB®. Additionally, a new module has been developed for this code to solve half-space acoustic problems in the presence of an impedance surface. The code is capable of post-processing operation to display sound source localizations and providing the data to be assessed by means of sound source characterization. This program which can be used for active noise control has been tested first for the theoretical acoustic sources; a dilating sphere and hemisphere. Then, as an engineering application, sound source characterization of a refrigerator has been performed. Passive noise control effect of an impedance surface under the refrigerator also has been examined. Sound measurements for the acoustic field of the refrigerator have been accomplished and compared with the numerical solutions.

Keywords: Vibro-acoustics, Boundary element method, Helmholtz integral equation, Sound source characterization, Impedance surface, Active noise control, Passive noise control, Dilating sphere, Refrigerator.

TİTREŞEN CİSİMLERİN SES KAYNAĞI DAVRANIŞ ÖZELLİKLERİNİN TEORİK VE DENEYSEL YÖNTEMLERLE BELİRLENMESİ

ÖZ

Sınır elemanları yöntemi (BEM) yaygın olarak kullanılan, bir çok yapısal ve akustik problemde başarıyla uygulanmış bir yöntemdir. Bu çalışmanın temel konusu olan, titreşen cisimlerin ses kaynağı karakterizasyonu, Helmholtz integral denkleminin yüzey hız ölçümleri ile beslenen BEM ile çözülmesi yoluyla gerçekleştirilmiştir. Bu işlemler için, tam ve yarım uzayda bulunan titreşen cisimlerin akustik analizi amacıyla bünyemizde geliştirilmiş olan bir bilgisayar programı MatLAB®'da yeniden yazılmıştır. Ayrıca bu program için, ses yutucu bir yüzeye sahip yarım uzaydaki akustik problemleri çözebilen yeni bir modül geliştirilmiştir. Program, ses kaynaklarının yerlerini göstermek için sonuçların işlenmesini ve bu kaynakların davranış özelliklerinin değerlendirilmesini mümkün kılmaktadır. Aktif gürültü kontrolüne yönelik olarak kullanılabilecek bu bilgisayar programı, öncelikle düzgün titreşen küre ve yarım küre gibi teorik akustik kaynaklar için denenmiştir. Daha sonra bir mühendislik uygulaması olarak, bir buzdolabının ses kaynaklarının belirlenmesi ve değerlendirilmesi işlemi gerçekleştirilmiştir. Buzdolabının altında bulunan ses yutucu bir yüzeyin pasif gürültü azaltımı etkisi de incelenmiştir. Buzdolabının akustik alanı için ses ölçümleri yapılmış ve bu ölçümlerden elde edilen sonuçlar, sayısal çözümler ile karşılaştırılmıştır.

Anahtar sözcükler : Vibroakustik, Sınır elemanları yöntemi, Helmholtz integral denklemi, Ses kaynağı karakterizasyonu, Ses yutucu yüzey, Aktif gürültü kontrolü, Pasif gürültü kontrolü, Düzgün titreşen küre, Buzdolabı.

CONTENTS

Page

CHAPTER ONE
INTRODUCTION

1.1 Introduction

Machinery has become much more complicated to satisfy customer expectations and legislations by the technological development. This causes complex dynamic problems leading to high noise and vibration levels and thus irritates the daily-life. It is expected from a reputable product to have low-noise characteristics together with a good quality-price property. Therefore, some active and passive treatments before and during the design stage have to be performed to deal with these dynamic problems. For this purpose, the designer has to have a satisfactory information about the vibro-acoustic characteristics of the machinery parts; localization, radiation characteristics, time, spatial and frequency dependent behaviours of the sound sources. Furthermore, it has to be accurately obtained, the interaction between the structural and acoustic parts of that machinery taking into account of reflection effects of the surrounding surfaces.

Noise source identification and characterization has become a powerful tool for the design and production of modern and noiseless machines and systems. Various techniques have been developed for this purpose. In general, measurements of surface velocity and exterior sound pressure are practical ways to perform a simple source localization analysis. The capability of these measurement approaches is very restricted due to the fact that it directly depends on the accuracy of the test set-up and expertise of the measurement technician. In the identification of acoustical characteristics of sound sources, some methods are available for researchers. For example; inverse and reciprocity methods (Fahy, 2003; Verheij, 1997a, 1997b) presenting characteristics of sources and transmission paths; pseudo-forces method (Janssens & Verheij, 2000; Janssens, Verheij & Loyau, 2002) where the internal excitation in a source component is reproduced by fictitious forces on the outer surface; and Inverse Boundary Element Method (IBEM) (Schuhmacher, Rasmussen & Hansen, 2003; Z. D. Zhang, Vlahopoulos, Raveendra, Allen & K. Y. Zhang, 2000)

that is a three-dimensional holography method joining boundary element modeling used in direct (forward) solution with inverse methods. The more industrialized tecniques are, Spatial Transformation of Sound Fields (STSF) (Ginn & Hald, 1989; Hald, 1989) that bases on measurements on a flat image of the source scanned on a reference plane; Near-field Acoustic Holography (NAH) (Maynard, Williams & Lee, 1985; Veronesi & Maynard, 1987), an approach to reconstruct the acoustic field on the surface of a planar source based on Helmholtz integral equation and the two-dimensional spatial Fourier transform; and beamforming (Castellini & Martarelli, 2008; Christensen & Hald, 2004), a technique that measures acoustic pressure by means of microphone arrays and locates sound sources by post-processing the measured signals. Different commercial software based on these techniques compatible to measurement hardware can be directly supplied by the test equipment sellers. In addition to these briefly explained techniques some other approaches such as, Statistically Optimal NAH (SONAH) (Hald, 2005a, 2005b); Non-Stationary STSF (Hald, 2000); Helmholtz integral equation, BEM with Singular Value Decomposition (SVD) (Bai, 1992; Veronesi & Maynard, 1989); Helmholtz Equation with Least Squares method (HELS) (Wang & Wu, 1997; Wu, 2000); Fast Multipole BEM (FMBEM) (Sakuma & Yasuda, 2002; Yasuda & Sakuma, 2005) are also available. All these methods have pros and cons depending on the accuracy, operation time and expenses, required equipment and software costs.

Analytical solutions of sound sources having uniform geometry are available for many years (Morse & Feshbach, 1953; Morse & Ingard, 1968; Pierce, 1981; Skudrzyk, 1971). However, closed form solutions have not been generally possible for arbitrarily shaped sources and the sources embedded in a complex structure. Therefore, for such cases, some efficient numerical techniques according to the objective of the analyses have to be considered.

Helmholtz integral equations constitute the foundation of many studies accomplished by numerical methods (Bell, Meyer & Zinn, 1977; Burton & Miller, 1971; Chertock, 1964; Copley, 1967; Koopmann & Benner, 1982; Piaszczyk & Klosner, 1984; Sarigül, 1999; Sarigül & Kiral, 1999; Sarigül & Seçgin, 2004; Seçgin

& Sarigül, 2010; Seybert, Soenarko, Rizzo & Shippy, 1985). In the application of Helmholtz integral to acoustic radiation problems, either the acoustic surface pressure or surface normal velocity distribution of the vibrating body has to be pre-defined. In practice, normal velocity is the pre-known variable obtained from structural analyses or measurements. In this case, the first step is to apply the surface Helmholtz integral equation for the determination of acoustic pressure distribution on the surface of the sound source by using boundary conditions. Secondly, predicted surface pressures are used for the computation of sound pressure field around the source via exterior Helmholtz integral equation.

In general, methods that are based on the numerical solution of a surface integral, such as Helmholtz integral, are known as Boundary Element Method (BEM). This method is similar to the Finite Element Method (FEM) due to its properties; discretization of the body, use of the shape functions and obtaining a set of algebraic equations. However, in the FEM, the body is entirely discretized while only the surface of the body is discretized in the BEM. Therefore, the BEM reduces the dimension and thus it is faster and less dense than the FEM.

In practice, machines sit on a floor or are mounted to at least one wall. The floor or the walls can be regarded as rigid or impedance surfaces which limit the analysis domain. If only one theoretically infinite surface restricts the domain, it is called as half-space condition. For such cases, the surface reflection effects have to be taken into account. The half-space algorithm for Helmholtz integral originally developed by Seybert & Soenarko (1988) and Seybert & Wu (1989) can be reliably used for such a problem.

In this thesis, an efficient methodology for sound source characterization based on the solution of Helmholtz integral equation via BEM fed by surface velocity data is presented. For this purpose, an in-house computer code previously developed in Vibration and Acoustic Laboratory has been rewritten in MatLAB® and improved for solving half-space problems with impedance surfaces. The impedance surface solutions constitute the contribution of this thesis to the literature. This redeveloped

code promises high resolution post-processed data that is displayed as 2D sound source localizations. The code also provides raw data ready for the assessment by means of sound source characterization. These analyses form the background of an effective active noise control. The tests of the computer program have been realized by making comparisons between the analytical and numerical results for spherical and hemispherical sources. As a practical application, sound source localization and characterization of a refrigerator been performed. The effect of an impedance surface under the refrigerator was examined as a sound absorbing material. The BEM results for this passive noise control application have been compared with those from the sound measurements.

1.2 Thesis Organization

This thesis comprises six chapters including introduction and conclusions, and appendices.

Chapter 1 mainly discusses the importance of sound source localization and characterization of vibrating bodies and presents a literature review.

Chapter 2 gives the theory and solution of Helmholtz integral equations via BEM for full-space, half-space and half-space contact cases in detail.

Chapter 3 presents the surface and exterior pressures of a dilating sphere in full space and a hemisphere in contact with a surface; for both the rigid and impedance bounding surface cases. Furthermore, this chapter presents the comparison of computed results with the analytical solutions.

Chapter 4 presents the sound source identification of a refrigerator. The measured surface velocity distribution together with calculated and displayed surface and exterior pressure distribution of the refrigerator make possible this assessment. Moreover, the numerical results of the refrigerator are compared with the sound measurements in this chapter.

Chapter 5 gives detailed explanations about the computer program.

Chapter 6 presents a short review and underlines the outcomes of the thesis.

Appendix A presents a brief information about the determination of reflection coefficient of a reflecting surface; Appendix B gives the geometrical data of spherical and hemispherical sources; Appendix C presents the surface pressures of spherical and hemispherical sources; Appendix D gives geometrical and surface velocity data of the refrigerator; consequently Appendix E presents the computer code.

CHAPTER TWO
THEORETICAL CONSIDERATIONS

2.1 Introduction

In this chapter, derivation of the Helmholtz integral equation for the three-dimensional full space is presented and expressed in terms of the acoustic variables, pressure and particle velocity. Numerical solution of the surface integrals in the Helmholtz integral formulation is accomplished by using boundary element method and Gaussian quadrature technique. Helmholtz integral formulations and their numerical expressions are also presented for the three-dimensional half-space and half-space contact problems.

2.2 Derivation of the Helmholtz Integral Equation

2.2.1 Green's Theorem and Helmholtz Equation

The derivation of the Helmholtz integral equation starts with the three-dimensional wave equation,

$$\nabla^2 p - \frac{1}{c^2}\frac{\partial^2 p}{\partial t^2} = 0 \tag{2.1}$$

where p is the acoustic pressure and c is the speed of sound. Assuming a harmonic time dependence $e^{i2\pi ft}$, acoustic pressure can be written as,

$$p = \bar{p}\, e^{i2\pi ft} \tag{2.2}$$

where f is the wave frequency. Substituting Equation (2.2) in Equation (2.1), the wave equation becomes

$$\left(\nabla^2 + k^2\right)p = 0\,. \tag{2.3}$$

Equation (2.3) is known as the Helmholtz equation, where $k = 2\pi f/c$ is the wavenumber. If the Helmholtz operator, $\bar{L}$, is defined as,

$$\bar{L} = \nabla^2 + k^2 \tag{2.4}$$

the non-homogeneous Helmholtz equation is given as (Morse & Feshbach, 1953),

$$\bar{L}v = -4\pi\delta(Q - P) \tag{2.5}$$

where δ is the Dirac-delta function, Q and P represent two points in the medium. The fundamental solution of Equation (2.5), in the three-dimensional space is the free-space Green's function,

$$v = \frac{e^{-ikR}}{R},\ R = |Q - P|\,. \tag{2.6}$$

Green's theorem relates the surface integral over S' to the volume integral over V bounded by S' for any two smooth and non-singular functions p and v in volume V (Kinsler, Frey, Coppens & Sanders, 1982).

$$\int_V \left(p\nabla^2 v - v\nabla^2 p\right)dV = \int_{S'}\left(p\frac{\partial v}{\partial n'} - v\frac{\partial p}{\partial n'}\right)dS \tag{2.7}$$

where n' is the outward normal of the surface S'. Forming the difference $p\bar{L}v - v\bar{L}p$ and by using Equations (2.3) and (2.4), the following relation is obtained:

$$\begin{aligned} p\bar{L}v - v\bar{L}p &= p\nabla^2 v - v\nabla^2 p\,, \\ p\bar{L}v &= p\nabla^2 v - v\nabla^2 p\,. \end{aligned} \tag{2.8}$$

If two sides of Equation (2.8) are integrated over the volume V, and if Green's theorem in Equation (2.7) is used, the following equality is obtained:

$$\int_V p\bar{L}v\,dV = \int_{S'}\left(p\frac{\partial v}{\partial n'} - v\frac{\partial p}{\partial n'}\right)dS\,. \tag{2.9}$$

Substituting Equation (2.5) into Equation (2.9) and by using the Dirac-delta function property,

$$\int_V p(Q)\,\delta(Q-P)\,dV = p(P) \tag{2.10}$$

the following equation is obtained,

$$-4\pi\,p(P) = \int_{S'}\left(p\frac{\partial v}{\partial n'} - v\frac{\partial p}{\partial n'}\right)dS\,. \tag{2.11}$$

2.2.2 Exterior Helmholtz Integral Equation

As shown in Figure 2.1, if point Q is on the surface S and point P is inside the field V, between the surface S and the infinite surface $\sum$, Equation (2.11) may be rewritten by using free-space Green's function in Equation (2.6) and expressed as the summation of two integrals:

$$4\pi\,p(P) = \int_{S+\sum}\left[-p\frac{\partial\left(e^{-ikR}/R\right)}{\partial n'} + \frac{e^{-ikR}}{R}\frac{\partial p}{\partial n'}\right]dS\ . \tag{2.12}$$

The surface $\sum$ at intifinity is identical to a sphere with a radius of $R = R' \to \infty$ (Skudrzyk, 1971). By using the relation $\partial/\partial n' = \partial/\partial R'$, the contribution of this surface to the integral in Equation (2.12) may be rewritten as,

$$\lim_{R'\to\infty} \int_{\Sigma} \left[- p \frac{\partial\left(e^{-ikR'}/R'\right)}{\partial R'} + \frac{e^{-ikR'}}{R'} \frac{\partial p}{\partial R'} \right] dS \,. \tag{2.13}$$

By using the spherical co-ordinates, the following relation

$$dS = R'^2 \sin\theta \, d\theta \, d\phi = R'^2 d\Omega \tag{2.14}$$

may be rewritten. Here Ω is the space angle. By substituting Equation (2.14) in Equation (2.13) and taking the derivatives, Equation (2.13) takes the form,

$$\lim_{R'\to\infty} \int_{\Sigma} R' \left[\frac{\partial p}{\partial R'} + ikp + \frac{p}{R'} \right] e^{-ikR'} d\Omega \,. \tag{2.15}$$

Thus, the contributions of the regions infinitely far away vanish if,

$$\lim_{R\to\infty} \left[R \left(\frac{\partial p}{\partial R} + ikp \right) \right] = 0 \tag{2.16}$$

which is known as Sommerfield radiation condition. This condition explains that there isn't any source at infinity, there isn't any reflection coming from infinity and the function p vanishes as $R \to \infty$.

When Sommerfeld radiation condition is used, the integral in Equation (2.12) involves only the surface of the source. Since the outward normal of the surface S is $n = -n'$, Equation (2.12) may be rewritten as,

$$4\pi p(P) = \int_{S} \left[p \frac{\partial\left(e^{-ikR}/R\right)}{\partial n} - \frac{e^{-ikR}}{R} \frac{\partial p}{\partial n} \right] dS \,. \tag{2.17}$$

which is called as exterior Helmholtz integral equation.

2.2.3 General Expression of the Helmholtz Integral Equation

If S is a smooth surface and if point P is allowed to approach to the surface, Equation (2.17) takes the form (Courant & Hilbert, 1962)

$$2\pi p(P) = \int_S \left[p \frac{\partial\left(e^{-ikR}/R\right)}{\partial n} - \frac{e^{-ikR}}{R} \frac{\partial p}{\partial n} \right] dS \tag{2.18}$$

which is known as surface Helmholtz integral equation.

If point P is inside the surface S, since there will not be a singularity problem in V, by using Dirac-delta function property,

$$0 = \int_S \left[p \frac{\partial\left(e^{-ikR}/R\right)}{\partial n} - \frac{e^{-ikR}}{R} \frac{\partial p}{\partial n} \right] dS \tag{2.19}$$

is obtained. Equation (2.19) is known as the interior Helmholtz integral equation. Equations (2.17), (2.18) and (2.19) together, may be written in a compact form as the general Helmholtz integral equation:

$$C(P)\, p(P) = \int_S \left[p \frac{\partial\left(e^{-ikR}/R\right)}{\partial n} - \frac{e^{-ikR}}{R} \frac{\partial p}{\partial n} \right] dS \,. \tag{2.20}$$

Here $C(P)$ takes the following values according to the position of the field point P (Figure 2.1):

$$C(P) = \begin{cases} 4\pi & \text{if } P \text{ is inside } V \\ 2\pi & \text{if } P \text{ is on } S \\ 0 & \text{if } P \text{ is outside } V \end{cases}$$

If P is at a corner or edge of S which has no unique tangent plane at that point, a more general expression for $C(P)$ is given as (Seybert, Soenarko, Rizzo & Shippy, 1985),

$$C(P) = 4\pi + \int_S \left[\frac{\partial(1/R)}{\partial n} \right] dS \,. \tag{2.21}$$

If Equation (2.21) is used in Equation (2.20), the equation known as the general surface Helmholtz integral is obtained:

$$\left(4\pi + \int_S \left[\frac{\partial(1/R)}{\partial n} \right] dS \right) p(P) = \int_S \left[p \frac{\partial\left(e^{-ikR}/R\right)}{\partial n} - \frac{e^{-ikR}}{R} \frac{\partial p}{\partial n} \right] dS \,. \tag{2.22}$$

Using the particle velocity u and the density of the fluid in the medium ρ_o, the linear Euler's equation is written as,

$$\rho_o \frac{\partial u}{\partial t} = -\nabla p \,. \tag{2.23}$$

Assuming a harmonic change for the acoustic particle velocity $u = U e^{i2\pi ft}$

$$\frac{\partial u}{\partial t} = i2\pi f u \tag{2.24}$$

may be written. Substituting Equation (2.24) in Equation (2.23), the following equality is obtained:

$$\frac{\partial p}{\partial n} = -iz_o k u_n \tag{2.25}$$

where $z_o = \rho_o c$ is the characteristic acoustic impedance of the medium, u_n is the component of the surface velocity in the direction of the outward normal. Substituting Equation (2.25) in Equation (2.20), the Helmholtz integral can be written in terms of acoustic pressure and velocity:

$$C(P)\,p(P) = \int_S \left[p\,\frac{\partial\left(e^{-ikR}/R\right)}{\partial n} + iz_o k u_n \frac{e^{-ikR}}{R} \right] dS\,. \tag{2.26}$$

The partial derivative of the free-space Green's function (Equation 2.6) with respect to n is,

$$\frac{\partial\left(e^{-ikR}/R\right)}{\partial n} = -\left(\frac{1}{R} + ik\right)\frac{e^{-ikR}}{R}\cos\gamma \tag{2.27}$$

where γ is the angle between the vectors R and n (Figure 2.2). By using Equation (2.27), Equation (2.26) may be rewritten as,

$$C(P)\,p(P) + \int_S \left[p\left(\frac{1}{R} + ik\right)\cos\gamma\ \frac{e^{-ikR}}{R} \right] dS = \int_S \left[iz_o k u_n \frac{e^{-ikR}}{R} \right] dS\,. \tag{2.28}$$

Taking the derivative of the $C(P)$ term in Equation (2.21) with respect to n yields,

$$\frac{\partial(1/R)}{\partial n} = -\frac{1}{R^2}\cos\gamma \tag{2.29}$$

Considering Equation (2.29), the general surface Helmholtz integral may be written as,

$$\left[4\pi - \int_S \left(\frac{1}{R^2}\cos\gamma\right) dS\right] p(P) + \int_S \left[p\left(\frac{1}{R} + ik\right)\frac{e^{-ikR}}{R}\cos\gamma\right] dS = \int_S \left[iz_o k u_n \frac{e^{-ikR}}{R}\right] dS \tag{2.30}$$

2.3 Numerical Solution of the Helmholtz Integral Equation

In order to determine the radiation characteristics of acoustic sources, acoustic pressure and normal velocity distributions on the surface should be known. In mechanical problems, generally the surface velocity distribution is prescribed. Therefore firstly, by using the Neumann boundary condition, acoustic pressures on the surface are calculated from the surface Helmholtz integral equation. Subsequently, by using the calculated surface pressures as input for the exterior Helmholtz integral equation, field pressures of the acoustic sources can be evaluated.

2.3.1 Numerical Expression of the General Surface Helmholtz Integral Equation

Before the numerical integration of the general surface Helmholtz integral, the variables in Equation (2.30) can be written in terms of the related points as,

$$\begin{aligned}&\left[4\pi - \int_S \left(\frac{1}{R^2(P,Q)}\cos\gamma(P,Q)\right) dS(Q)\right] p(P) \\ &\quad + \int_S \left[p(Q)\left(\frac{1}{R(P,Q)} + ik\right)\frac{e^{-ikR(P,Q)}}{R(P,Q)}\cos\gamma(P,Q)\right] dS(Q) \\ &\quad = \int_S \left[iz_o k u_n(Q)\frac{e^{-ikR(P,Q)}}{R(P,Q)}\right] dS(Q)\,.\end{aligned} \tag{2.31}$$

In the present study, the boundary element method is used to solve the surface integrals in Equation (2.31). In order to apply this method, the surface of the body is discretized by using L quadrilateral elements shown in Figure 2.3. The surface integrals in Equation (2.31) are rewritten as the summations of the elemental surface integrals,

$$\left[4\pi - \sum_{\lambda=1}^{L} \int_{S_\lambda} \left(\frac{1}{R_\lambda{}^2} \cos\gamma_\lambda \right) dS \right] p(P) + \sum_{\lambda=1}^{L} \int_{S_\lambda} p_\lambda \left(\frac{1}{R_\lambda} + ik \right) \frac{e^{-ikR_\lambda}}{R_\lambda} \cos\gamma_\lambda \, dS$$

$$= iz_o k \sum_{\lambda=1}^{L} \int_{S_\lambda} (u_n)_\lambda \frac{e^{-ikR_\lambda}}{R_\lambda} dS \,. \qquad (2.32)$$

In the isoparametric element formulation technique, global Cartesian co-ordinates and acoustic variables, such as pressure and normal velocity, of a point on an element are written in terms of the nodal variables of the corresponding element;

$$x_\lambda(\xi,\eta) = \sum_{\alpha=1}^{8} N_\alpha(\xi,\eta)\, x_{\lambda\alpha}$$

$$y_\lambda(\xi,\eta) = \sum_{\alpha=1}^{8} N_\alpha(\xi,\eta)\, y_{\lambda\alpha} \qquad \text{(a)}$$

$$z_\lambda(\xi,\eta) = \sum_{\alpha=1}^{8} N_\alpha(\xi,\eta)\, z_{\lambda\alpha}$$

$$p_\lambda(\xi,\eta) = \sum_{\alpha=1}^{8} N_\alpha(\xi,\eta)\, p_{\lambda\alpha} \qquad \text{(b)} \qquad (2.33)$$

$$(u_n)_\lambda(\xi,\eta) = \sum_{\alpha=1}^{8} N_\alpha(\xi,\eta)\, (u_n)_{\lambda\alpha} \qquad \text{(c)}$$

where ξ and η represent the local co-ordinates. x_λ, y_λ and z_λ are the global co-ordinates, p_λ and $(u_n)_\lambda$ are the acoustic pressure and the normal velocity of a point on the λ_{th} element, respectively. The variables with the subscript $\lambda\alpha$ represent the nodal values of the element λ. $\alpha = 1,2,3...,8$ denotes the node number. N_α denotes the second order shape functions for an 8-noded quadrilateral element (Sarigül, 1990).

The surface integrals in Equation (2.32) may be written in the local co-ordinates as,

$$\int_S dS = \int_S J(\xi,\eta)\, d\xi\, d\eta \tag{2.34}$$

where J is the Jacobian of the co-ordinate transformation in Equation (2.33)(a).

Substituting Equations (2.33) and (2.34) in Equation (2.32) leads to

$$\left[4\pi - \sum_{\lambda=1}^{L} s_{\lambda d}\right] p_d + \sum_{\lambda=1}^{L}\sum_{\alpha=1}^{8} t_{\lambda d}^{\alpha}\, p_{\lambda\alpha} = iz_o k \sum_{\lambda=1}^{L}\sum_{\alpha=1}^{8} v_{\lambda d}^{\alpha}\, (u_n)_{\lambda\alpha} \tag{2.35}$$

where $d = 1 \rightarrow D$ and D is the total number of nodes on the surface of the body. The coefficients in Equation (2.35) are,

$$s_{\lambda d} = \int_{S_\lambda} \left(\frac{1}{R_d(\xi,\eta)}\right)^2 \cos\gamma_d(\xi,\eta)\, J(\xi,\eta)\, d\xi\, d\eta \quad ,$$

$$t_{\lambda d}^{\alpha} = \int_{S_\lambda} N_\alpha(\xi,\eta)\left[\frac{1}{R_d(\xi,\eta)} + ik\right] \cos\gamma_d(\xi,\eta) \cdot \left[\frac{e^{-ikR_d(\xi,\eta)}}{R_d(\xi,\eta)}\right] J(\xi,\eta)\, d\xi\, d\eta \quad , \tag{2.36}$$

$$v_{\lambda d}^{\alpha} = \int_{S_\lambda} N_\alpha(\xi,\eta)\left[\frac{e^{-ikR_d(\xi,\eta)}}{R_d(\xi,\eta)}\right] J(\xi,\eta)\, d\xi\, d\eta \quad ,$$

where $R_d(\xi,\eta)$ denotes the distance between the node d and the points representing the element λ.

In Equation (2.36) singularity occurs due to the term $1/R_d(\xi,\eta)$ when $R_d(\xi,\eta) = 0$. In order to solve the ordinary surface integrals in Equation (2.36), Gaussian quadrature is used. This is a powerful integration technique and very

suitable for the removal of the singularity problem (Sarigül, 1990). Using Gaussian points that never coincide with the nodes, $R_d(\xi,\eta) \neq 0$ condition can be satisfied.

In the Gaussian quadrature, a surface integral for a function which is indicated by ψ is written as two numerical summations,

$$\int_S \psi(\xi,\eta)\, d\xi\, d\eta = \int_{-1}^{1}\int_{-1}^{1} \psi(\xi,\eta)\, d\xi\, d\eta = \sum_{i=1}^{n}\sum_{j=1}^{m} A_i A_j \psi(\xi_i,\eta_j) \tag{2.37}$$

where A_i and A_j represent Gaussian weights, n and m denote the number of Gaussian points in the ξ and η directions, respectively. Local co-ordinates and weights of these points are tabulated in numerical analysis books. If the approach in Equation (2.37) is applied to Equation (2.36), coefficients of Equation (2.35) become

$$s_{\lambda d} = \sum_{i=1}^{n}\sum_{j=1}^{m} A_i A_j \left[\frac{1}{R_d(\xi_i,\eta_j)}\right]^2 \cos\gamma_d(\xi_i,\eta_j)\, J(\xi_i,\eta_j) \quad ,$$

$$t^{\alpha}_{\lambda d} = \sum_{i=1}^{n}\sum_{j=1}^{m} A_i A_j N_\alpha(\xi_i,\eta_j)\left[\frac{1}{R_d(\xi_i,\eta_j)} + ik\right]\cos\gamma_d(\xi_i,\eta_j) \cdot\left[\frac{e^{-ikR_d(\xi_i,\eta_j)}}{R_d(\xi_i,\eta_j)}\right] J(\xi_i,\eta_j) \quad , \tag{2.38}$$

$$v^{\alpha}_{\lambda d} = \sum_{i=1}^{n}\sum_{j=1}^{m} A_i A_j N_\alpha(\xi_i,\eta_j)\left[\frac{e^{-ikR_d(\xi_i,\eta_j)}}{R_d(\xi_i,\eta_j)}\right] J(\xi_i,\eta_j) \quad .$$

2.3.2 Matrix Representation of the General Surface Helmholtz Integral Equation

Surface Helmholtz integral has a suitable form for matrix solution. If Equation (2.35) is written for each of the nodes on the surface of the body, a system of

equations involving 2D (D real, D imaginary) algebraic equations are obtained. This set of equations can be written in the matrix form as,

$$[G]\{p\}+[C]\{p\}=[V]\{u_n\} \tag{2.39}$$

where $[G]$ is 2Dx2D diagonal matrix which includes the geometrical data, $[C]$ and $[V]$ are 2Dx2D matrices. $\{p\}$ and $\{u_n\}$ are 2Dx1 vectors including the acoustic pressure and normal velocity of all nodes, respectively. Equation (2.39) may be written as follows,

$$[[G]+[C]]\{p\}=[V]\{u_n\}. \tag{2.40}$$

By defining a new matrix $[M]=[G]+[C]$ and subsituting this matrix in Equation (2.40) leads to

$$[M]\{p\}=[V]\{u_n\}. \tag{2.41}$$

If the right-hand side of Equation (2.41) is rearranged as $\{h\}=[V]\{u_n\}$, Equation (2.41) becomes

$$[M]\{p\}=\{h\}. \tag{2.42}$$

Acoustic pressure of each node on the surface of the vibrating body can be evaluated by solving Equation (2.42).

The field pressures can be calculated by substituting the determined surface pressures of the body, to the exterior Helmholtz equation:

$$4\pi\, p_f = -\sum_{\lambda=1}^{L}\sum_{\alpha=1}^{8} t_{\lambda d}^{\alpha}\; p_{\lambda\alpha} + iz_o k \sum_{\lambda=1}^{L}\sum_{\alpha=1}^{8} v_{\lambda d}^{\alpha}\,(u_n)_{\lambda\alpha} \tag{2.43}$$

where p_f is the acoustic pressure of a field point, $t_{\lambda d}^{\alpha}$ and $v_{\lambda d}^{\alpha}$ are the related coefficients defined in Equation (2.38). In order to evaluate acoustic pressures of field points, the solution of Equation (2.43) is performed separately for each field point.

2.4 Helmholtz Integral Equation for Half-Space

v being free-space Green's function, Helmholtz integral in Equation (2.20) can be written in closed form as,

$$C(P)p(P) = \int_S \left[p\frac{\partial v}{\partial n} - v\frac{\partial p}{\partial n} \right] dS \,. \tag{2.44}$$

In the case where there exists an infinite reflecting plane that makes the acoustic domain V a half-space, the surface S is given by the summation $S = S_o + S_p$. Here, S_o represents the surface of the vibrating body whereas S_p denotes the surface of the infinite plane that forms the half space (Figure 2.4)

In most radiation problems the Neumann boundary condition ($\partial p/\partial n$ known) is specified on the surface of the vibrating body S_o. For a reflecting plane S_p, the impedance boundary condition expressed in p is given as,

$$ikp + \frac{Z}{z_o}\frac{\partial p}{\partial n} = 0 \tag{2.45}$$

where Z is the acoustical impedance of the surface. Equation (2.45) is used in Equation (2.44) for the integrand of the S_p integral.

The solution of the Helmholtz integral in Equation (2.44) requires the calculation of surface integrals over the entire body S which includes the infinite reflecting

plane S_p. In practice, numerical solution of Equation (2.44) should be performed by a reasonable number of surface elements. However, the integral over infinite plane S_p causes to some numerical modelling and computational difficulties. Under this circumstance, the inclusion of the surface S_p puts forward the question of where to terminate the discretization of the infinite plane. Indeed, there is no specific answer to this question.

Boundary element method provides considerable flexibility in the selection of the kernel functions in Equation (2.44). Any regular solution of the wave equation may be added to the usual free-space Green's function and the resulting function may be used instead of v in Equation (2.44). For that reason, it is required to select a modified Green's function v_H which causes the integral over infinite plane S_p to vanish in Equation (2.44),

$$\int_{S_p}\left[p\frac{\partial v_H}{\partial n} - v_H \frac{\partial p}{\partial n}\right] dS_p = 0. \tag{2.46}$$

Thus, the selection of appropriate Green's function gives the opportunity to implement boundary element discretization only to the vibrating body S_o.

The selected v_H should satisfy the boundary condition in Equation (2.45), on the infinite plane S_p,

$$ikv_H + \frac{Z}{z_o}\frac{\partial v_H}{\partial n} = 0. \tag{2.47}$$

Therefore, the integrand in Equation (2.46) is identically zero which can be verified by the substitution of Equations (2.45) and (2.47) into Equation (2.46).

Equation (2.47) may be satisfied for two important cases:

- when S_p is a rigid plane ($\partial p/\partial n = 0$, $u_n = 0$, $Z = \infty$ on S_p),
- when S_p is a free surface ($p = 0$, $Z = 0$ on S_p).

For these two conditions the modified Green's function may be chosen as,

$$v_H = \frac{e^{-ikR}}{R} + R_p \frac{e^{-ikR'}}{R'} \tag{2.48}$$

which is formed by adding a second term to the free-space Green's function due to a image point P' of the point P with respect to the infinite plane as shown in Figure 2.4 (Seybert & Soenarko, 1988). Here, R' is the distance between points Q and P' ($R' = |Q - P'|$) and R_p is the reflection coefficient of the reflecting plane. The value of R_p depends on the sound absorption coefficient of the reflecting plane. For Q is on S_p, R_p can be chosen as:

- when S_p is a rigid plane $R_p = 1$,
- when S_p is a free surface $R_p = -1$,
- when S_p is an impedance surface $R_p = \sqrt{1-\alpha^2}$,

where α is the sound absorption coefficient of the reflecting plane. The relationship between R_p and α ($R_p = \sqrt{1-\alpha^2}$) is derived in Appendix A. The value of R_p reaches to 1 when $\alpha = 0$ which means that S_p is a rigid plane.

Equation (2.48) which is known as the usual "half-space Green's function", is used in theoretical acoustics, for example in the determination of the field produced by a point source near a reflecting plane. Seybert & Soenarko (1988) have successfully applied the half-space Green's function to the finite body problems for the first time.

The selection of the appropriate Green's function v_H as it is given in Equation (2.48) removes the requirement of integration over the infinite plane S_p. Thus, all discretizations and numerical approximations are performed only for the body S_o. In this regard, for half-space radition problems Equation (2.44) leads to

$$C(P)p(P)=\int_{S_o}\left[p\frac{\partial v_H}{\partial n}-v_H\frac{\partial p}{\partial n}\right]dS_o\,. \tag{2.49}$$

In this thesis, numerical solutions are performed for both rigid and impedance infinite surfaces. The general surface Helmholtz integral in Equation (2.22) can be rewritten in closed form for a surface point P of a body in half-space as,

$$\left(4\pi+\int_{S_o}\left[\frac{\partial(1/R)}{\partial n}\right]dS_o\right)p(P)-\int_{S_o}\left[\frac{\partial v_H(R,R',k)}{\partial n}\right]p(Q)\,dS_o = \int_{S_o} iz_o k\,v_H(R,R',k)\,u_n(Q)\,dS_o\,. \tag{2.50}$$

2.4.1 Numerical Expression of the General Surface Helmholtz Integral Equation for Half-Space

The discretized form of the Helmholtz integral in Equation (2.35) is also valid for this case. The coefficient $s_{\lambda d}$ remains unchanged, whereas the expressions for coefficients $t^{\alpha}_{\lambda d}$ and $v^{\alpha}_{\lambda d}$ take the following forms

$$s_{\lambda d}=\sum_{i=1}^{n}\sum_{j=1}^{m}A_i A_j\left(\frac{1}{R_d(\xi_i,\eta_j)}\right)^2\cos\gamma_d(\xi_i,\eta_j)\,J(\xi_i,\eta_j)\qquad,$$

$$t^{\alpha}_{\lambda d}=\sum_{i=1}^{n}\sum_{j=1}^{m}A_i A_j N_{\alpha}(\xi_i,\eta_j)\left\{\left[\frac{1}{R_d(\xi_i,\eta_j)}+ik\right]\left[\frac{e^{-ikR_d(\xi_i,\eta_j)}}{R_d(\xi_i,\eta_j)}\right]\cos\gamma_d(\xi_i,\eta_j)\right.$$

$$+ R_p\left[\frac{1}{R'_d(\xi_i,\eta_j)} + ik\right]\left[\frac{e^{-ikR'_d(\xi_i,\eta_j)}}{R'_d(\xi_i,\eta_j)}\right]\cos\gamma'_d(\xi_i,\eta_j)\Bigg\} J(\xi_i,\eta_j)\ , \qquad (2.51)$$

$$v^{\alpha}_{\lambda d} = \sum_{i=1}^{n}\sum_{j=1}^{m} A_i A_j N_\alpha(\xi_i,\eta_j)\left[\frac{e^{-ikR_d(\xi_i,\eta_j)}}{R_d(\xi_i,\eta_j)} + R_p\frac{e^{-ikR'_d(\xi_i,\eta_j)}}{R'_d(\xi_i,\eta_j)}\right] J(\xi_i,\eta_j)\ .$$

2.4.2 Matrix Representation of the General Surface Helmholtz Integral Equation for Half-Space

The general surface Helmholtz integral equation for half space has a similar matrix form as the general surface Helmholtz integral equation for free space. Therefore, the solution steps are the same for both surface and field pressures.

Despite the fact that, inclusion of new terms in the Helmholtz integral for half-space case increases the computer time and memory requirements, these are fairly small when compared with the computation time and memory required for the evaluation of the integrals on the reflecting plane S_p.

2.5 Helmholtz Integral Equation for Half-Space Contact Case

Half-space contact problem is a special case of the half-space position. If the vibrating body is sitting on the infinite reflecting plane S_p as demonstrated in Figure 2.5, some modifications are needed in the half-space formulation. In this case, the boundary S of the body is divided into two parts; the first part S_c in contact with S_p while the second part S_o exposed to the acoustic medium. Helmholtz integral equation for the contact case can be written as,

$$C(P)\,p(P) = \int_{S_o}\left[p\frac{\partial v_H}{\partial n} - v_H\frac{\partial p}{\partial n}\right]dS_o \qquad (2.52)$$

which is identical in form to Equation (2.49) written for the half-space case except that S_o here is a part of the boundary, not the total boundary. The coefficient $C(P)$ in Equation (2.52) is again 4π for P in V and zero for P in D'. However, special care should be taken in calculating $C(P)$ when P on S_o, if S_o does not have a unique tangent plane at P. Thus, there are two possible cases for P on S_o (Seybert & Wu, 1989):

- The first case is that P is on S_o but not in contact with the reflecting plane S_p. For this case $C(P)$ is given by,

$$C(P) = 4\pi + \int_{S_o+S_c} \left[\frac{\partial(1/R)}{\partial n} \right] d(S_o + S_c) \tag{2.53}$$

  where the integral is calculated on the total surface. Therefore, Equation (2.53) is identical to Equation (2.21) written for full space.

- The second case is that P is not only on S_o, but also in contact with the reflecting plane S_p. In this case $C(P)$ is given as,

$$C(P) = (1 + R_p) \left[2\pi + \int_{S_o+S_c} \left[\frac{\partial(1/R)}{\partial n} \right] d(S_o + S_c) \right] \tag{2.54}$$

  where $R_p = \sqrt{1-\alpha^2}$.

The elements of S_c which are called as “dummy elements”, don’t contribute to the Helmholtz integral in Equation (2.52) since there is no acoustic variable associated with these elements. However, these elements are used for integration in Equations (2.53) and (2.54) only to obtain geometrical data.

By using Equations (2.50) and (2.54), the general surface Helmholtz integral for a point P in contact with S_o and S_p can be rewritten in closed form as,

$$\left(1+R_p\right)\left[2\pi+\int_{S_o+S_c}\left[\frac{\partial(1/R)}{\partial n}\right]d\left(S_o+S_c\right)\right]p(P)$$

$$-\int_{S_o}\left[\frac{\partial v_H\left(R,R',k\right)}{\partial n}\right]p(Q)\,dS_o=\int_{S_o}iz_o k\,v_H\left(R,R',k\right)u_n(Q)\,dS_o\,. \qquad (2.55)$$

After implementing boundary element discretization, co-ordinate transformation and Gaussian quadrature, Equation (2.55) takes the form

$$\left[\left(1+R_p\right)\left(2\pi-\sum_{\lambda=1}^{L}s_{\lambda d}\right)\right]p_d+\sum_{\lambda=1}^{L}\sum_{\alpha=1}^{8}t_{\lambda d}^{\alpha}\,p_{\lambda\alpha}=iz_o k\sum_{\lambda=1}^{L}\sum_{\alpha=1}^{8}v_{\lambda d}^{\alpha}\left(u_n\right)_{\lambda\alpha} \qquad (2.56)$$

where the coefficients $s_{\lambda d}$, $t_{\lambda d}^{\alpha}$ and $v_{\lambda d}^{\alpha}$ are identical to those in Equation (2.51).

The general surface Helmholtz integral equation for half-space contact case has a similar matrix form as the general surface Helmholtz integral equation for free space. Therefore, the solution steps are the same for both surface and field pressures.

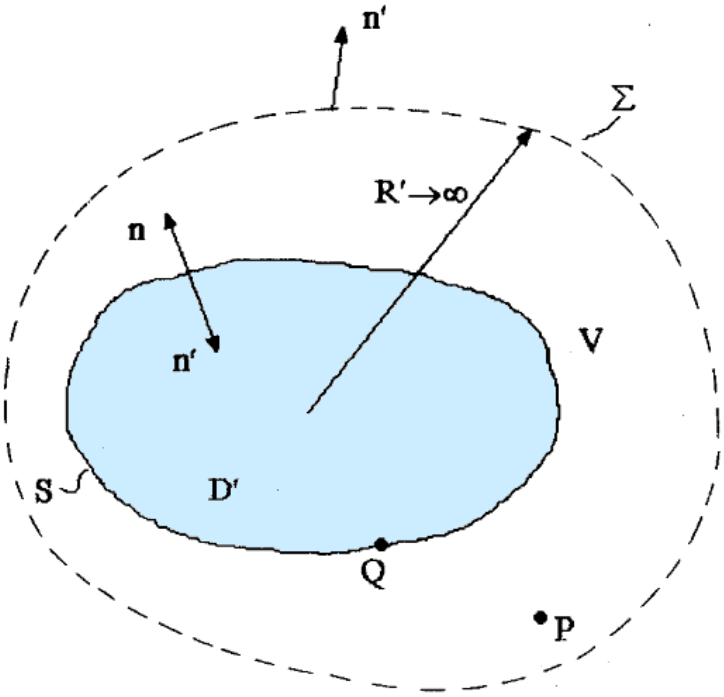

Figure 2.1 Exterior acoustic problem geometry.

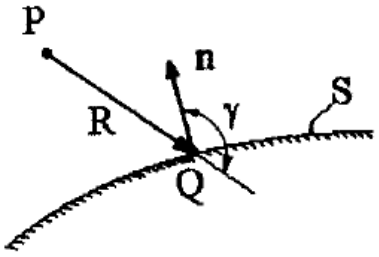

Figure 2.2 R vector and γ angle.

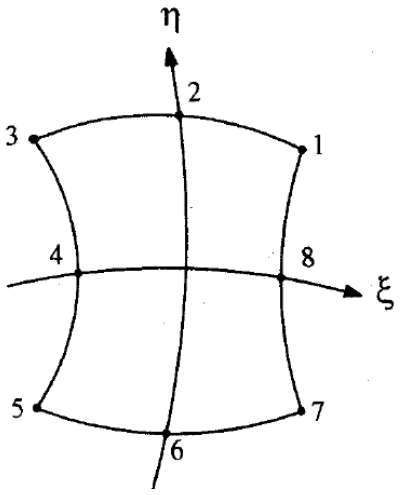

Figure 2.3 8-noded curvilinear quadrilateral element.

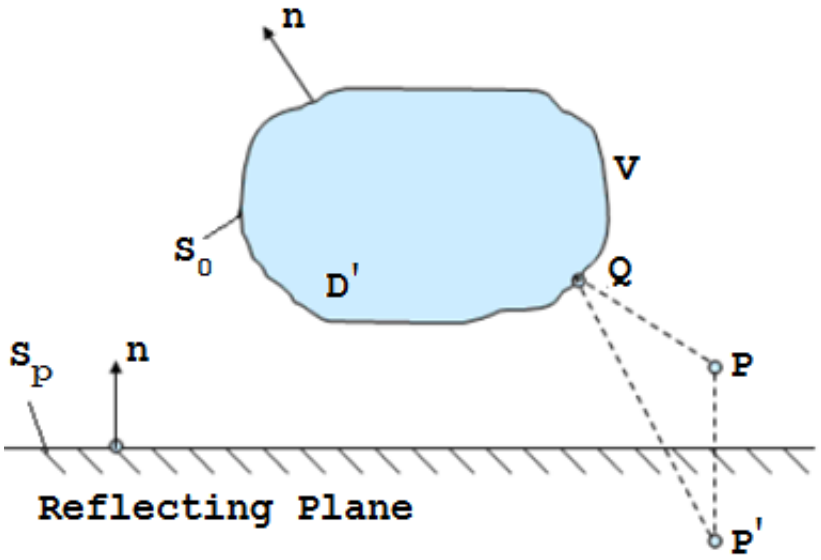

Figure 2.4 Half-space acoustic problem geometry.

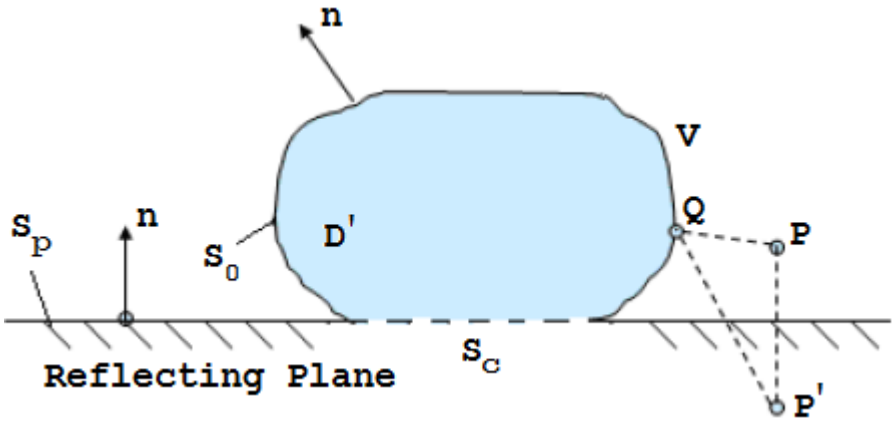

Figure 2.5 Half-space contact acoustic problem geometry.

CHAPTER THREE
NUMERICAL RESULTS OF SPHERICAL SOURCES

3.1 Introduction

In this chapter, dilating spherical sources are considered in order to test the accuracy of the rewritten computer code in MatLAB®. For this purpose, BEM is applied to a dilating sphere in full space and to a dilating hemisphere in contact with a rigid infinite plane. The evaluated surface pressures of the spherical and hemispherical sources are compared with the theoretical solution.

In order to present the sound pressure distribution around the hemispherical source and to examine the effect of the sound absorbent surface as infinite plane, equal pressure contours are calculated and displayed for two cases: $\alpha = 0$ and $\alpha = 1$; that is, for rigid and anechoic infinite surfaces.

3.2 Analytical Expression for a Dilating Sphere

The exact analytical solution for the surface and field pressures of a dilating spherical source vibrating with a uniform radial velocity U_o is given as (Wu & Seybert – eds: Ciskowski & Brebbia, 1991),

$$p = \frac{a}{r} U_o \frac{iz_o ka}{1+ika} e^{-ik(r-a)} \tag{3.1}$$

where a is the radius of the sphere, r is the radial distance between the centre of the sphere and a field point.

3.3 Numerical Results of a Dilating Sphere for Full-Space Case

In the numerical solution of a dilating sphere in full space, the boundary element discretization presented by (Sarigül, 1990) was used. This model has 24 elements

and 82 nodes as illustrated in Figure 3.1. As a necessity of the BEM solution the data concerning nodal co-ordinate matrix and incidence matrix is fed to the computer. Incidence matrix is composed of node arrays in each element. The nodal co-ordinate and the incidence matrices of the sphere are given in Appendix B (Tables B.1 and B.2). 16 Gaussian points were used in the numerical integration of each element.

In order to verify the computer program for full-space case, a dilating sphere of radius $a = 1$ m was examined. It is assumed that there is a uniform normal velocity at the surface of the sphere as $U_o = u_n = 1$ m/s ($n = 1,2,3,...,82$). The wavenumber is $k = 1\,\text{m}^{-1}$, the density of the fluid in the medium is $\rho_o = 1.2$ kg/m^3 and the speed of sound is $c = 340$ m/s. Since it is not possible to obtain a unique value for each node in a numerical solution, average of the surface pressures of the dilating sphere is presented in Table 3.1 together with the theoretical result as solution of Equation 3.1. The pressure distribution over 82 nodes of the spherical source is tabulated in Appendix C (Table C.1). It is seen that although the surface pressures vary from node to node, their average value is very approximate to the theoretical result.

Table 3.1 Comparison of surface pressures predicted by BEM and theory for a spherical source ($a = 1$ m, $u_n = 1$ m/s, $k = 1$ m^{-1}, $\rho_o = 1.2$ kg/m^3, $c = 340$ m/s)

Theory (Pa)	**BEM (Pa)**
288.500	288.697

3.4 Numerical Results of a Dilating Hemisphere for Half-Space Contact Case

In the numerical solution of a dilating hemisphere for half-space contact case, the boundary element discretization in Figure 3.2 was formed by taking one-half of the sphere model in Figure 3.1. The elements in the bottom surface of the hemisphere are "dummy elements". The nodes of the "dummy elements", except the nodes that are at edges and at corners, are "dummy nodes". There is no acoustical variable associated with these nodes. Therefore, they are only taken into account in the evaluation of the $C(P)$ integrals in Equations (2.53) and (2.54) to obtain the geometrical data. This boundary element model has 4 dummy elements among 16

elements and 5 dummy nodes among 54 nodes as demonstrated in Figure 3.2. The co-ordinates of these nodes and the incidence matrix of the hemisphere are given in Appendix B (Tables B.3 and B.4). 16 Gaussian points were used in the numerical integration of each element.

3.4.1 Numerical Results of a Dilating Hemisphere in Contact with a Rigid Infinite Surface

The problem considered is the radiation from a hemisphere sitting on a rigid infinite surface which has a sound absorption coefficient of $\alpha = 0$. This configuration is analogous to a sphere in the full space as presented in Figure 3.3. The hemisphere examined has a radius of $a = 1$ m and vibrating with a uniform velocity $U_o = u_n = 1$ m/s ($n = 1,2,3,...,49$). The wavenumber is $k = 1$ m^{-1}, the density of the fluid in the medium is $\rho_o = 1.2$ kg/m^3 and the speed of sound is $c = 340$ m/s. The average value of the computed nodal pressures is compared with the average of the surface pressures of the dilating sphere in full space. As seen in Table 3.2, the results of hemispherical source are computed with sufficient accuracy.

Table 3.2 Comparison of surface pressures of spherical and hemispherical sources ($a = 1$ m, $u_n = 1$ m/s, $k = 1$ m^{-1}, $\rho_o = 1.2$ kg/m^3, $c = 340$ m/s)

Spherical source (Pa)	**Hemispherical source (Pa)**
288.697	288.832

Equal pressure contours were computed at the vertical ($x = 0$) plane in dB and demonstrated in Figure 3.4 in order to display the sound pressure level distribution around the hemisphere sitting on a rigid infinite surface. Since the hemisphere and the infinite surface system is symmetric with respect to the $x - z$ plane, the contours are also symmetric with respect to this plane. Furthermore, as the rigid surface has no sound absorbent property, the distribution of the contours is homogenous and circular as seen in Figure 3.4.

3.4.2 Numerical Results of a Dilating Hemisphere in Contact with an Impedance Infinite Surface

The hemisphere examined here is identical to the hemispherical source that was introduced in the previous section. However, it is in contact with an anechoic surface which is an impedance surface with a sound absorption coefficient of $\alpha = 1$.

In order to show the effect of the impedance surface on the sound pressure level distribution around the hemisphere, equal pressure contours evaluated at the vertical ($x = 0$) plane are presented in Figure 3.5. Since the hemisphere and the impedance system are again symmetric with respect to the $x - z$ plane, the contours are also symmetric with respect to this plane. Comparison of Figure 3.4 with Figure 3.5 shows that sound pressure levels around the hemisphere decrease due to the presence of anechoic surface. Moreover, the circular contours in Figure 3.4 tend to take elliptical shape in Figure 3.5, as a consequence of vanishing reflection effect of infinite surface.

The surface pressures of a dilating hemispherical source sitting on infinite impedance surfaces with various sound absorption coefficients ($\alpha = 0, 0.25, 0.50, 0.75$ and 1) are tabulated in Appendix C. In the literature survey of this thesis, no study on the half spaces with impedance surfaces could be found. Therefore, any comparison for the results of this new module could not be performed. However, the logical and consistent solutions for different α values indicate the validity of the developed module. Table C.2 shows evidently the decrease in the surface pressures with the increase of the sound absorbing coefficient of the infinite surface.

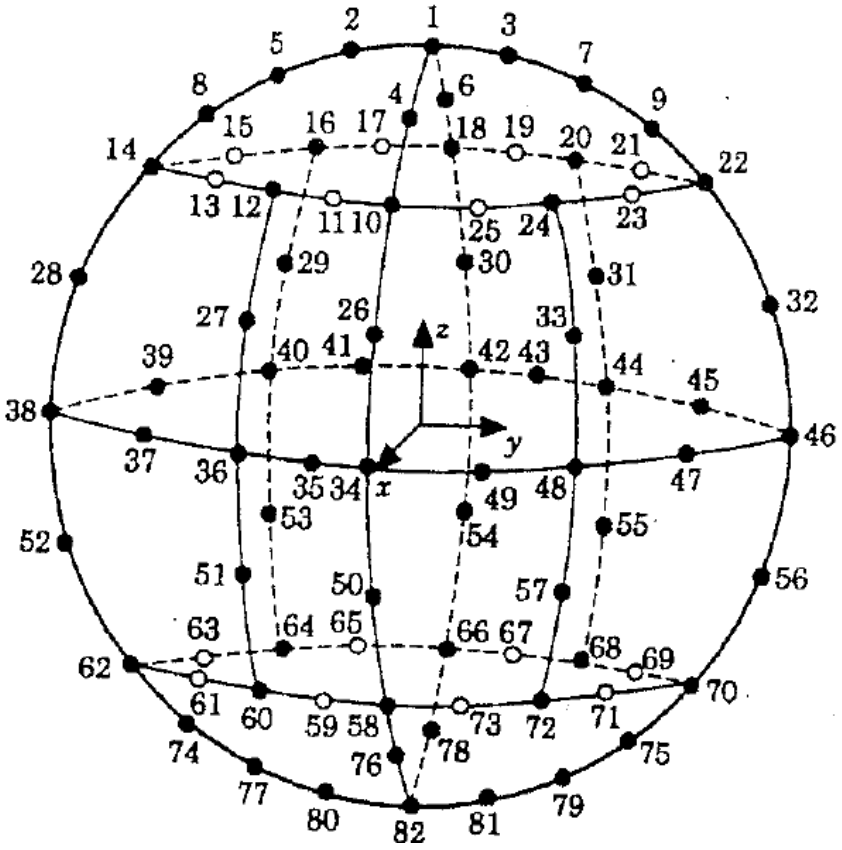

Figure 3.1 The boundary element discretization of a sphere with 24 elements and 82 nodes (Sarigül, 1990).

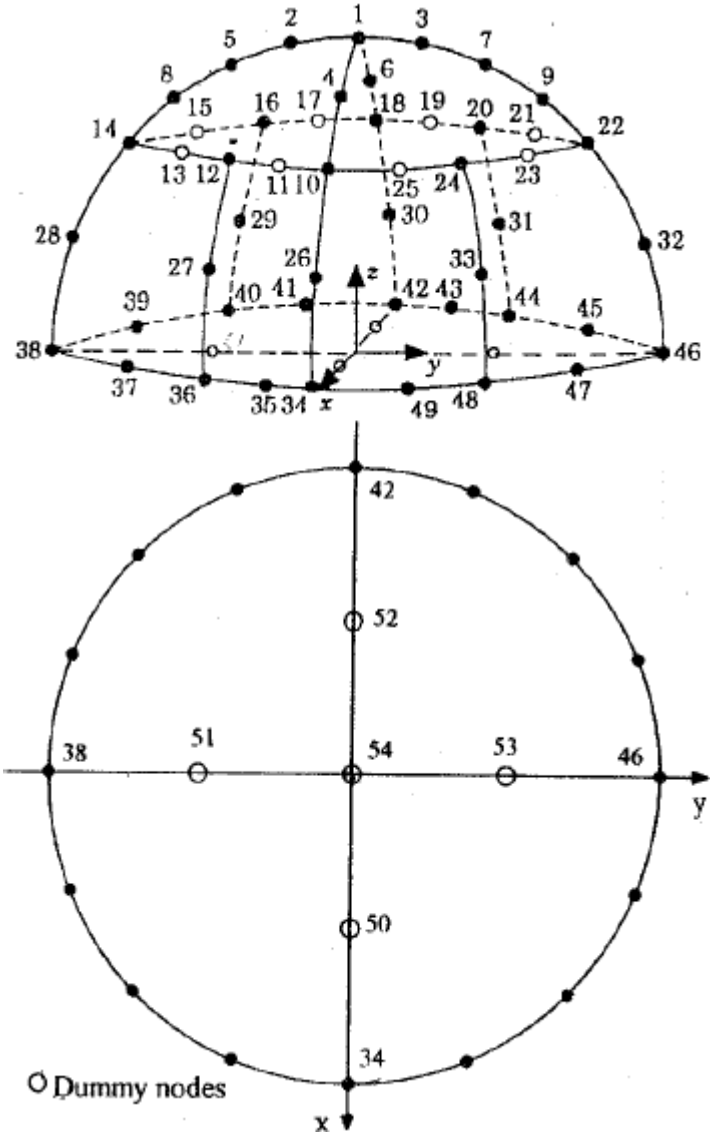

Figure 3.2 Boundary element discretization of a hemisphere with dummy elements and nodes 50-54.

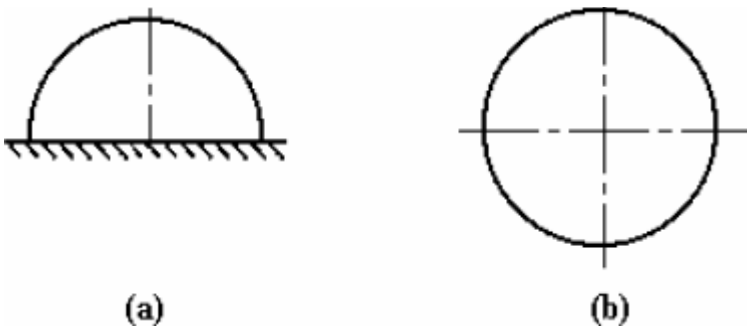

Figure 3.3 (a) A hemisphere sitting on a rigid infinite surface.
(b) A sphere in a full space.

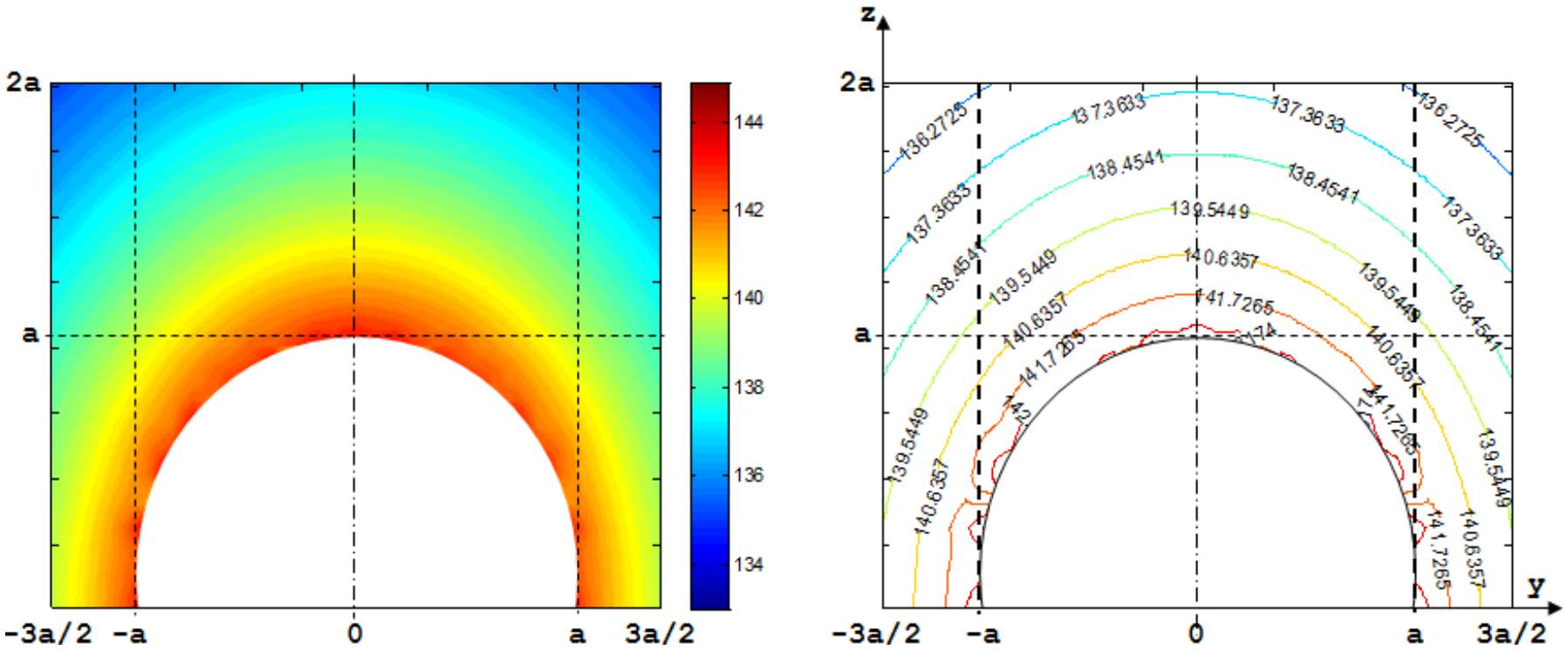

Figure 3.4 Equal pressure contours of a dilating hemisphere sitting on a rigid infinite surface, at the $x = 0$ plane ($\alpha = 0$, $a = 1$ m).

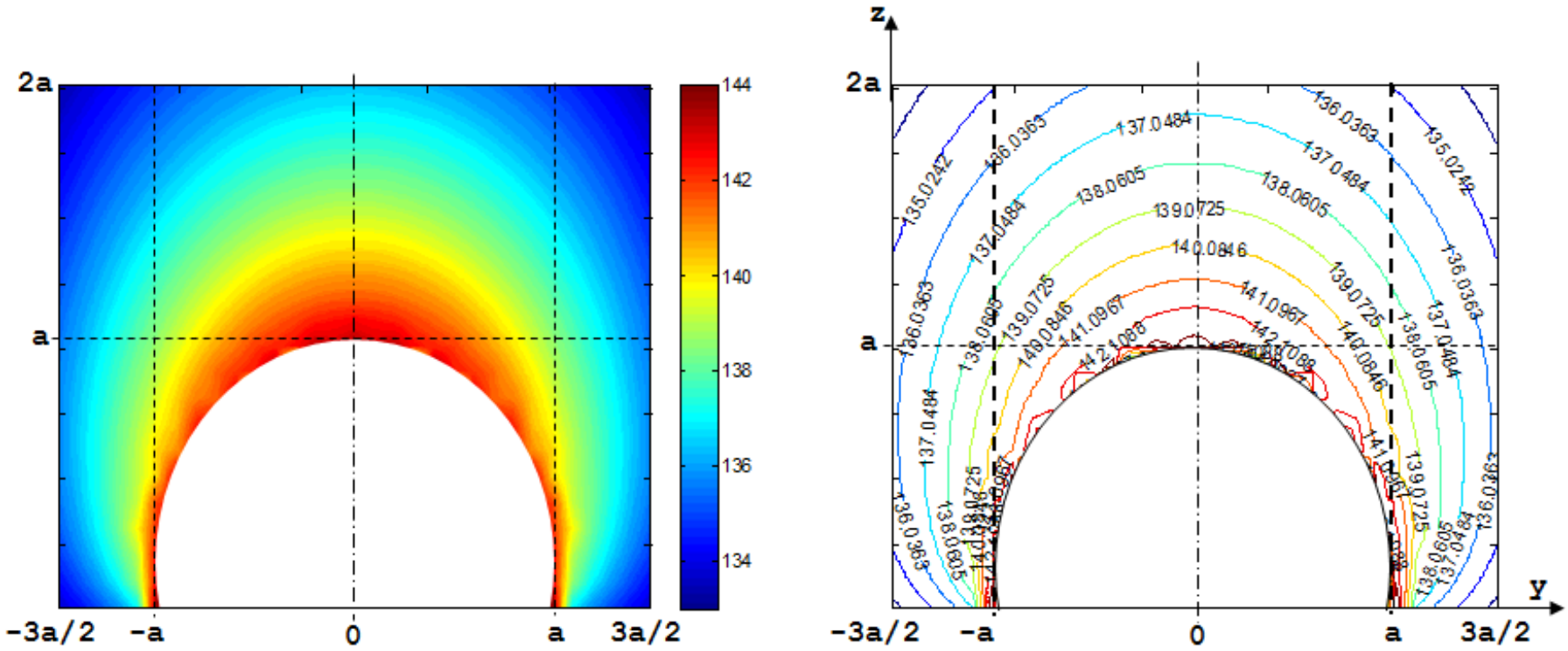

Figure 3.5 Equal pressure contours of a dilating hemisphere sitting on an anechoic infinite surface, at the $x = 0$ plane ($\alpha = 1$, $a = 1$m).

CHAPTER FOUR
SOUND SOURCE CHARACTERIZATION OF A REFRIGERATOR

4.1 Introduction

As the main practical application of this thesis, sound source localization and characterization of a refrigerator was performed. On the other hand, the sound reduction effect of an absorbent material placed under the refrigerator was examined. Therefore, the analyses were accomplished for two cases: the refrigerator is sitting on a rigid surface and on an impedance surface. These problems constitute an application of the half-space contact case as displayed in Figure 4.1. The determination of the surface and exterior pressures requires the surface velocities to be prescribed. For these analyses, surface velocity data of the refrigerator was obtained by vibration measurements in Sound and Vibration Laboratory. By using the velocity data, BEM was applied in order to obtain the surface and exterior pressure distributions of the refrigerator. Sound source characterization was accomplished with regard to the displayed surface velocity and pressure distributions together with field pressure distribution. Numerical results for the field pressure levels of the refrigerator sitting on both rigid and impedance surfaces were compared with sound measurements at several points.

4.2 Model Description of the Refrigerator

The refrigerator shown in Figure 4.2 is of energy class A; has two lids and dimensions of 690 mm x 710 mm x 1875 mm. As schematized in Figure 4.1, it has symmetry with respect to the central $x-z$ plane. For the BEM analysis, the refrigerator surface was discretized into 192 quadrilateral isoparametric elements with 578 nodes. As demonstrated in Figure 4.3, the width and length of each side surface were divided into 4 and 10 pieces, respectively. Meanwhile, both the width and length of the top and bottom surfaces were divided into 4 pieces. As a result of these, each of the side surfaces has 40 elements with 149 nodes whereas each of the top and bottom surfaces has 16 elements with 65 nodes. Due to the half-space contact

algorithm, 16 elements and 33 nodes at the bottom surface were regarded as “dummy” for which no acoustical variables were specified. Figure 4.4 shows the lay-out of the half-space contact boundary element model of the refrigerator. As mentioned in Chapter 3, as a necessity of the BEM solution the data concerning nodal co-ordinate and incidence matrices were fed to the computer. These matrices for the refrigerator are introduced in Appendix D (Tables D.1 and D.2).

4.3 Surface Velocity Measurements of the Refrigerator

As input for the computer code, surface velocities of the refrigerator were measured by a simple vibration system presented in Figure 4.5. The vibration test system consisted of a vibration meter, a tunable band-pass filter, an accelerometer and a data-logger. Measurements were performed with respect to ISO 8187:1991 standard that dictates characteristics and test methods of refrigerators. According to this standard the following conditions should be satisfied during the measurements:

- All shelves in the refrigerator should be fixed.
- The internal temperature of the refrigerator should be 5 ºC ± 2 ºC.
- The temperature of the medium should be 22 ºC ± 3 ºC while the relative humidity and the atmospheric pressure should be 50 % ± 20 % and 96 kPA ± 10 kPa, respectively.

The surface velocity measurements were accomplished at the optimal operation condition of the refrigerator “med-med”. The measurements of the internal temperature of the refrigerator were performed by using two thermocouples with a weight of 10 gr. The variation of the internal temperature with time illustrated in Figure 4.6 was obtained from the data-logger. Figure 4.6 also presents the operation condition of the compressor. All the surface velocity measurements should be performed while the compressor and fan of the refrigerator are running. Figure 4.6 shows that the time interval where both compressor is running and the internal temperature is within 3 ºC - 7 ºC range is the filled region. Therefore, measurements were accomplished when the refrigerator is running at this mode.

The frequency analysis was performed by setting the filter to 1/3 octave band center frequencies when the accelerometer was placed on the rectangular meshes drawn on the surface panels of the refrigerator. In this analysis, 50 Hz and 100 Hz were determined as the dominant frequencies. Therefore, the surface velocity distribution on each side surface and top surface of the refrigerator was examined at these two resonance frequencies. Consequently, the gathered velocity data of the nodes was fed to the computer for the acoustic surface pressures of the refrigerator to be computed. The velocity data for both 50 Hz and 100 Hz frequencies are given in Appendix D (Tables D.3 and D.4).

4.4 Sound Source Characterization of the Refrigerator

In order to perform sound source localization of the refrigerator, the first step is the examination of the surface velocity distribution. Measured velocity distribution of the refrigerator was presented on the model lay-out in Figure 4.7 for both 50 Hz and 100 Hz frequencies.

As seen in Figure 4.7, vibrations at 50 Hz are more critical than the vibrations at 100 Hz. Higher velocities on top-front and top-rear regions imply vibrations of fan and air-circulation due to the fan blades. Higher velocities on bottom-rear region indicate compressor surface vibrations. The reasons of panel vibrations are:

- Transmission of compressor vibrations by joints fixing the compressor to the refrigerator chassis at both 50 Hz and 100 Hz.
- Vibration of the cooler grid at 100 Hz.
- The effect of fan at both 50 Hz and 100 Hz.

The second step of sound source localization of the refrigerator is the determination of the surface and exterior sound pressure distributions. In the solution process, 16 Gaussian points were used for the numerical integration of each element.

The surface and exterior sound pressure distributions were acquired for the following two cases:

- when the refrigerator is in contact with a rigid surface that has a sound absorption coefficient of $\alpha = 0$,
- when the refrigerator is in contact with an impedance surface that has a sound absorption coefficient of $\alpha = 0.30$.

4.4.1 Rigid Surface

In this case, the refrigerator sits on the floor. Since the floor does not have any absorbent characteristic, it is rigid. Therefore, the surface and field pressure distributions of the refrigerator were calculated for the case $\alpha = 0$ for both 50 Hz and 100 Hz frequencies.

The surface pressure distribution of the refrigerator is demonstrated in Figure 4.8.a for 50 Hz and in Figure 4.8.b for 100 Hz. As seen from Figure 4.8 the compressor dominates the sound radiation on the rear side for both of the two frequencies. Moreover, compressor vibrations do not only cause higher surface pressures on the rear side, but also influence the other sides. This situation can be explained by the coupling phenomena leading to structure-structure and structure-acoustic interactions. Although the coupling phenomenon is observed at both of the two frequencies, it is more obvious at 100 Hz, despite lower pressure levels. Furthermore, cooler grid placed at the rear of the refrigerator is affected by the vibrations of the compressor and fan at 100 Hz. Therefore, it behaves as if a planar sound source.

Equal pressure contours of the refrigerator at the horizontal cross-section through the compressor are displayed in Figures 4.9 and 4.10 for 50 Hz and 100 Hz, respectively. The influence of the compressor vibrations on the other sides can be obviously seen in these contours. The compressor mostly affects the sound pressures

of the left side at 50 Hz and causes a more regular distribution all around the refrigerator at 100 Hz.

Sound radiation pattern of the refrigerator at the horizontal cross-section through the fan is presented in Figures 4.11 and 4.12 for 50 Hz and 100 Hz, respectively. Figure 4.11 shows that the sound radiation is almost at the same level for all sides at 50 Hz. This distribution means that the circulated air causes uniform sound radiation to all sides. Figure 4.12 implies that the radiation pattern at 100 Hz is mostly originated from the cooler grid vibrations. However, fan is also effective at this frequency and due to this effect equal pressure contours incline towards to left-front side of the refrigerator.

Consequently, displayed results expose that the compressor is the dominant sound source of the refrigerator. Furthermore, the surface and field pressures of the refrigerator is more critical at 50 Hz compared with those of 100 Hz. As a result, three main sound sources are determined for this refrigerator:

- Compressor is a point source at 50 Hz and 100 Hz.
- Fan is a point source at 50 Hz and 100 Hz.
- Cooler grid is a planar source at 100 Hz.

The field pressures around the rear side of the refrigerator were also computed and presented in Figures 4.13 and 4.14 for 50 Hz and 100 Hz, respectively. Equal pressure contours show a symmetrical sound radiation with respect to the central axis.

4.4.2 Impedance Surface

In this case, it is assumed as the refrigerator sits on an impedance surface with a sound absorption coefficient of $\alpha = 0.30$ for both 50 Hz and 100 Hz frequencies. In order to examine the sound absorption effect of the impedance surface, previous analyses for rigid floor were repeated.

The surface pressure distribution of the refrigerator for this case is demonstrated in Figure 4.15. Figures 4.16 and 4.17 display equal pressure contours of the refrigerator at the horizontal cross-section through the compressor for 50 Hz and 100 Hz, respectively. Sound radiation patterns of the refrigerator at the horizontal cross-section through the fan are shown in Figures 4.18 and 4.19 for 50 Hz and 100 Hz, respectively. Finally, Figures 4.20 and 4.21 present the field pressures around the rear side of the refrigerator for 50 Hz and 100 Hz, respectively.

Comparison of Figures 4.15-4.21 with Figures 4.8-4.14 shows that the surface pressure and field pressure patterns of the refrigerator are not affected by the impedance surface. However, a light decrease arises especially in the field pressure levels.

4.5 Sound Measurements of the Refrigerator

In the present work, sound measurements of the refrigerator were performed at several field points and results were compared with the boundary element solutions introduced in the previous section.

Sound measurements were accomplished by a Type 1 sound level meter. Measurements were performed with respect to ISO 8187:1991 standard which was introduced in Section 4.3. Field pressures of the refrigerator were obtained for the following two cases:

- when the refrigerator is in contact with a rigid surface,
- when the refrigerator is in contact with an impedance surface.

4.5.1 Rigid Surface

In this case, sound measurements were performed from the rear side of the refrigerator when the refrigerator was sitting on the floor as seen in Figure 4.22.

Background noise level was measured as 41.4 dB at 50 Hz and 35.9 dB at 100 Hz. The measurements were accomplished for two different height;

- corresponding to the middle of the refrigerator ($z = 0$),
- 580 mm above the floor ($z = -357.5\,\text{mm}$)

and at four different distance;

- 500 mm apart from the rear side of the refrigerator ($x = -845\,\text{mm}$),
- 700 mm (one characteristic length) apart from the rear side of the refrigerator ($x = -1045\,\text{mm}$),
- 1000 mm apart from the rear side of the refrigerator ($x = -1345\,\text{mm}$),
- 1400 mm (two characteristic lengths) apart from the rear side of the refrigerator ($x = -1745\,\text{mm}$).

Results of the measurements and BEM are compared in Tables 4.1 and 4.2 for 50 Hz and 100 Hz, respectively. In the measurements there is almost at least 10 dB difference between the sound pressure levels of the refrigerator and the background noise for both 50 Hz and 100 Hz frequencies.

Table 4.1 Comparison of sound pressure levels of the refrigerator at 50 Hz ($\alpha = 0$)

x (mm)	y (mm)	z (mm)	BEM (dB)	Measurement (dB)
-845	0	0	40.7	55.3
-1045	0	0	39.6	53.1
-1345	0	0	38.2	52.9
-1745	0	0	36.7	51.3
-845	0	-357.5	41.7	55.6
-1045	0	-357.5	40.5	54.5
-1345	0	-357.5	39.0	53.4
-1745	0	-357.5	37.3	53.0

In Figures 4.23 and 4.24 sound pressure levels at $z = 0$, $y = 0$ and different x distances obtained via BEM are compared with measurements for 50 Hz and 100 Hz, respectively. Figures 4.25 and 4.26 show the comparison of sound pressure levels

calculated via BEM with measurements at $z = -357.5$ mm, $y = 0$ and different x distances for 50 Hz and 100 Hz, respectively.

Table 4.2 Comparison of sound pressure levels of the refrigerator at 100 Hz ($\alpha = 0$)

x (mm)	y (mm)	z (mm)	BEM (dB)	Measurement (dB)
-845	0	0	31.4	49.2
-1045	0	0	30.4	46.5
-1345	0	0	29.2	45.3
-1745	0	0	28.1	46.3
-845	0	-357.5	32.7	47.3
-1045	0	-357.5	31.9	45.9
-1745	0	-357.5	29.6	45.6

It is seen in Tables 4.1, 4.2 and Figures 4.23-4.26, as getting closer to the floor the sound pressure levels increase. This situation is the evidence of that the compressor is the dominant sound source of the refrigerator. On the other hand, sound pressure levels decrease as getting further from the refrigerator. BEM results obey these two realities strictly whereas measurements disobey in some cases. Additionally, all comparisons show very higher values of measurements than BEM solutions. The differences tend to increase toward further distances. The main reasons of these differences may be;

- The variation of the refrigerator's working status.
- Effect of reflecting surfaces around. The perfect free field condition couldn't be satisfied.
- Effect of background noise during the measurements.

As a result, it is seen that sound measurements have been affected highly by the environmental conditions. This is due to the facts that the refrigerator has comparatively low sound levels and also has large dimensions. Low sound property causes it to be affected by the background noise. On the other hand, due to its large dimensions, its far field is very distant where reflection effects dominate. For precise measurements, large anechoic chambers are required. The cost of construction such a chamber is very high. Therefore, numerical solution is more advantageous for many

practical cases. As it is shown, BEM is a powerful technique for sound source identification and characterization; and may be confidentially used.

4.5.2 Impedance Surface

In this case sound measurements were performed from the rear side of the refrigerator when the refrigerator was sitting on glass wool as seen in Figure 4.27. Technical properties of the glass wool used in the measurements are given in Table 4.3.

Table 4.3 Technical properties of the glass wool

Thickness (cm)	**Width x Length (cm)**	**Frequency (Hz)**	**Sound Absorption Coefficient (α)**
5	60 x 120	125	0.30

Background noise level was measured as 35.9 dB at 100 Hz. The measurements were performed for 580 mm above the impedance surface ($z = -357.5\,\text{mm}$) and at the four distances as in the rigid surface case.

Sound absorption coefficient of the used glass wool has been declared as $\alpha = 0.30$ at 125 Hz. Since the refrigerator has a critical frequency at 100 Hz, the BEM solution was performed at this frequency with $\alpha = 0.30$. The glass wool has no absorption for lower frequencies as many of the sound absorbent materials. Therefore, measurement and BEM comparisons could be made only for 100 Hz as shown in Table 4.4. In the measurements almost at least 10 dB difference between the refrigerator's sound and the background noise was satisfied.

Table 4.4 Comparison of sound pressure levels of the refrigerator at 100 Hz ($\alpha = 0.30$)

x (mm)	**y (mm)**	**z (mm)**	**BEM (dB)**	**Measurement (dB)**
-845	0	-357.5	32.5	46.3
-1045	0	-357.5	31.5	45.7
-1345	0	-357.5	30.4	46.9
-1745	0	-357.5	29.1	46.0

Figure 4.28 displays the comparison of sound pressure levels obtained via BEM with sound measurements. There is again quite large differences between two sets of results and these differences tend to increase toward further distances as in the case of rigid surface. Because, the measurement results loose their consistency towards further distances due to the reflection effects whereas BEM solutions are always conformable. On the other hand, comparison of Table 4.2 with Table 4.4 or Figure 4.26 with Figure 4.28 indicates that the sound pressure levels in latters are smaller as a result of sound absorption effect of the impedance surface. This phenomenon is more obvious for the BEM solutions. Consequently, as in the case of rigid surfaces, the BEM code for impedance surfaces in half space gives more reliable results rather than sound measurements.

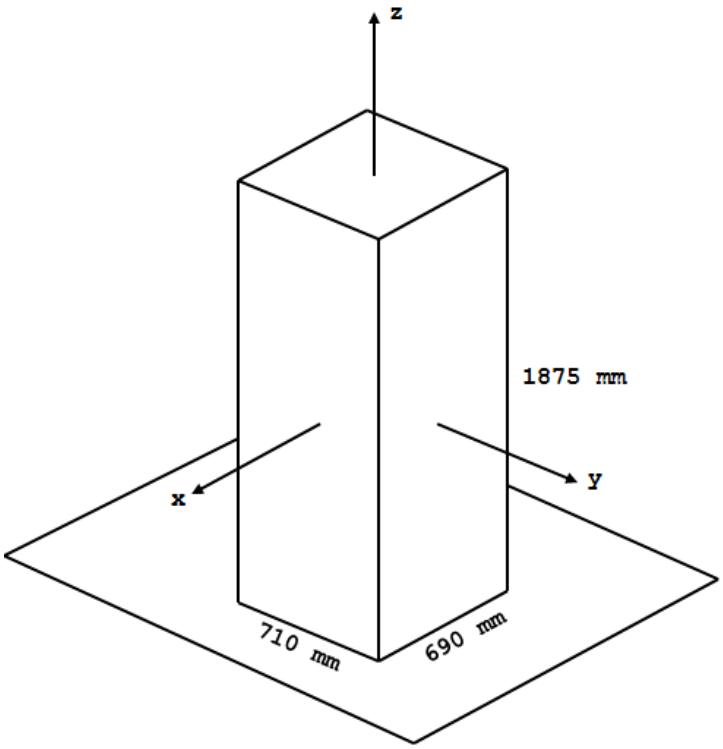

Figure 4.1 Schematic representation of the refrigerator sitting on a surface.

Figure 4.2 The tested refrigerator.

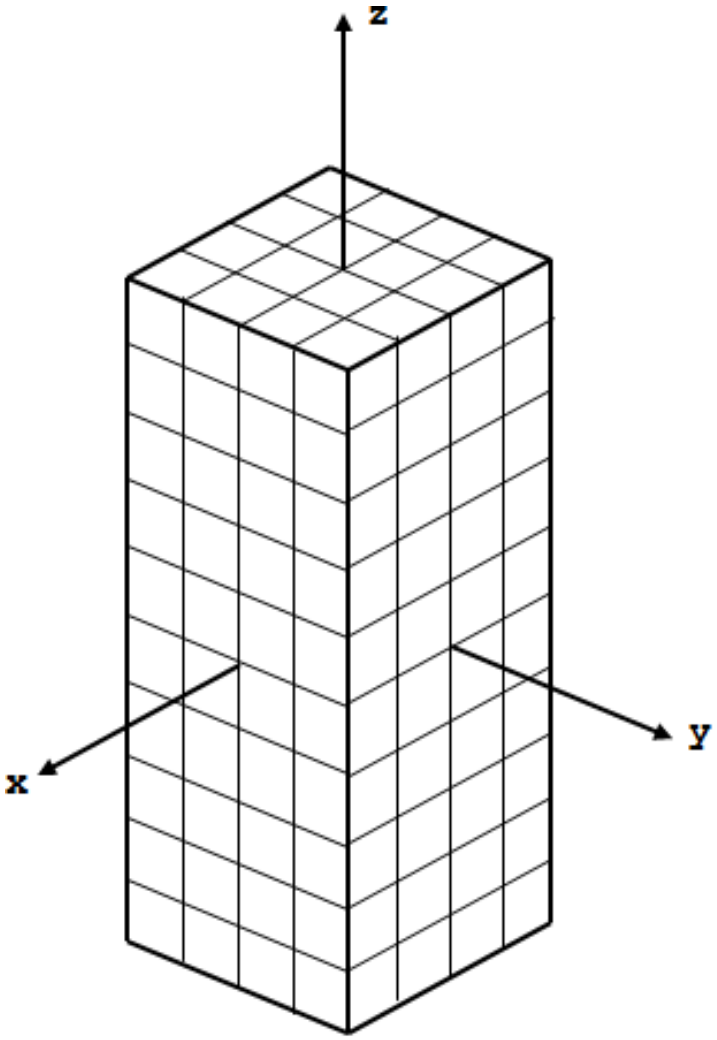

Figure 4.3 Schematic representation of the boundary element discretization of the refrigerator.

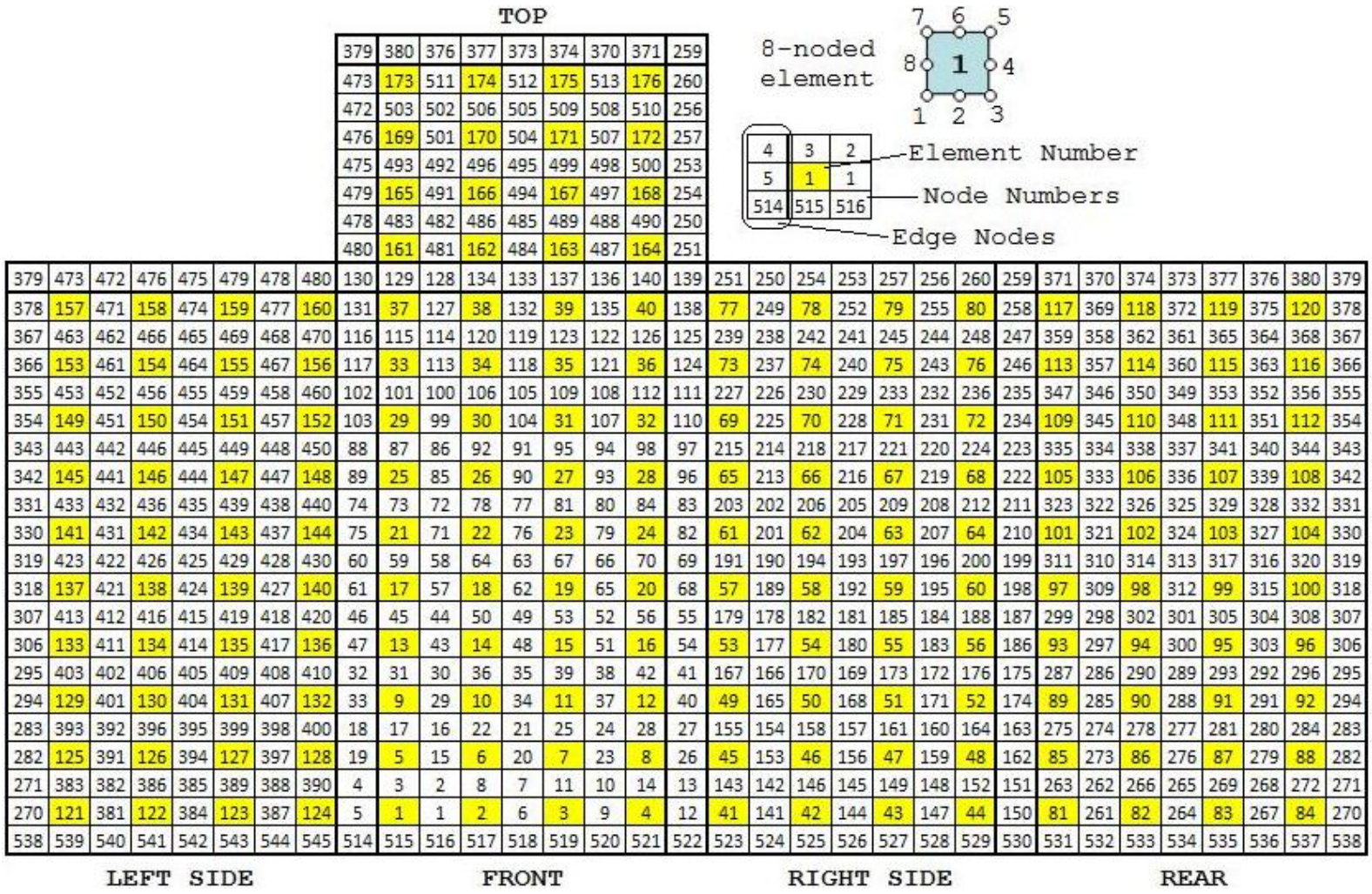

Figure 4.4 Lay-out of the boundary element model.

Figure 4.5 Surface velocity measurement system.

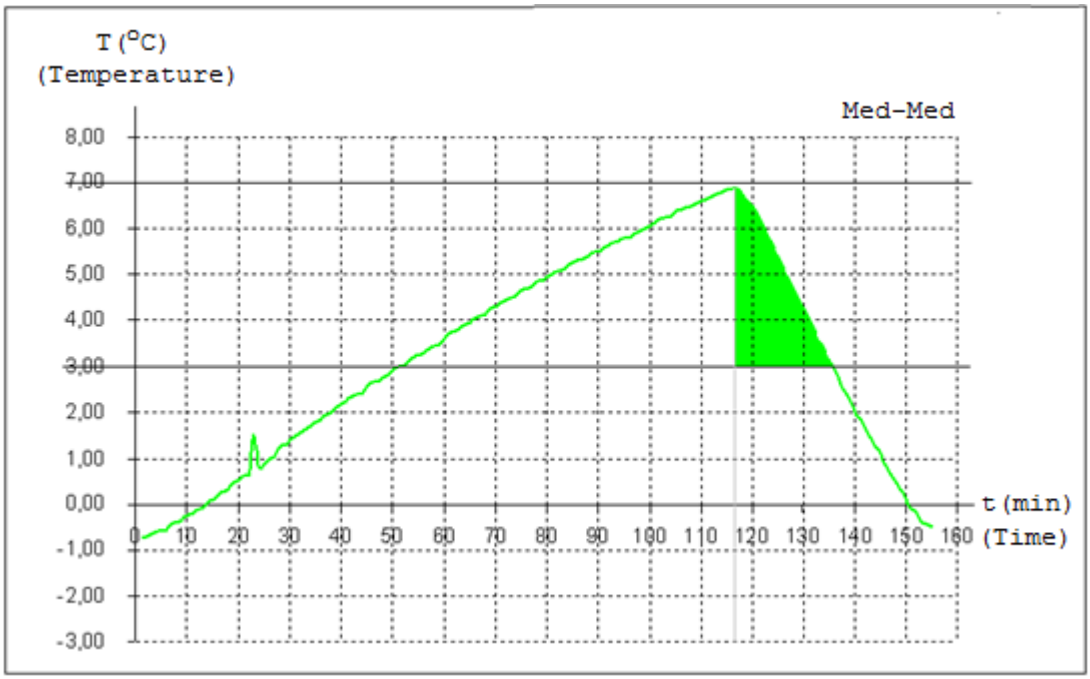

Figure 4.6 Variation of internal temperature of the refrigerator with time.

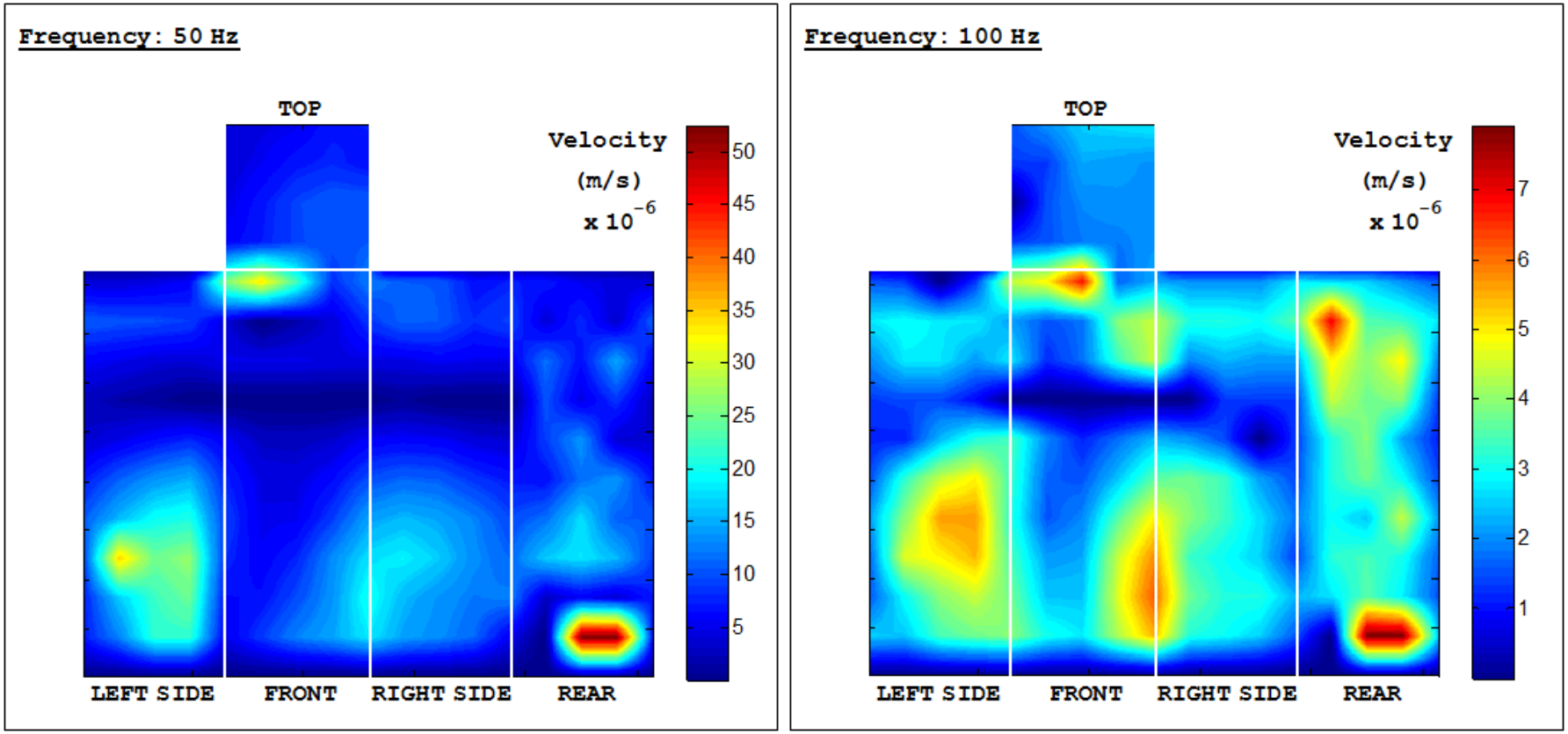

(a) **(b)**

Figure 4.7 Measured surface velocity distribution of the refrigerator a) at 50 Hz, b) at 100 Hz.

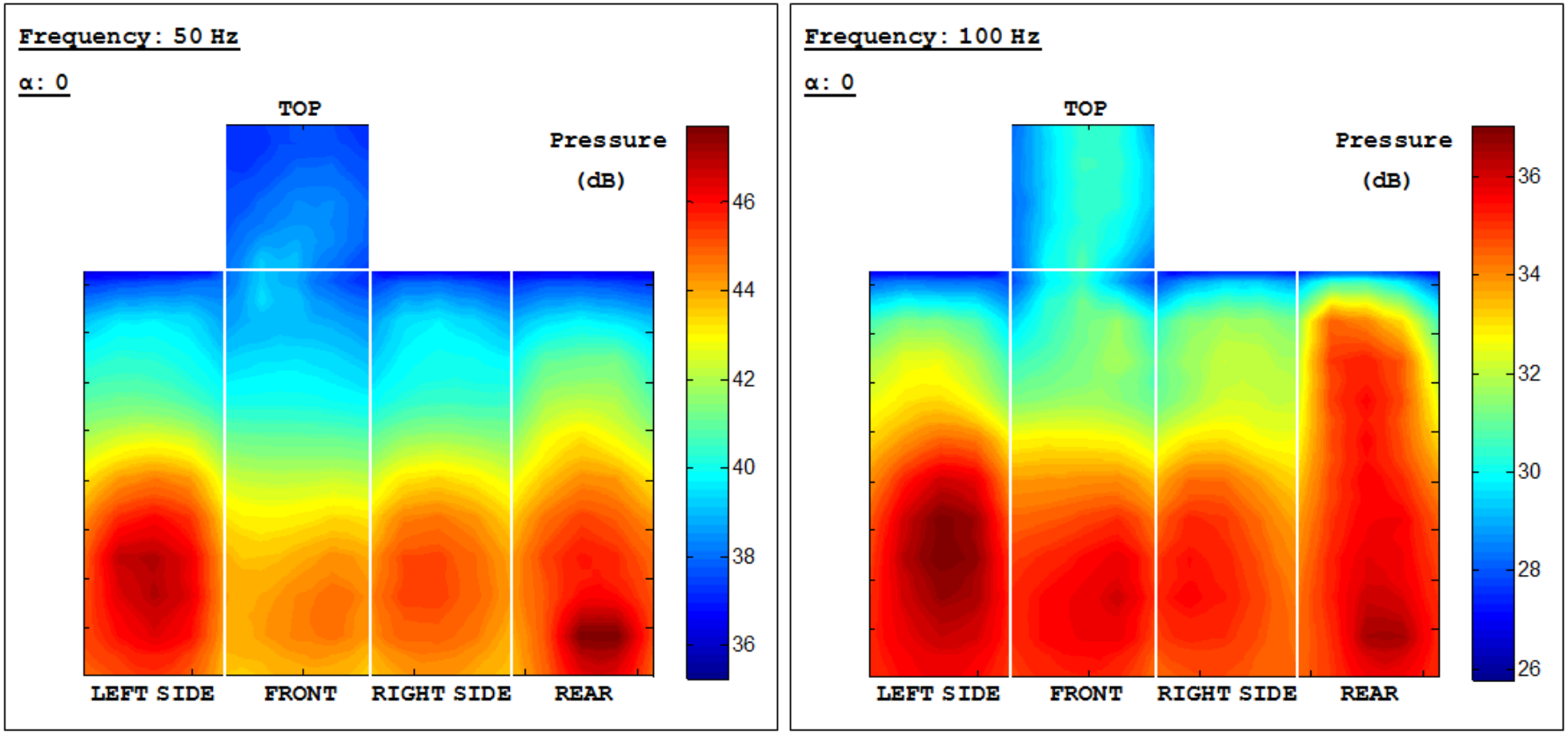

(a) **(b)**

Figure 4.8 Predicted surface pressure distribution of the refrigerator by the half-space contact BEM ($\alpha = 0$) a) at 50 Hz, b) at 100 Hz.

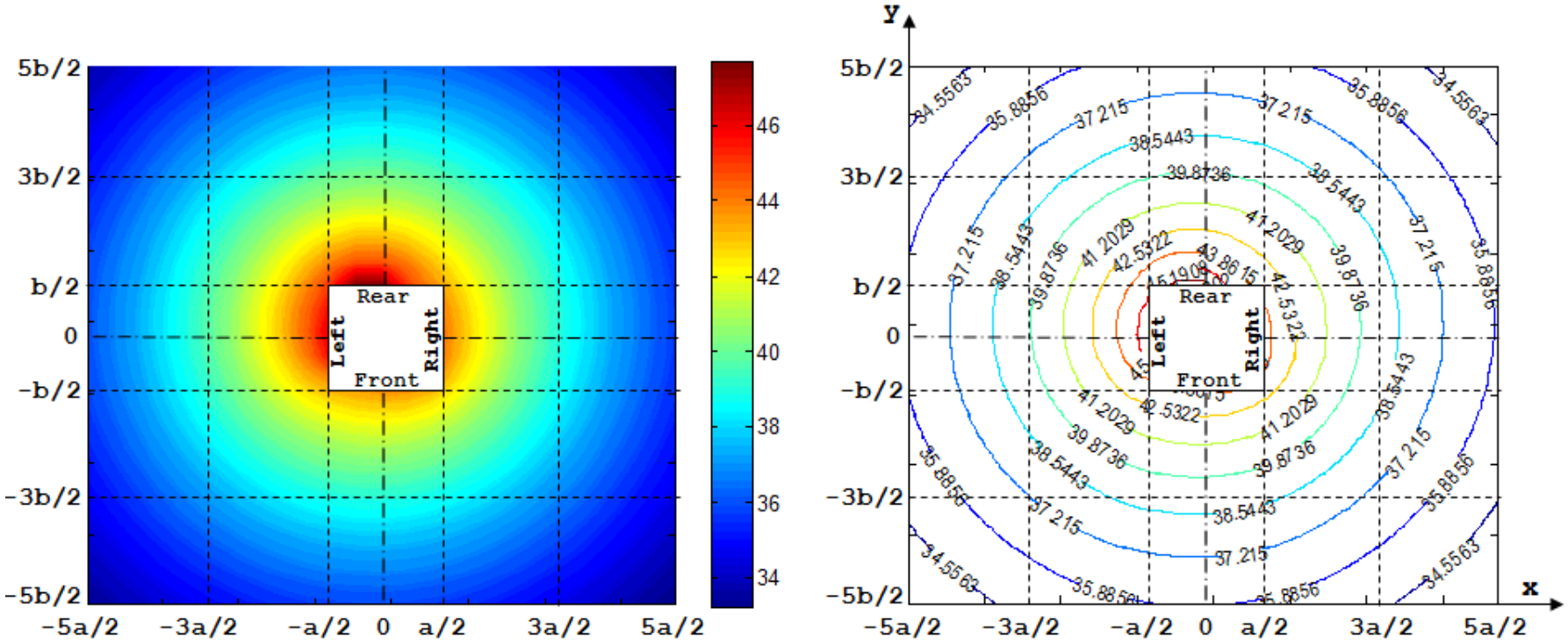

Figure 4.9 Equal pressure contours of the refrigerator at the horizontal cross-section through the compressor for 50 Hz ($\alpha = 0$, $a = 710$ mm, $b = 690$ mm).

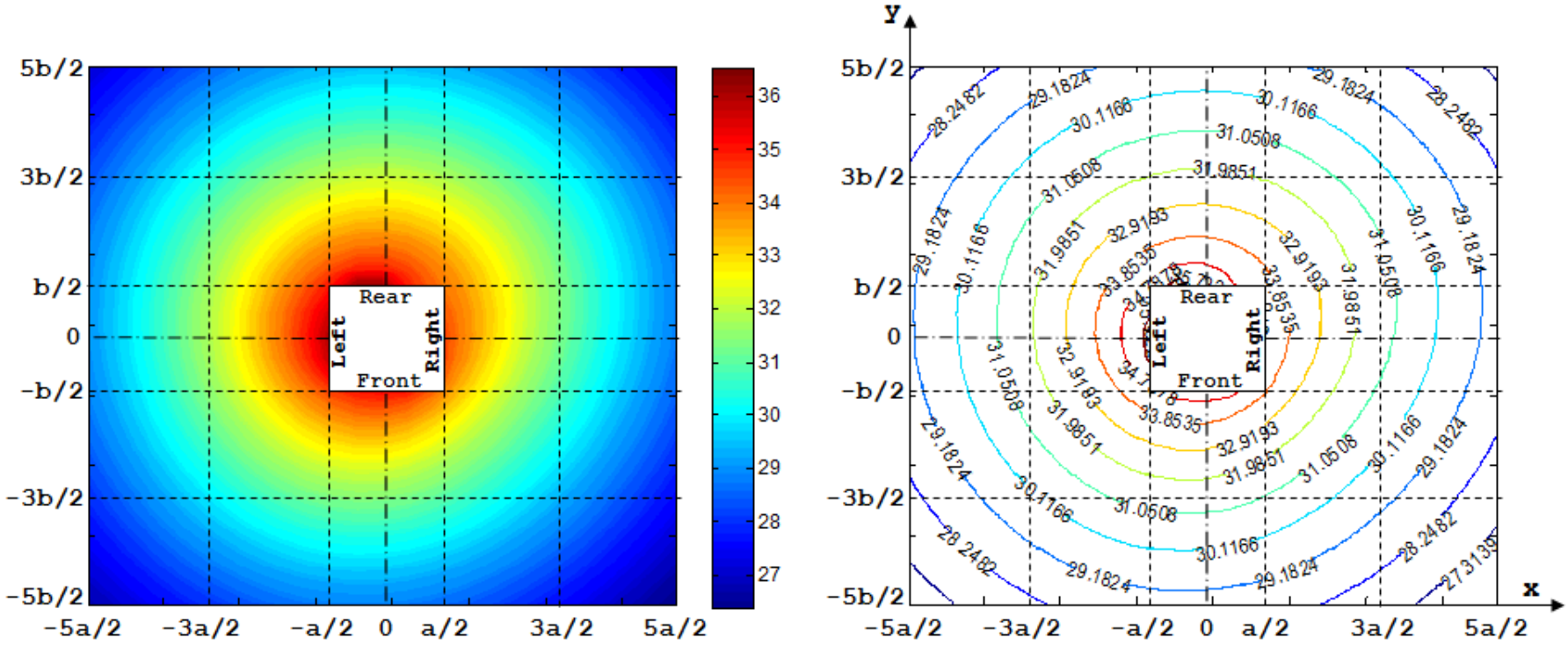

Figure 4.10 Equal pressure contours of the refrigerator at the horizontal cross-section through the compressor for 100 Hz ($\alpha = 0$, $a = 710$ mm, $b = 690$ mm).

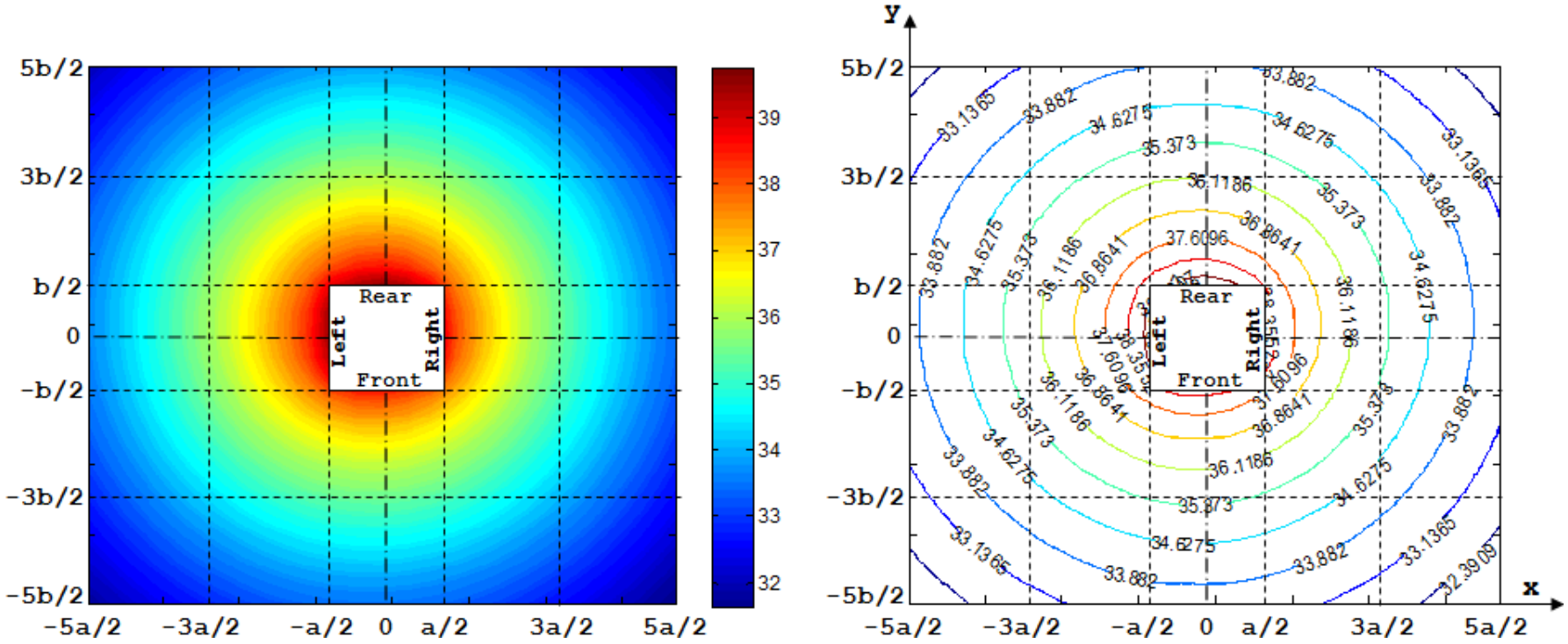

Figure 4.11 Equal pressure contours of the refrigerator at the horizontal cross-section through the fan for 50 Hz ($\alpha = 0$, $a = 710$ mm, $b = 690$ mm).

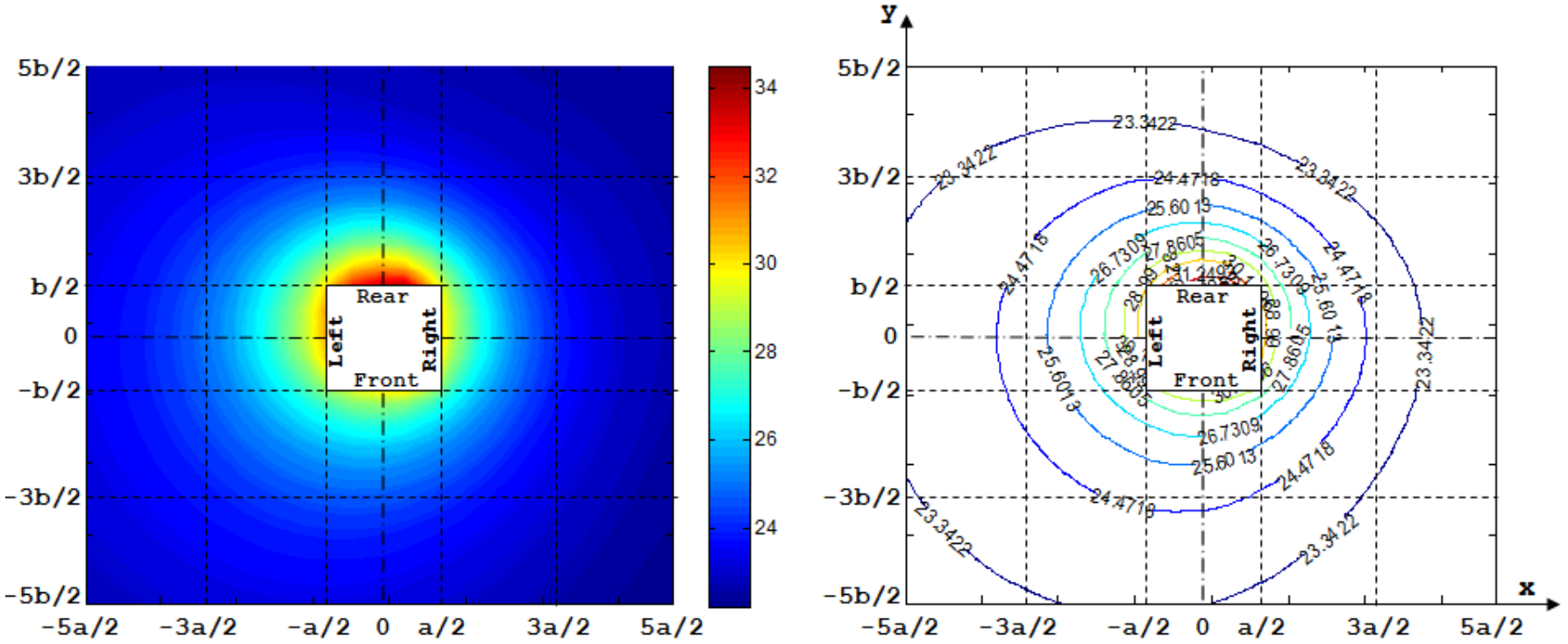

Figure 4.12 Equal pressure contours of the refrigerator at the horizontal cross-section through the fan for 100 Hz ($\alpha = 0$, $a = 710$ mm, $b = 690$ mm).

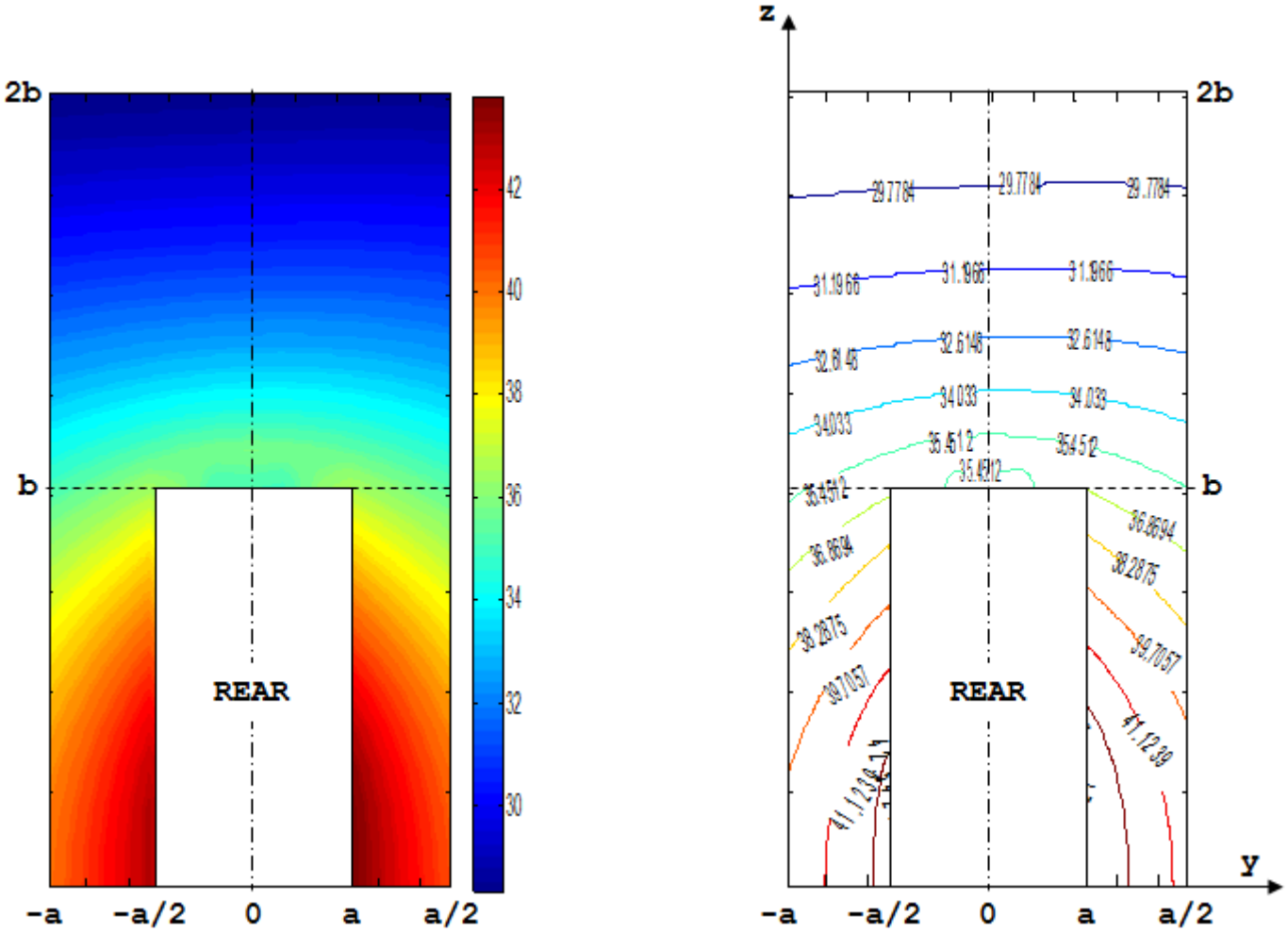

Figure 4.13 Equal pressure contours of the refrigerator at $x = -345$ mm plane for 50 Hz ($\alpha = 0$, $a = 710$ mm, $b = 1875$ mm).

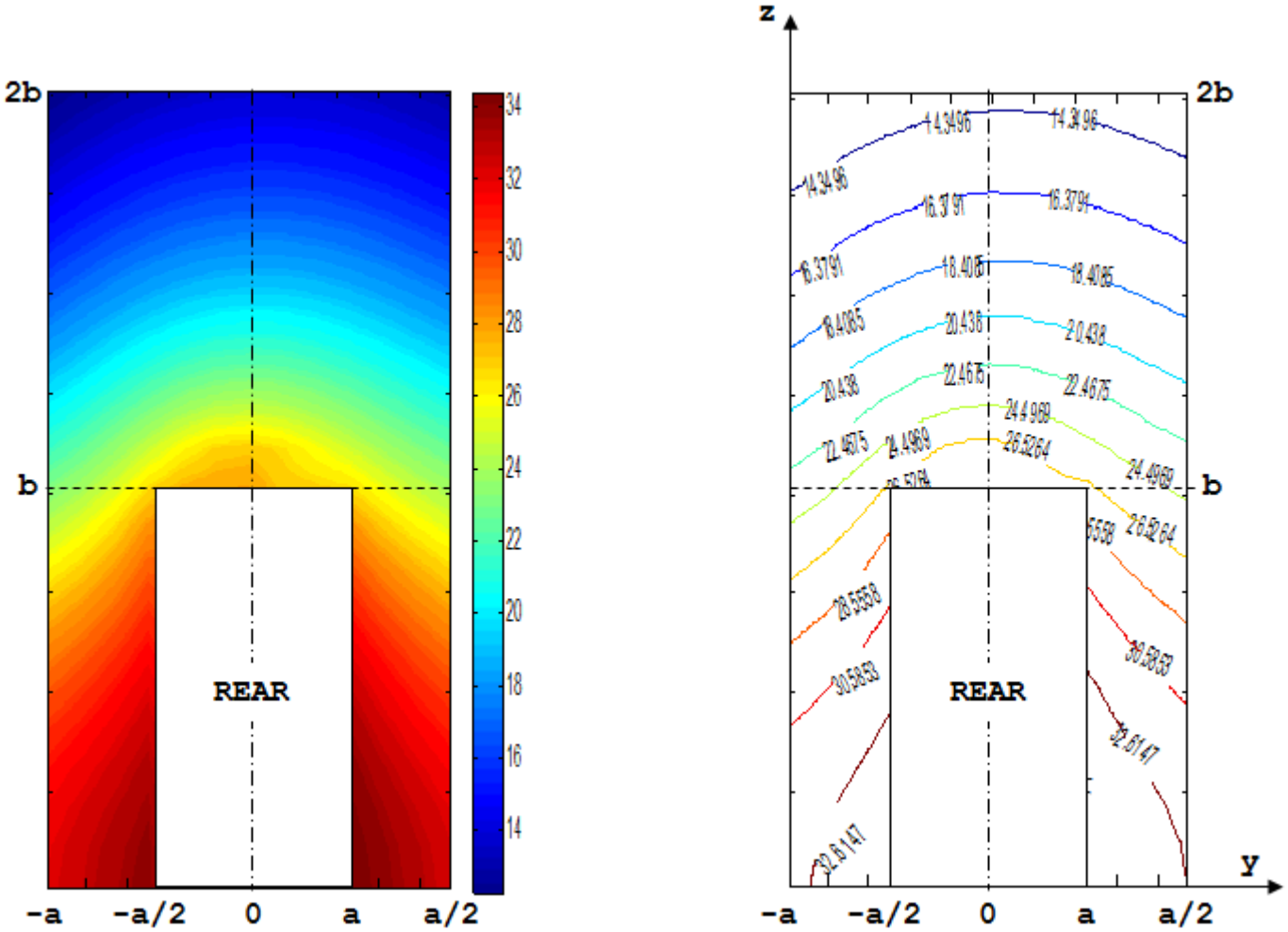

Figure 4.14 Equal pressure contours of the refrigerator at $x = -345$ mm plane for 100 Hz ($\alpha = 0$, $a = 710$ mm, $b = 1875$ mm).

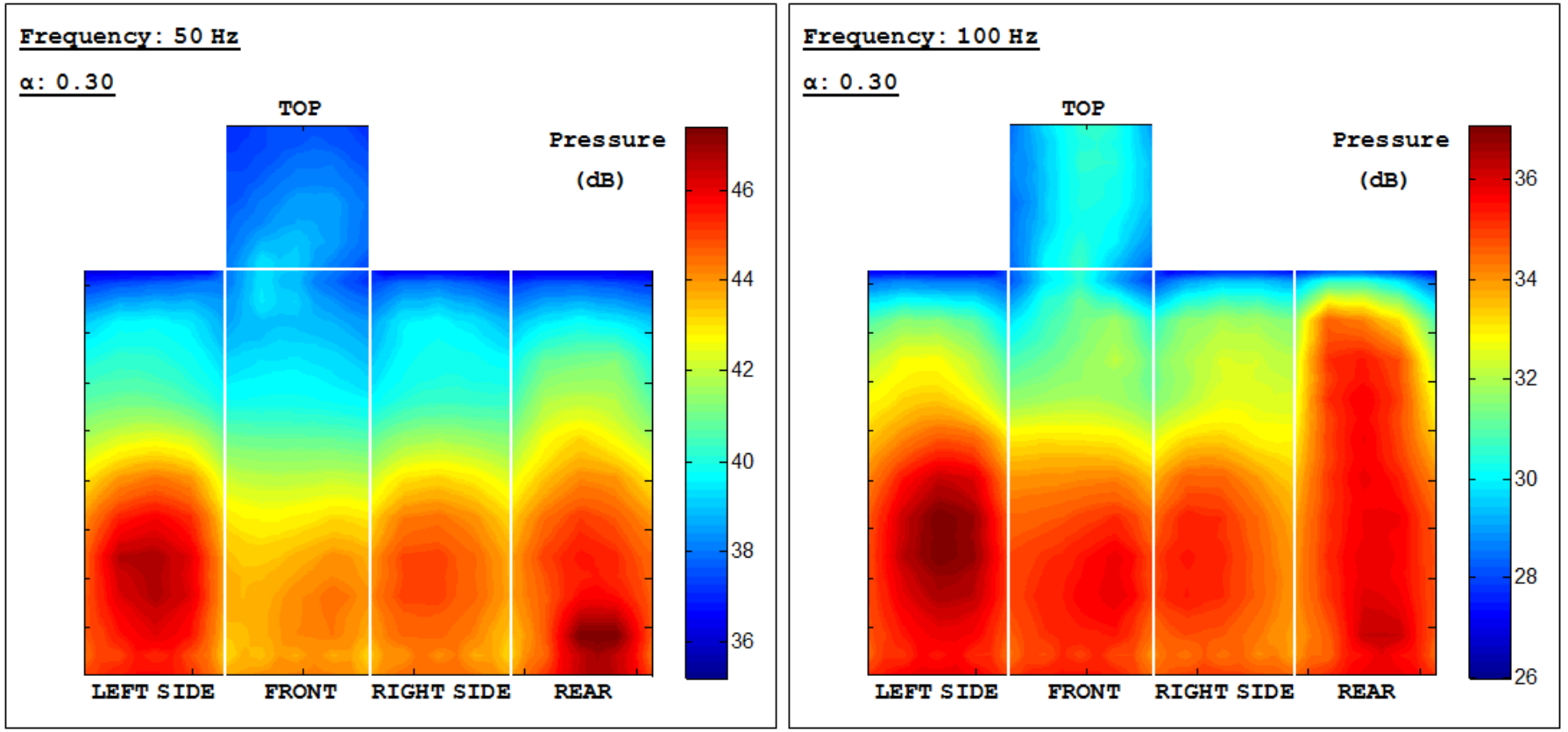

Figure 4.15 Predicted surface pressure distribution of the refrigerator by the half-space contact BEM ($\alpha = 0.30$) a) at 50 Hz, b) at 100 Hz.

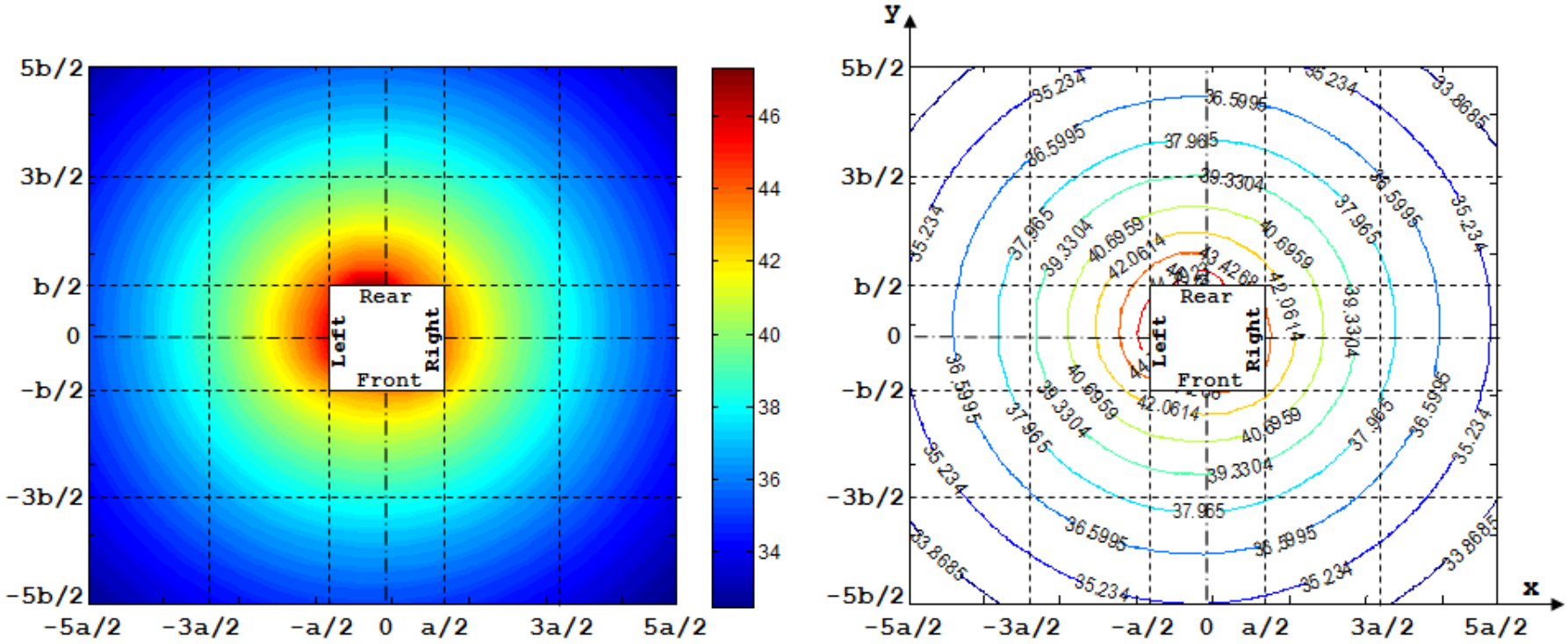

Figure 4.16 Equal pressure contours of the refrigerator at the horizontal cross-section through the compressor for 50 Hz ($\alpha = 0.30$, $a = 710$ mm, $b = 690$ mm).

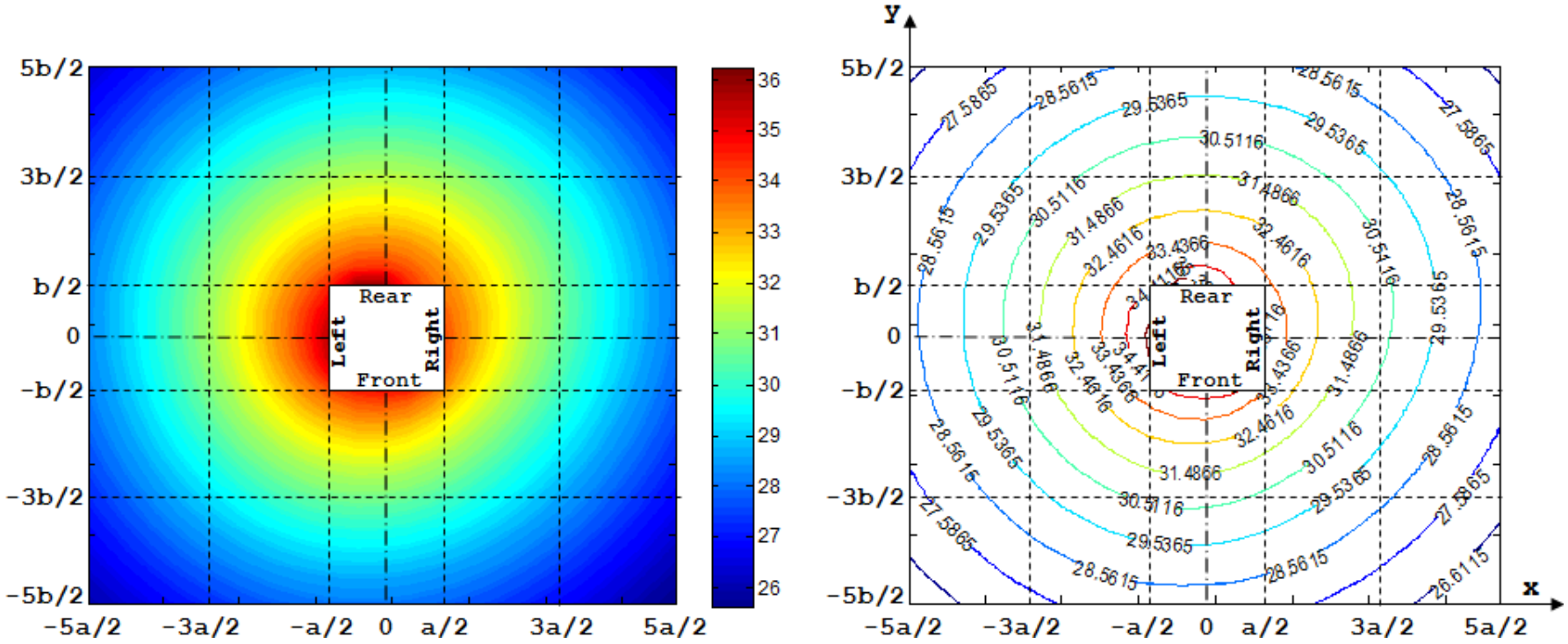

Figure 4.17 Equal pressure contours of the refrigerator at the horizontal cross-section through the compressor for 100 Hz ($\alpha = 0.30$, $a = 710\,\text{mm}$, $b = 690\,\text{mm}$).

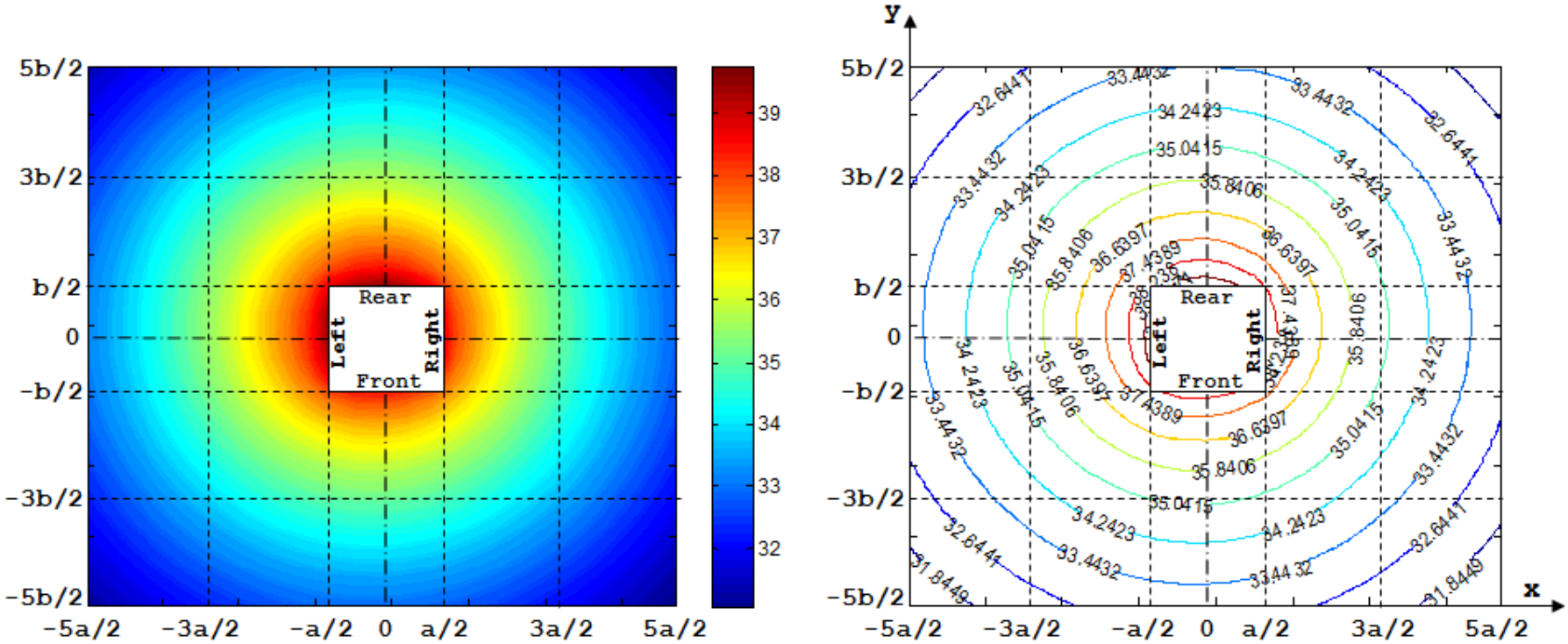

Figure 4.18 Equal pressure contours of the refrigerator at the horizontal cross-section through the fan for 50 Hz ($\alpha = 0.30$, $a = 710$ mm, $b = 690$ mm).

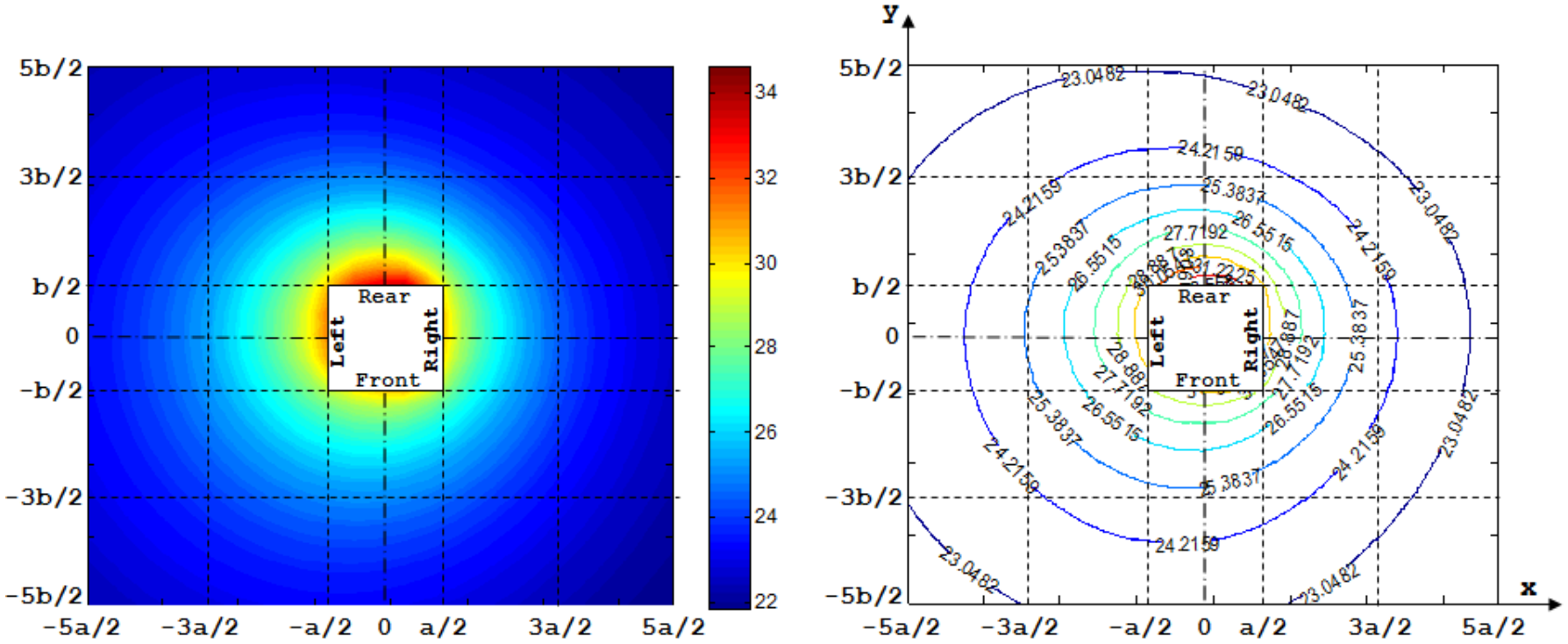

Figure 4.19 Equal pressure contours of the refrigerator at the horizontal cross-section through the fan for 100 Hz ($\alpha = 0.30$, $a = 710\,\text{mm}$, $b = 690\,\text{mm}$).

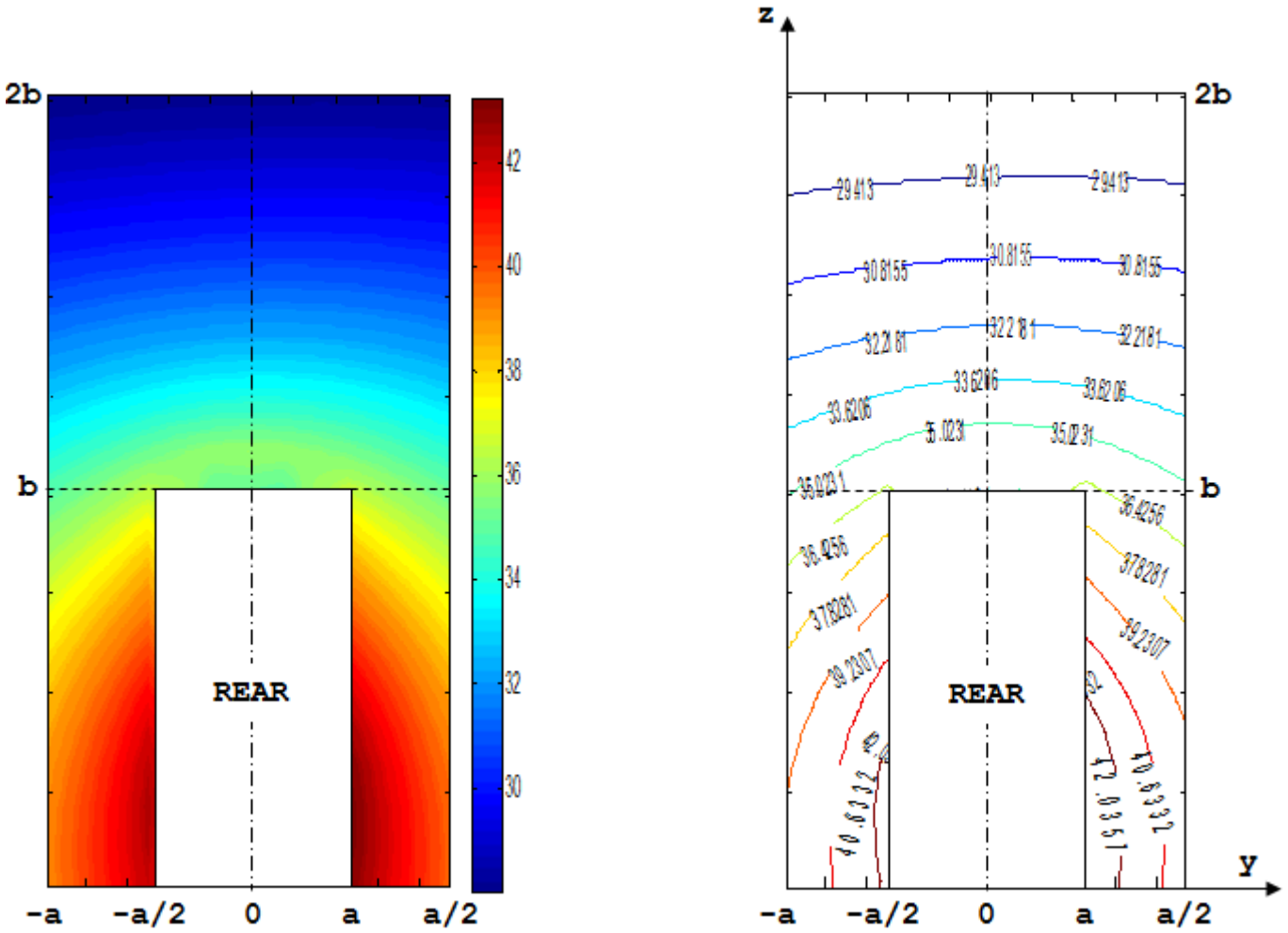

Figure 4.20 Equal pressure contours of the refrigerator at $x = -345$ mm plane for 50 Hz ($\alpha = 0.30$, $a = 710$ mm, $b = 1875$ mm).

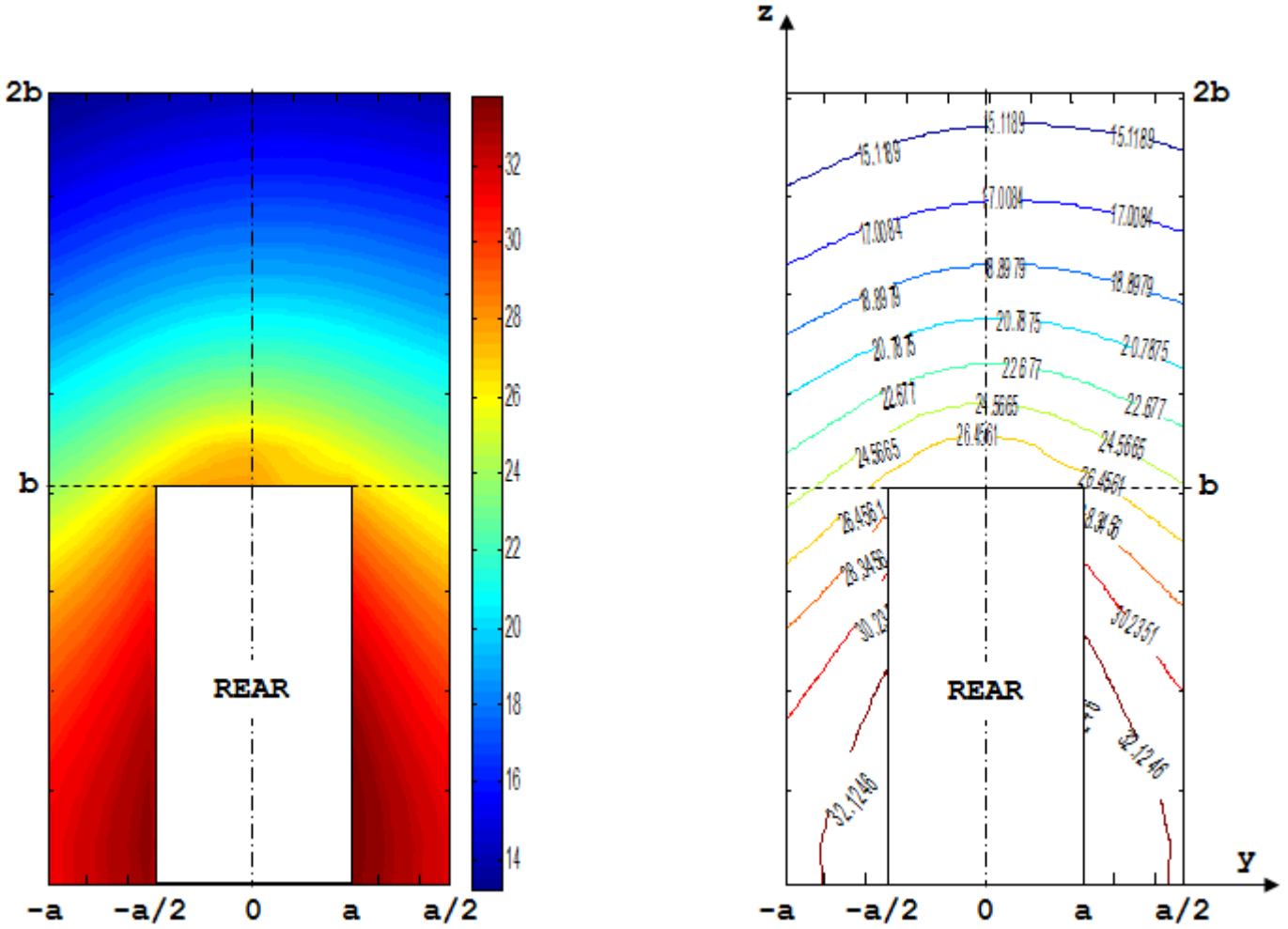

Figure 4.21 Equal pressure contours of the refrigerator at $x = -345$ mm plane for 100 Hz ($\alpha = 0.30$, $a = 710$ mm, $b = 1875$ mm).

Figure 4.22 Sound measurement when the refrigerator is sitting on the floor ($\alpha = 0$).

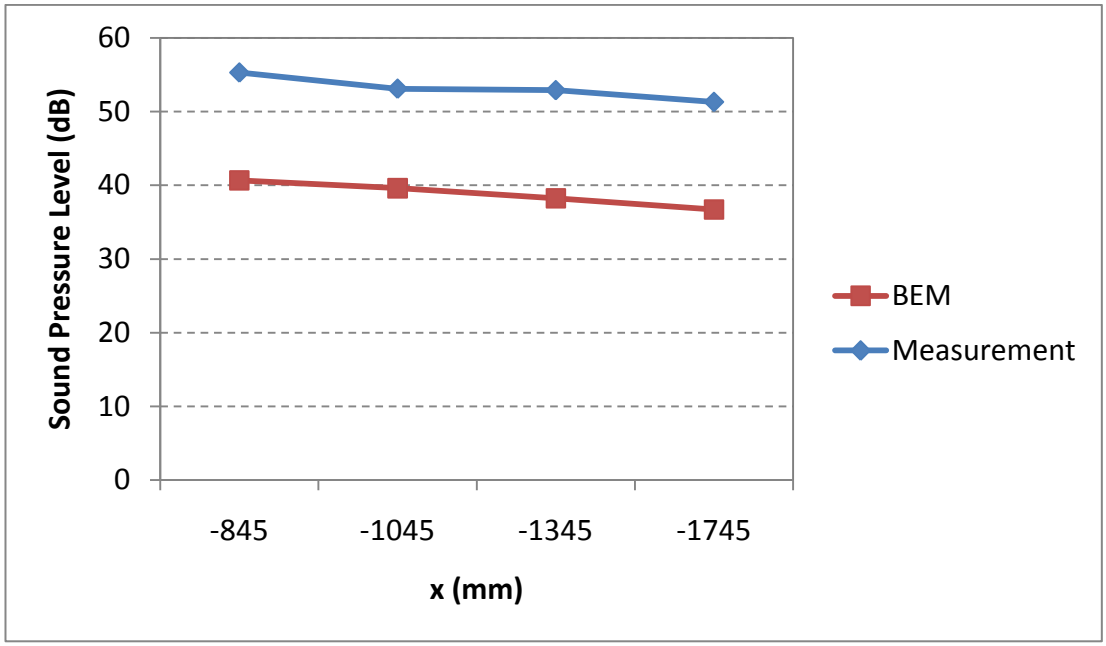

Figure 4.23 Comparison of sound pressure levels calculated via BEM with measurement results at 50 Hz ($\alpha = 0,\ y = 0,\ z = 0$).

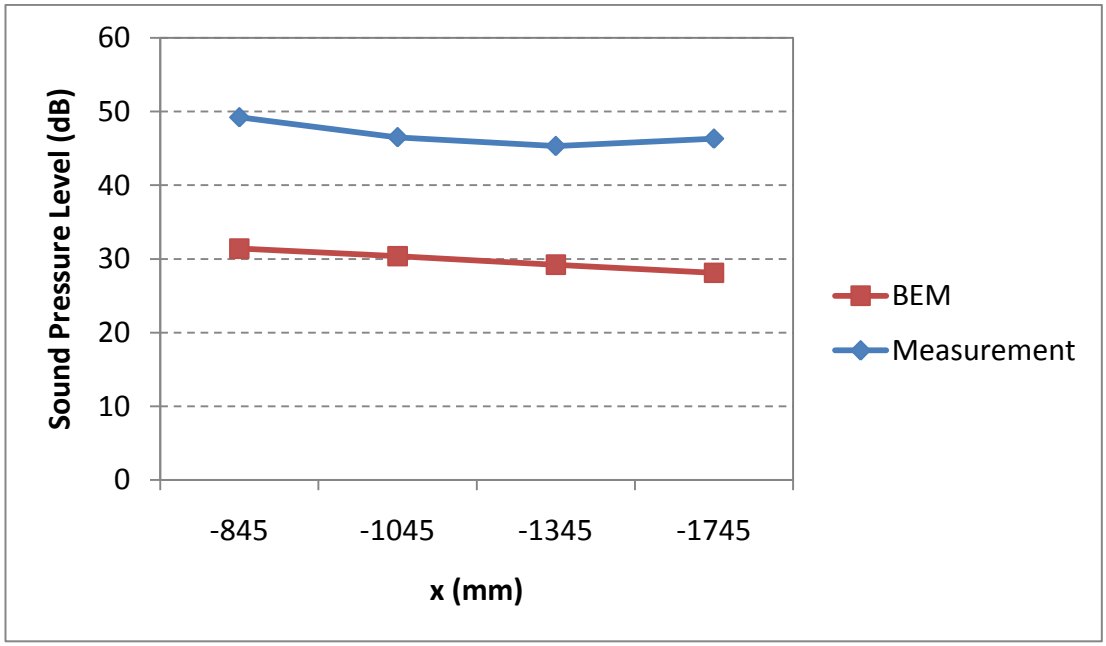

Figure 4.24 Comparison of sound pressure levels calculated via BEM with measurement results at 100 Hz ($\alpha = 0,\ y = 0,\ z = 0$).

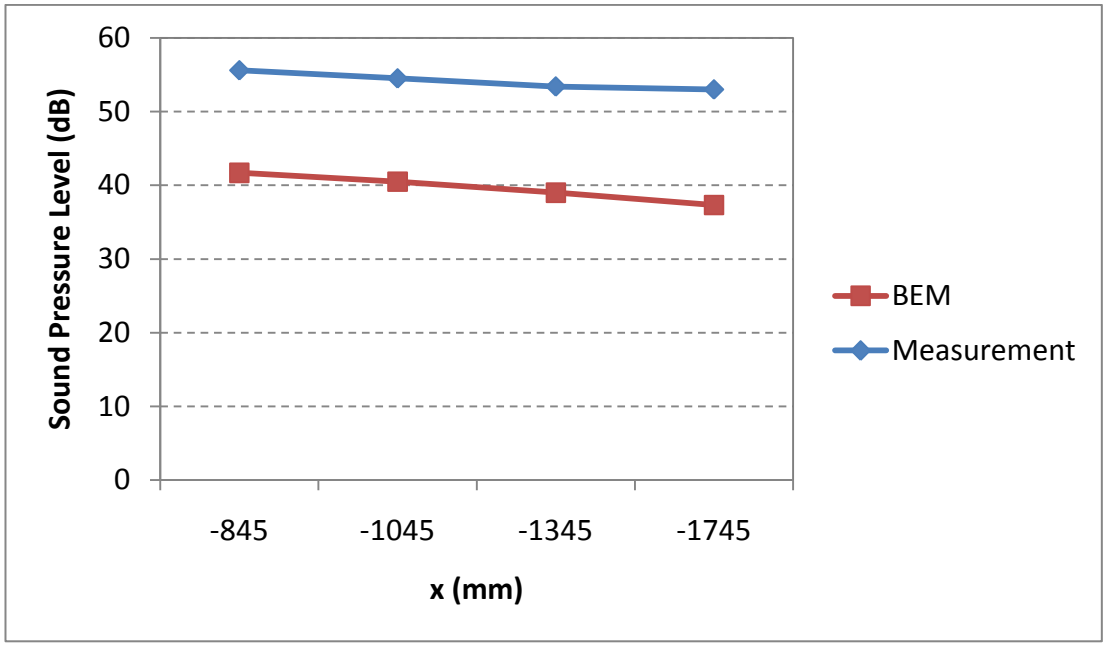

Figure 4.25 Comparison of sound pressure levels calculated via BEM with measurement results at 50 Hz ($\alpha = 0$, $y = 0$, $z = -357.5\,\text{mm}$).

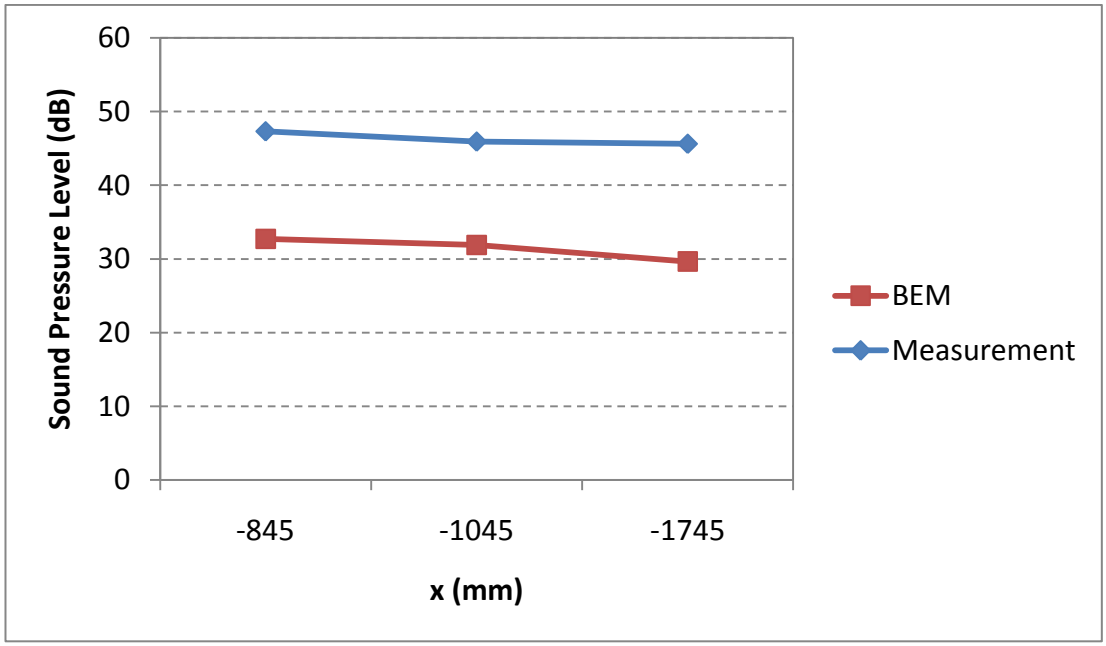

Figure 4.26 Comparison of sound pressure levels calculated via BEM with measurement results at 100 Hz ($\alpha = 0$, $y = 0$, $z = -357.5\,\text{mm}$).

Figure 4.27 Sound measurement when the refrigerator is sitting on glass wool ($\alpha = 0.30$).

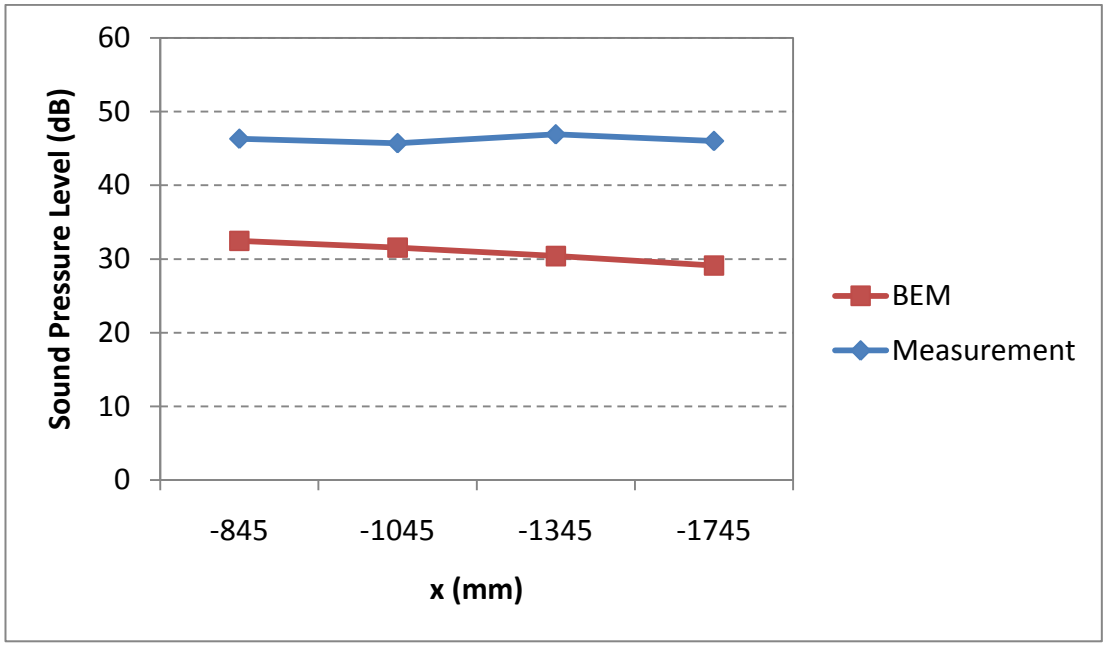

Figure 4.28 Comparison of sound pressure levels calculated via BEM with measurement results at 100 Hz ($\alpha = 0.30$, $y = 0$, $z = -357.5$ mm).

CHAPTER FIVE
EXPLANATIONS ABOUT THE COMPUTER CODE

5.1 Introduction

In the present work, a computer code, which had been written by Avşar (2000) in Visual Basic programming language, was adopted to MatLAB®. Avşar's program solves acoustic radiation problems in different sub-spaces. In the present study, only half-space algorithm was adopted, however impedance surface approach was included. The computer code named main_bem was successfully used to obtain surface and field pressures of spheres and a refrigerator in half space with rigid and impedance surfaces. The users can run this code easily without having any necessary information about the computer programming language.

5.2 Explanations about main_bem

main_bem calculates the surface and exterior field pressures of vibrating arbitrarily shaped bodies in full or half space with rigid or impedance surfaces. The acoustical information about the bodies gives the opportunity to perform sound source identification and characterization analysis.

There are basically two sub programs of main_bem; surhel and exthel, which perform the calculations and evaluate the acoustic pressures. The other sub programs prepare geometrical and velocity data to these programs.

main_bem calculates the acoustical impedance of the medium and runs the sub programs data_input, vel, av_aa, coeff, depar, corn, surhel, swrite, exdata, depar1, exthel and extwrite which are explained in the following section.

5.3 Explanations about Sub Programs

In this section, explanations about the sub programs used in the main_bem are given. Information given in parenthesis denotes the variables used in the code.

5.3.1 data_input

This program reads data of the discretized boundary element model of the vibrating body from the input file "indat.txt". The input file "indat.txt" contains:

- Wave number (kwn),
- Dimension transformation coefficient (aba),
- Number of nodes except "dummy nodes" (nod),
- Number of nodes which are not in contact with bounding surface (nod1),
- Total number of nodes (nod2),
- Total number of elements (AE),
- Number of elements except "dummy elements" (ae2),
- Number of Gaussian points on the local horizontal axis (AB),
- Number of Gaussian points on the local vertical axis (AB),
- Sound absorption coefficient of the bounding surface (alfa),
- The co-ordinates of nodes (alm),
- Incidence matrix (AI),
- The angles between the local and global co-ordinates (aci),
- The distances from the global co-ordinate's origin to the local co-ordinate's origin in directions x, y and z (dxyzb),

respectively.

5.3.2 vel

This program reads the nodal velocity data (AH) of the vibrating body from the input file "inv.txt".

5.3.3 av_aa

This program reads Gaussian weights (AV, AA) from the input file “ava.txt”.

5.3.4 coeff

This program calculates

- Gaussian weight functions A_i and A_j (AU),
- Shape functions N_α (ALtS),
- Jacobian matrix (AJ),
- The co-ordinates of Gaussian points (AF).

5.3.5 depar

This program calculates the distances (R) between the nodes and Gaussian points. In addition to this, evaluates the cosines of the angles (O) between R and n vectors.

5.3.6 corn

This program calculates the term $C(P)$, including the effect of edges and corners and adds this term to the diagonal elements of the coefficient matrix of the nodal pressure vector.

5.3.7 surhel

This program calculates the surface pressures of the vibrating body by using the surface Helmholtz integral equation and makes use of the data calculated by data_input, vel, coeff, depar and corn. The output of this program is the nodal sound pressure vector (surf_pres) in Pa.

5.3.8 swrite

This program uses the nodal sound pressure vector (surf_pres) and calculates the sound pressure levels of the nodes in dB. The output of this program is the file “surfpres.txt”. The first column in the output file is the node number whereas the second column is the sound pressure levels of the nodes.

5.3.9 exdata

This program reads the number and co-ordinates of the field points from the input file “ext_data.txt”.

5.3.10 depar1

This program calculates the distances (Rr) between the field points and Gaussian points. In addition to this, evaluates the cosines of the angles (Oo) between Rr and n vectors.

5.3.11 exthel

This program uses the surface pressures which had been calculated by surhel in the exterior Helmholtz integral and calculates the field pressures. Exthel makes use of the data calculated by data_input, vel, coeff, exdata and depar1. The output of this program is sound pressure vector (ext_pres) of the field points.

5.3.12 extwrite

This program uses sound pressure vector (ext_pres) of the field points in Pa and calculates the sound pressure levels of the field points in dB. The output of this program is the file “extpres.txt”. The first column in the output file is the node number whereas the second column is the sound pressure levels of the field points.

CHAPTER SIX
CONCLUSIONS

In the present study, an available in-house computer code solving full-space problems and half-space problems in the presence of a rigid surface has been rewritten in MatLAB®. In addition to this, a new module has been developed to solve half-space problems with an impedance surface. The code performs this task by using the boundary element method implementation of the Helmholtz integral equation. The validity of the code was tested by examining a dilating spherical source and a dilating hemispherical source by comparison of the analytical result. This code enables to obtain acoustic surface and field pressures of a vibrating body. The code is also capable of post-processing operation to display sound source localizations and providing the data to be assessed by means of sound source characterization of the vibrating bodies in half space with rigid and impedance surfaces.

A dilating sphere in full space and a hemisphere sitting on a rigid surface that forms half space were computed in order to test the accuracy of the rewritten code. Then the effect of a sound absorbent surface on the sound pressure distribution around the hemispherical source was examined. In this regard, equal pressure contours of the hemisphere were calculated and displayed for two cases. In the rigid case, since there is no sound absorbent property, the distributions of the contours are homogenous and circular. However, in the anechoic case, the circular contours tend to take elliptical shape as a consequence of vanishing reflection effect of the surface. As it is expected, in the second case, sound pressures around the hemisphere decrease due to the presence of anechoic surface. On the other hand, surface pressures of hemispheres sitting on surfaces with different sound absorption coefficients were computed. The decreasing pressures with increasing absorption coefficients indicate the validity of the recently developed module.

As the practical application of this thesis, sound source characterization of a refrigerator was performed for two cases: the refrigerator is sitting on a rigid floor

and on a glass wool which has sound absorbent property. For the determination of the surface and field pressure distributions, firstly the boundary element model of the refrigerator was developed. After that, in conformity with this model, the surface velocity data of the refrigerator was obtained by vibration measurements with respect to ISO 8187:1991 standard. During the measurements, two dominant frequencies; 50 Hz and 100 Hz for which velocities have considerable levels were determined. Therefore, the surface velocity distribution of the refrigerator was examined at these resonance frequencies and it was seen that vibration levels at 50 Hz are greater than those at 100 Hz. By feeding the gathered nodal velocity data to the computer code and by operating the BEM algorithm, the surface and exterior pressure distributions of the refrigerator were obtained for both frequencies.

Sound source localization and characterization were accomplished with regard to the displayed surface velocity and pressure distributions of the refrigerator together with the field pressure distribution around the refrigerator. Displayed results exposed that the refrigerator has three main sound sources. The compressor was determined as the dominant one vibrating as if a point source at both 50 and 100 Hz frequencies. The second sound source was detected as fan which acts as a point source at the two frequencies while the cooler grid which behaves like a planar source at 100 Hz was regarded as the third one.

On the other hand, sound measurements were performed while the refrigerator was sitting firstly on rigid floor and secondly on glass wool for comparison purposes with the BEM results. The measurements were accomplished for two different heights and at four different distances from the rear side of the refrigerator. In the measurements, it was paid attention that at least 10 dB difference to be between the measured sound pressure and the background noise levels for both 50 Hz and 100 Hz frequencies.

When the results of rigid floor and glass wool cases are compared, it is noticed in both the BEM solutions and sound measurements that the sound pressure levels in the glass wool case are smaller than the levels in the rigid floor case as a

consequence of sound absorption effect of the impedance surface. It is a fact that sound pressure levels increase as getting closer to both the refrigerator and the floor. When the BEM solutions are examined, it is seen that they are in agreement with these expectations. However, some deviations from these realities are noticed in the sound measurements. Furthermore, it is obviously seen that sound pressure levels obtained in the measurements are greater than the levels evaluated by the BEM. The main reasons of these differences may be the variation of the refrigerator's working status together with the effect of reflecting surfaces around the refrigerator. Moreover, during the measurements, sound pressure levels might be affected from the background noise. In order to prevent the influence of environmental conditions on the measurements, a large anechoic chamber is required for a quite big body working without too much noise, such as refrigerator. In most cases, the cost of construction such a chamber may not be feasible. However, the BEM has proven its power for all the computations performed in this thesis.

Consequently, the results show that the presented procedure in this study may be effectively used in sound source characterization of vibrating bodies. This procedure provides satisfactory information, about the vibro-acoustic characteristics of the machinery parts; localization, radiation characteristics, spatial and frequency dependent behaviours of sound sources, to the machinery designers and researchers for the purpose of active noise control. On the other hand, this analysis exposes that the effectiveness of passive noise control treatments may be tested in the form of computer simulations without making real applications causing waste of time and money.

REFERENCES

Avsar, E. (2000). *Determination of the acoustic radiation characteristics of vibrating bodies near reflecting surfaces.* M.Sc Thesis, DEÜ, Graduate School of Natural and Applied Sciences, İzmir.

Bai, M. R. (1992). Application of BEM (Boundary element method)-based acoustic holography to radiation analysis of sound sources with arbitrarily shaped geometries. *Journal of the Acoustical Society of America,* 92(1), 533-549.

Bell, W. A., Meyer, W. L., & Zinn, B. T. (1977). Predicting acoustics of arbitrarily shaped bodies using an integral approach. *AIAA Journal,* 15(6), 813-820.

Burton, A. J., & Miller, G. F. (1971). Application of integral equation methods to numerical solution of some exterior boundary-value problems. *Proceedings of the Royal Society of London A,* 323(1553), 201-210.

Castellini, P., & Martarelli, M. (2008). Acoustic beamforming: Analysis of uncertainty and metrological performances. *Mechanical Systems and Signal Processing,* 22(3), 672-692.

Chertock, G. (1964). Sound radiation from vibrating surfaces. *Journal of the Acoustical Society of America,* 36(7), 1305-1313.

Christensen, J. J., & Hald, J. (2004). Beamforming. *Bruel & Kjaer Technical Review,* 1, 1-48.

Courant, R., & Hilbert, D. (1962). *Methods of mathematical physics*. New York: Interscience.

Copley, L. G. (1967). Integral equation method for radiation from vibrating bodies. *Journal of the Acoustical Society of America,* 41(4), 807-816.

Fahy, F. J. (2003). Some applications of the reciprocity principle in experimental vibroacoustics. *Acoustical Physics*, 48(2), 217–229.

Ginn, K. B., & Hald, J. (1989). STSF - Practical instrumentation and applications. *Bruel & Kjaer Technical Review,* 2, 1-27.

Hald, J. (1989). STSF - A unique technique for scan-based near-field acoustic holography without restrictions on coherence. *Bruel & Kjaer Technical Review,* 1, 1-50.

Hald, J. (2000). Non-Stationary STSF. *Bruel & Kjaer Technical Review,* 1, 1-36.

Hald, J. (2005a). Combined NAH and Beamforming using the same array. *Bruel & Kjaer Technical Review,* 1, 11-39.

Hald, J. (2005b). Patch near-field acoustical holography using a new statistically optimal method. *Bruel & Kjaer Technical Review,* 1, 40-50.

Janssens, M. H. A., & Verheij, J. W. (2000). A pseudo-forces methodology to be used in characterization of structure-borne sound sources. *Applied Acoustics,* 61(3), 285-308.

Janssens, M. H. A., Verheij, J. W., & Loyau, T. (2002). Experimental example of the pseudo-forces method used in characterisation of a structure-borne sound source. *Applied Acoustics*, 63(1), 9-34.

Kinsler, L. E., Frey, A. R., Coppens, A. B., & Sanders, J. V. (1982). *Fundamentals of acoustics*. New York: John-Wiley & Sons.

Koopmann, G. H., & Benner, H. (1982). Method for computing the sound power of machines based on the Helmholtz integral. *Journal of the Acoustical Society of America*, 71(1), 78-89.

Maynard, J. D., Williams, E. G., & Lee, Y. (1985). Nearfield acoustic holography: 1. Theory of generalized holography and the development of NAH. *Journal of the Acoustical Society of America*, 78(4), 1395-1413.

Morse, P. M., & Feshbach, H. (1953). *Methods of theoretical physics*. New York: McGraw-Hill.

Morse, P. M., & Ingard, K.U. (1968). *Theoretical acoustics*. New York: McGraw-Hill.

Piaszczyk, C. M., & Klosner, J. M. (1984). Acoustic radiation from vibrating surfaces at characteristic frequencies. *Journal of the Acoustical Society of America*, 75(2), 363-375.

Pierce, A. D. (1981). *Acoustics: An introduction to its physical principles and applications*. New York: McGraw-Hill.

Sakuma, T., & Yasuda, Y. (2002). Fast multipole boundary element method for large-scale steady-state sound field analysis. Part I: Setup and validation. *Acta Acustica United with Acustica*, 88(4), 513-525.

Sarigül, A. S. (1990). *Çok cisimli ses alanlarinin Helmholtz integral denklemi ile hesaplanmasi.* Doktora Tezi, DEÜ, Fen Bilimleri Enstitüsü, Izmir.

Sarigül, A. S. (1999). Sound attenuation characteristics of right-angle pipe bends. *Journal of Sound and Vibration*, 228(4), 837-844.

Sarigül, A. S., & Kiral, Z. (1999). Interior acoustics of a truck cabin with hard and impedance surfaces. *Engineering Analysis with Boundary Elements*, 23(9), 769-775.

Sarigül, A. S., & Seçgin, A. (2004). A study on the applications of the acoustic design sensitivity analysis of vibrating bodies. *Applied Acoustics,* 65(11), 1037-1056.

Schuhmacher, A., Rasmussen, K. B., & Hansen, P. C. (2003). Sound source reconstruction using inverse boundary element calculations. *Journal of the Acoustical Society of America*, 113(1), 114-127.

Seçgin, A., & Sarigül, A. S. (2010). *Acoustic design sensitivity analysis for vibrating bodies*. Saarbrücken, Germany: Lambert Academic Publishing.

Seybert, A. F., Soenarko, B., Rizzo, F. J., & Shippy, D. J. (1985). An advanced computational method for radiation and scattering of acoustic-waves in three dimensions. *Journal of the Acoustical Society of America,* 77(2), 362-368.

Seybert, A. F., & Soenarko, B. (1988). Radiation and scattering of acoustic-waves from bodies of arbitrary shape in a three-dimensional half-space. *Journal of Vibration Acoustics Stress and Reliability in Design,* 110(1), 112-117.

Seybert, A. F., & Wu, T. W. (1989). Modified Helmholtz integral-equation for bodies sitting on an infinite-plane. *Journal of the Acoustical Society of America,* 85(1), 19-23.

Skudrzyk, E. (1971). *Foundations of acoustics: Basic mathematics and basic acoustics*. Vienna: Springer-Verlag.

Verheij, J. W. (1997a). Inverse and reciprocity methods for machinery noise source characterization and sound path quantification. Part 1: Sources. *International Journal of Acoustics and Vibration,* 2, 11–20.

Verheij, J. W. (1997b). Inverse and reciprocity methods for machinery noise source characterization and sound path quantification. Part 2: Transmission paths. *International Journal of Acoustics and Vibration,* 3, 103–112.

Veronesi, W. A., & Maynard, J. D. (1987). Nearfield acoustic holography (NAH): 2. Holographic reconstruction algorithms and computer implementation. *Journal of the Acoustical Society of America,* 81(5), 1307-1322.

Veronesi, W. A., & Maynard, J. D. (1989). Digital holographic reconstruction of sources with arbitrarily shaped surfaces. *Journal of the Acoustical Society of America*, 85(2), 588-598.

Wang, Z. X., & Wu, S. F. (1997). Helmholtz equation least-squares method for reconstructing the acoustic pressure field. *Journal of the Acoustical Society of America*, 102(4), 2020-2032.

Wu, S. F. (2000). On reconstruction of acoustic pressure fields using the Helmholtz equation least squares method. *Journal of the Acoustical Society of America,* 107(5), 2511-2522.

Wu, T. W., & Seybert, A. F. (1991). Acoustic radiation and scattering. Boundary element methods in acoustics. R. D. Ciskowski, & C. A. Brebbia, C.A., (Eds.). *Computational Mechanics Publications-Elsevier Applied Science,* 61-76.

Yasuda, Y., & Sakuma, T. (2005). A technique for plane-symmetric sound field analysis in the fast multipole boundary element method. *Journal of Computational Acoustics,* 13(1), 71-85.

Zhang, Z. D., Vlahopoulos, N., Raveendra, S. T., Allen, T., & Zhang, K. Y. (2000). A computational acoustic field reconstruction process based on an indirect boundary element formulation. *Journal of the Acoustical Society of America,* 108(5), 2167-2178.

APPENDICES

APPENDIX A
DETERMINATION OF REFLECTION COEFFICIENT OF A SURFACE

A.1 Reflection Coefficient

When a wave (incident wave) encounters a reflecting surface, part of the wave is reflected (reflected wave) backward from the surface and part of the wave is transmitted (transmitted wave) across the surface as shown in Figure A.1. Here, I denotes incident wave, R represents reflected wave and T is transmitted wave.

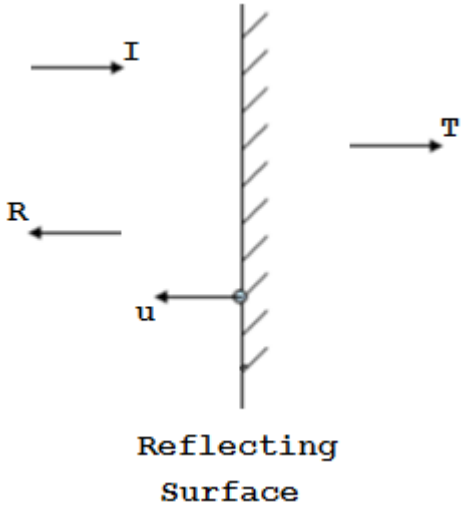

Figure A.1 Schematic representation of reflection and transmission of an incident wave from a reflecting surface

The reflection coefficient, R_p, of the surface can be written in terms of acoustical pressure of reflected and incident waves as,

$$R_p = \frac{p_R}{p_I} \tag{A.1}$$

where p_R denotes the acoustical pressure of reflected wave and p_I represents the acoustical pressure of incident wave.

One-dimensional form of the Helmholtz Equation (2.3) may be written as,

$$\frac{\partial^2 p}{\partial x^2} + k^2 p = 0. \tag{A.2}$$

Let p be the sum of p_R and p_I as the following form

$$p = p_R + p_I = Ae^{i\omega t}e^{-ikx} + Be^{i\omega t}e^{ikx} \tag{A.3}$$

which satisfies Equation (A.2). Here, ω denotes the radiation frequency. In order to calculate p, it is necessary to evaluate coefficients *A* and *B* in Equation (A.3). Therefore, it is required to apply Euler's equation as boundary condition. One-dimensional form of Euler's Equation (2.23) is written as,

$$\rho_o \frac{\partial u}{\partial t} = -\frac{\partial p}{\partial x} \tag{A.4}$$

Taking the derivative of p in Equation (A.3) with respect to x,

$$\frac{\partial p}{\partial x} = Ae^{i\omega t}(-ik)e^{-ikx} + Be^{i\omega t}(ik)e^{ikx}. \tag{A.5}$$

Substituting Equation (A.5) into Equation (A.4) yields

$$\rho_o \frac{\partial u}{\partial t} = Ae^{i\omega t}(ik)e^{-ikx} - Be^{i\omega t}(ik)e^{ikx}. \tag{A.6}$$

If two sides of Equation (A.6) are integrated with respect to t; normal velocity u of the surface is obtained as,

$$u = \frac{e^{i\omega t}}{\rho_o c}\left(Ae^{-ikx} - Be^{ikx}\right) \tag{A.7}$$

where $c = \omega / k$.

There are three ways of obtaining the reflection coefficient R_p of the surface:

- If u and p are known for a specified value of x, coefficients A and B can be calculated by using Equations (A.3) and (A.7). Then, R_p may be evaluated by using Equations (A.1) and (A.3).

- Max and min value of p in Equation (A.3) can be written as,

$$p_{\max} = p_R + p_I, \qquad \text{(a)}$$

$$p_{\min} = p_R - p_I. \qquad \text{(b)} \qquad \text{(A.8)}$$

If $p_{\max}$ and $p_{\min}$ are known, p_I and p_R may be calculated and R_p can be determined by using Equation (A.1).

- R_p may be obtained by using sound absorption coefficient, α, of the reflecting surface. α is related with the acoustical energy of the transmitted and incident waves in the following form,

$$\alpha = \frac{E_T}{E_I} \qquad \text{(A.9)}$$

where E_T and E_I denote the acoustical energies of the transmitted and incident waves, respectively. Energy conservation law gives,

$$E_I = E_R + E_T \qquad \text{(A.10)}$$

where E_R represents the acoustical energy of the reflected wave. Equation (A.10) can be rewritten as,

$$E_T = E_I - E_R . \tag{A.11}$$

By substituting Equation (A.11) into Equation (A.9), the following equation is obtained:

$$\alpha = 1 - \frac{E_R}{E_I} . \tag{A.12}$$

Since acoustical power is proportional to acoustical energy, Equation (A.12) can be written in terms of acoustical power as

$$\alpha = 1 - \frac{W_R}{W_I} \tag{A.13}$$

where W_R and W_I denotes the acoustical power of reflected and incident waves, respectively. On the other hand, the acoustical power of a wave may be written in terms of its pressure and particle velocity as,

$$W = p \cdot u \tag{A.14}$$

For a one-dimensional (plane) wave, the particle speed is in phase with the pressure and given as, (Kinsler, Frey, Coppens & Sanders, 1982)

$$u = \frac{p}{\rho_o c} . \tag{A.15}$$

Substitution of Equation (A.15) into Equation (A.14) yields

$$W = \frac{p^2}{\rho_o c}. \tag{A.16}$$

In this regard, the acoustical power of reflected and incident waves can be written as,

$$W_R = \frac{{p_R}^2}{\rho_o c}, \quad \text{(a)}$$

$$W_I = \frac{{p_I}^2}{\rho_o c}, \quad \text{(b)} \tag{A.17}$$

respectively. The sound absorption coefficient of the reflecting surface is obtained by substituting Equation (A.17) into Equation (A.13) as,

$$\alpha = 1 - \frac{{p_R}^2}{{p_I}^2}. \tag{A.18}$$

By using Equation (A.1), Equation (A.18) may be rewritten as,

$$\alpha = 1 - {R_p}^2 \tag{A.19}$$

which yields reflection coefficient as,

$$R_p = \sqrt{1-\alpha^2}\,. \tag{A.20}$$

APPENDIX B

GEOMETRICAL DATA OF SPHERICAL AND HEMISPHERICAL SOURCES

Table B.1 Nodal Co-ordinates of the Spherical Source

Node No	x (mm)	y (mm)	z (mm)
1	0.000000	0.000000	1.000000
2	0.000000	-0.195090	0.980785
3	0.000000	0.195090	0.980785
4	0.382683	0.000000	0.923880
5	0.000000	-0.382683	0.923880
6	-0.382683	0.000000	0.923880
7	0.000000	0.382683	0.923880
8	0.000000	-0.555570	0.831470
9	0.000000	0.555570	0.831470
10	0.707107	0.000000	0.707107
11	0.653281	-0.270598	0.707107
12	0.500000	-0.500000	0.707107
13	0.270598	-0.653281	0.707107
14	0.000000	-0.707107	0.707107
15	-0.270598	-0.653281	0.707107
16	-0.500000	-0.500000	0.707107
17	-0.653281	-0.270598	0.707107
18	-0.707107	0.000000	0.707107
19	-0.653281	0.270598	0.707107
20	-0.500000	0.500000	0.707107
21	-0.270598	0.653281	0.707107
22	0.000000	0.707107	0.707107
23	0.270598	0.653281	0.707107
24	0.500000	0.500000	0.707107
25	0.653281	0.270598	0.707107
26	0.923880	0.000000	0.382683
27	0.653281	-0.653281	0.382683
28	0.000000	-0.923880	0.382683
29	-0.653281	-0.653281	0.382683
30	-0.923880	0.000000	0.382683
31	-0.653281	0.653281	0.382683
32	0.000000	0.923880	0.382683
33	0.653281	0.653281	0.382683
34	1.000000	0.000000	0.000000
35	0.923880	-0.382683	0.000000
36	0.707107	-0.707107	0.000000
37	0.382683	-0.923880	0.000000
38	0.000000	-1.000000	0.000000
39	-0.382683	-0.923880	0.000000
40	-0.707107	-0.707107	0.000000
41	-0.923880	-0.382683	0.000000
42	-1.000000	0.000000	0.000000
43	-0.923880	0.382683	0.000000
44	-0.707107	0.707107	0.000000
45	-0.382683	0.923880	0.000000
46	0.000000	1.000000	0.000000
47	0.382683	0.923880	0.000000
48	0.707107	0.707107	0.000000
49	0.923880	0.382683	0.000000
50	0.923880	0.000000	-0.382683
51	0.653281	-0.653281	-0.382683
52	0.000000	-0.923880	-0.382683
53	-0.653281	-0.653281	-0.382683
54	-0.923880	0.000000	-0.382683
55	-0.653281	0.653281	-0.382683
56	0.000000	0.923880	-0.382683
57	0.653281	0.653281	-0.382683
58	0.707107	0.000000	-0.707107
59	0.653281	-0.270598	-0.707107
60	0.500000	-0.500000	-0.707107
61	0.270598	-0.653281	-0.707107
62	0.000000	-0.707107	-0.707107
63	-0.270598	-0.653281	-0.707107
64	-0.500000	-0.500000	-0.707107

Table B.1 (Continued)

Node No	x (mm)	y (mm)	z (mm)
65	-0.653281	-0.270598	-0.707107
66	-0.707107	0.000000	-0.707107
67	-0.653281	0.270598	-0.707107
68	-0.500000	0.500000	-0.707107
69	-0.270598	0.653281	-0.707107
70	0.000000	0.707107	-0.707107
71	0.270598	0.653281	-0.707107
72	0.500000	0.500000	-0.707107
73	0.653281	0.270598	-0.707107
74	0.000000	-0.555570	-0.831470
75	0.000000	0.555570	-0.831470
76	0.382683	0.000000	-0.923880
77	0.000000	-0.382683	-0.923880
78	-0.382683	0.000000	-0.923880
79	0.000000	0.382683	-0.923880
80	0.000000	-0.195090	-0.980785
81	0.000000	0.195090	-0.980785
82	0.000000	0.000000	-1.000000

Table B.2 Incidence Matrix of the Spherical Source

Element No	nod1	nod2	nod3	nod4	nod5	nod6	nod7	nod8
1	1	2	5	8	14	12	10	4
2	5	2	1	6	18	16	14	8
3	1	3	7	9	22	20	18	6
4	7	3	1	4	10	24	22	9
5	10	11	12	27	36	35	34	26
6	12	13	14	28	38	37	36	27
7	14	15	16	29	40	39	38	28
8	16	17	18	30	42	41	40	29
9	18	19	20	31	44	43	42	30
10	20	21	22	32	46	45	44	31
11	22	23	24	33	48	47	46	32
12	24	25	10	26	34	49	48	33
13	34	35	36	51	60	59	58	50
14	36	37	38	52	62	61	60	51
15	38	39	40	53	64	63	62	52
16	40	41	42	54	66	65	64	53
17	42	43	44	55	68	67	66	54
18	44	45	46	56	70	69	68	55
19	46	47	48	57	72	71	70	56
20	48	49	34	50	58	73	72	57
21	58	60	62	74	77	80	82	76
22	62	64	66	78	82	80	77	74
23	66	68	70	75	79	81	82	78
24	70	72	58	76	82	81	79	75

Table B.3 Nodal Co-ordinates of the Hemispherical Source

Node No	x (mm)	y (mm)	z (mm)
1	0.000000	0.000000	1.000000
2	0.000000	-0.195090	0.980785
3	0.000000	0.195090	0.980785
4	0.382683	0.000000	0.923880
5	0.000000	-0.382683	0.923880
6	-0.382683	0.000000	0.923880
7	0.000000	0.382683	0.923880
8	0.000000	-0.555570	0.831470
9	0.000000	0.555570	0.831470
10	0.707107	0.000000	0.707107
11	0.653281	-0.270598	0.707107
12	0.500000	-0.500000	0.707107
13	0.270598	-0.653281	0.707107
14	0.000000	-0.707107	0.707107
15	-0.270598	-0.653281	0.707107
16	-0.500000	-0.500000	0.707107
17	-0.653281	-0.270598	0.707107
18	-0.707107	0.000000	0.707107
19	-0.653281	0.270598	0.707107
20	-0.500000	0.500000	0.707107
21	-0.270598	0.653281	0.707107
22	0.000000	0.707107	0.707107
23	0.270598	0.653281	0.707107
24	0.500000	0.500000	0.707107
25	0.653281	0.270598	0.707107
26	0.923880	0.000000	0.382683
27	0.653281	-0.653281	0.382683
28	0.000000	-0.923880	0.382683
29	-0.653281	-0.653281	0.382683
30	-0.923880	0.000000	0.382683
31	-0.653281	0.653281	0.382683
32	0.000000	0.923880	0.382683
33	0.653281	0.653281	0.382683
34	1.000000	0.000000	0.000000
35	0.923880	-0.382683	0.000000
36	0.707107	-0.707107	0.000000
37	0.382683	-0.923880	0.000000

Node No	x (mm)	y (mm)	z (mm)
38	0.000000	-1.000000	0.000000
39	-0.382683	-0.923880	0.000000
40	-0.707107	-0.707107	0.000000
41	-0.923880	-0.382683	0.000000
42	-1.000000	0.000000	0.000000
43	-0.923880	0.382683	0.000000
44	-0.707107	0.707107	0.000000
45	-0.382683	0.923880	0.000000
46	0.000000	1.000000	0.000000
47	0.382683	0.923880	0.000000
48	0.707107	0.707107	0.000000
49	0.923880	0.382683	0.000000
50	0.500000	0.000000	0.000000
51	0.000000	-0.500000	0.000000
52	-0.500000	0.000000	0.000000
53	0.000000	0.500000	0.000000
54	0.000000	0.000000	0.000000

Table B.4 Incidence Matrix of the Hemispherical Source

Element No	nod1	nod2	nod3	nod4	nod5	nod6	nod7	nod8
1	1	2	5	8	14	12	10	4
2	5	2	1	6	18	16	14	8
3	1	3	7	9	22	20	18	6
4	7	3	1	4	10	24	22	9
5	10	11	12	27	36	35	34	26
6	12	13	14	28	38	37	36	27
7	14	15	16	29	40	39	38	28
8	16	17	18	30	42	41	40	29
9	18	19	20	31	44	43	42	30
10	20	21	22	32	46	45	44	31
11	22	23	24	33	48	47	46	32
12	24	25	10	26	34	49	48	33
13	34	35	36	37	38	51	54	50
14	54	51	38	39	40	41	42	52
15	46	53	54	52	42	43	44	45
16	48	49	34	50	54	53	46	47

APPENDIX C
SURFACE PRESSURES OF DILATING SPHERICAL AND HEMISPHERICAL SOURCES

Table C.1 Surface Pressures of the Spherical Source ($a = 1$ m, $u_n = 1$ m/s)

Node No	Surface Pressures (Pa)
1	294.188
2	291.294
3	291.294
4	282.649
5	314.612
6	282.649
7	314.612
8	290.864
9	290.864
10	292.879
11	285.552
12	286.505
13	286.921
14	292.382
15	286.921
16	286.505
17	285.552
18	292.879
19	285.552
20	286.505
21	286.921
22	292.382
23	286.921
24	286.505
25	285.552
26	282.846
27	282.875
28	282.817
29	282.875
30	282.846
31	282.875
32	282.817

Node No	Surface Pressures (Pa)
33	282.875
34	295.369
35	283.226
36	295.343
37	283.209
38	295.351
39	283.209
40	295.343
41	283.226
42	295.369
43	283.226
44	295.343
45	283.209
46	295.351
47	283.209
48	295.343
49	283.226
50	282.846
51	282.8754
52	282.8169
53	282.8754
54	282.8464
55	282.8754
56	282.8169
57	282.8754
58	292.8794
59	285.552
60	286.5053
61	286.9212
62	292.3815
63	286.9212
64	286.5053

Table C.1 (Continued)

Node No	Surface Pressures (Pa)
65	285.552
66	292.8794
67	285.552
68	286.5053
69	286.9212
70	292.3815
71	286.9212
72	286.5053
73	285.552
74	290.864
75	290.864
76	282.6486
77	314.6115
78	282.6486
79	314.6115
80	291.2941
81	291.2941
82	294.1884

Table C.2 Surface Pressures of the Hemispherical Source ($a = 1$ m, $u_n = 1$ m/s)

Node No	Surface Pressures (Pa)				
	α=0	α=0.25	α=0.50	α=0.75	α=1.0
1	294.277	294.679	295.186	295.957	299.057
2	291.382	291.544	291.760	292.140	294.240
3	291.382	291.544	291.760	292.140	294.240
4	282.732	282.171	281.506	280.696	279.737
5	314.722	314.690	314.678	314.766	316.187
6	282.732	282.171	281.506	280.696	279.737
7	314.722	314.690	314.678	314.766	316.187
8	290.958	289.603	287.975	285.877	281.654
9	290.958	289.603	287.975	285.877	281.654
10	292.995	290.302	287.045	282.754	272.882
11	285.660	282.843	279.431	274.918	264.424
12	286.586	283.799	280.423	275.960	265.599
13	287.030	284.229	280.837	276.353	265.945
14	292.497	289.789	286.515	282.199	272.260
15	287.030	284.229	280.837	276.353	265.945
16	286.586	283.799	280.423	275.960	265.599
17	285.660	282.843	279.431	274.918	264.424
18	292.995	290.302	287.045	282.754	272.882
19	285.660	282.843	279.431	274.918	264.424
20	286.586	283.799	280.423	275.960	265.599
21	287.030	284.229	280.837	276.353	265.945
22	292.497	289.789	286.515	282.199	272.260
23	287.030	284.229	280.837	276.353	265.945
24	286.586	283.799	280.423	275.960	265.599
25	285.660	282.843	279.431	274.918	264.424
26	282.710	275.275	266.207	254.005	223.238
27	283.334	275.881	266.791	254.559	223.718
28	282.680	275.244	266.173	253.967	223.193
29	283.334	275.881	266.791	254.559	223.718
30	282.710	275.275	266.207	254.005	223.238
31	283.334	275.881	266.791	254.559	223.718
32	282.680	275.244	266.173	253.967	223.193
33	283.334	275.881	266.791	254.559	223.718
34	295.263	298.358	302.203	307.514	321.891
35	283.110	286.304	290.276	295.770	310.685
36	295.215	298.313	302.160	307.475	321.863

Table C.2 (Continued)

Node No	Surface Pressures (Pa)				
	α=0	**α=0.25**	**α=0.50**	**α=0.75**	**α=1.0**
37	283.093	286.287	290.259	295.752	310.669
38	295.245	298.341	302.185	307.496	321.873
39	283.093	286.287	290.259	295.752	310.669
40	295.215	298.313	302.160	307.475	321.863
41	283.110	286.304	290.276	295.770	310.685
42	295.263	298.358	302.203	307.514	321.891
43	283.110	286.304	290.276	295.770	310.685
44	295.215	298.313	302.160	307.475	321.863
45	283.093	286.287	290.259	295.752	310.669
46	295.245	298.341	302.185	307.496	321.873
47	283.093	286.287	290.259	295.752	310.669
48	295.215	298.313	302.160	307.475	321.863
49	283.110	286.304	290.276	295.770	310.685

APPENDIX D

GEOMETRICAL AND SURFACE VELOCITY DATA OF THE REFRIGERATOR

Table D.1 Nodal Co-ordinates of the Refrigerator

Node No	x (mm)	y (mm)	z (mm)
1	345.000	-177.500	-843.750
2	345.000	-177.500	-750.000
3	345.000	-266.250	-750.000
4	345.000	-355.000	-750.000
5	345.000	-355.000	-843.750
6	345.000	0	-843.750
7	345.000	0	-750.000
8	345.000	-88.750	-750.000
9	345.000	177.500	-843.750
10	345.000	177.500	-750.000
11	345.000	88.750	-750.000
12	345.000	355.000	-843.750
13	345.000	355.000	-750.000
14	345.000	266.250	-750.000
15	345.000	-177.500	-656.250
16	345.000	-177.500	-562.500
17	345.000	-266.250	-562.500
18	345.000	-355.000	-562.500
19	345.000	-355.000	-656.250
20	345.000	0	-656.250
21	345.000	0	-562.500
22	345.000	-88.750	-562.500
23	345.000	177.500	-656.250
24	345.000	177.500	-562.500
25	345.000	88.750	-562.500
26	345.000	355.000	-656.250
27	345.000	355.000	-562.500
28	345.000	266.250	-562.500
29	345.000	-177.500	-468.750
30	345.000	-177.500	-375.000
31	345.000	-266.250	-375.000
32	345.000	-355.000	-375.000

Node No	x (mm)	y (mm)	z (mm)
33	345.000	-355.000	-468.750
34	345.000	0	-468.750
35	345.000	0	-375.000
36	345.000	-88.750	-375.000
37	345.000	177.500	-468.750
38	345.000	177.500	-375.000
39	345.000	88.750	-375.000
40	345.000	355.000	-468.750
41	345.000	355.000	-375.000
42	345.000	266.250	-375.000
43	345.000	-177.500	-281.250
44	345.000	-177.500	-187.500
45	345.000	-266.250	-187.500
46	345.000	-355.000	-187.500
47	345.000	-355.000	-281.250
48	345.000	0	-281.250
49	345.000	0	-187.500
50	345.000	-88.750	-187.500
51	345.000	177.500	-281.250
52	345.000	177.500	-187.500
53	345.000	88.750	-187.500
54	345.000	355.000	-281.250
55	345.000	355.000	-187.500
56	345.000	266.250	-187.500
57	345.000	-177.500	-93.750
58	345.000	-177.500	0
59	345.000	-266.250	0
60	345.000	-355.000	0
61	345.000	-355.000	-93.750
62	345.000	0	-93.750
63	345.000	0	0
64	345.000	-88.750	0

Table D.1 (Continued)

Node No	x (mm)	y (mm)	z (mm)
65	345.000	177.500	-93.750
66	345.000	177.500	0
67	345.000	88.750	0
68	345.000	355.000	-93.750
69	345.000	355.000	0
70	345.000	266.250	0
71	345.000	-177.500	93.750
72	345.000	-177.500	187.500
73	345.000	-266.250	187.500
74	345.000	-355.000	187.500
75	345.000	-355.000	93.750
76	345.000	0	93.750
77	345.000	0	187.500
78	345.000	-88.750	187.500
79	345.000	177.500	93.750
80	345.000	177.500	187.500
81	345.000	88.750	187.500
82	345.000	355.000	93.750
83	345.000	355.000	187.500
84	345.000	266.250	187.500
85	345.000	-177.500	281.250
86	345.000	-177.500	375.000
87	345.000	-266.250	375.000
88	345.000	-355.000	375.000
89	345.000	-355.000	281.250
90	345.000	0	281.250
91	345.000	0	375.000
92	345.000	-88.750	375.000
93	345.000	177.500	281.250
94	345.000	177.500	375.000
95	345.000	88.750	375.000
96	345.000	355.000	281.250
97	345.000	355.000	375.000
98	345.000	266.250	375.000
99	345.000	-177.500	468.750
100	345.000	-177.500	562.500
101	345.000	-266.250	562.500
102	345.000	-355.000	562.500

Node No	x (mm)	y (mm)	z (mm)
103	345.000	-355.000	468.750
104	345.000	0	468.750
105	345.000	0	562.500
106	345.000	-88.750	562.500
107	345.000	177.500	468.750
108	345.000	177.500	562.500
109	345.000	88.750	562.500
110	345.000	355.000	468.750
111	345.000	355.000	562.500
112	345.000	266.250	562.500
113	345.000	-177.500	656.250
114	345.000	-177.500	750.000
115	345.000	-266.250	750.000
116	345.000	-355.000	750.000
117	345.000	-355.000	656.250
118	345.000	0	656.250
119	345.000	0	750.000
120	345.000	-88.750	750.000
121	345.000	177.500	656.250
122	345.000	177.500	750.000
123	345.000	88.750	750.000
124	345.000	355.000	656.250
125	345.000	355.000	750.000
126	345.000	266.250	750.000
127	345.000	-177.500	843.750
128	345.000	-177.500	937.500
129	345.000	-266.250	937.500
130	345.000	-355.000	937.500
131	345.000	-355.000	843.750
132	345.000	0	843.750
133	345.000	0	937.500
134	345.000	-88.750	937.500
135	345.000	177.500	843.750
136	345.000	177.500	937.500
137	345.000	88.750	937.500
138	345.000	355.000	843.750
139	345.000	355.000	937.500
140	345.000	266.250	937.500

Table D.1 (Continued)

Node No	x (mm)	y (mm)	z (mm)
141	172.500	355.000	-843.750
142	172.500	355.000	-750.000
143	258.750	355.000	-750.000
144	0	355.000	-843.750
145	0	355.000	-750.000
146	86.250	355.000	-750.000
147	-172.500	355.000	-843.750
148	-172.500	355.000	-750.000
149	-86.250	355.000	-750.000
150	-345.000	355.000	-843.750
151	-345.000	355.000	-750.000
152	-258.750	355.000	-750.000
153	172.500	355.000	-656.250
154	172.500	355.000	-562.500
155	258.750	355.000	-562.500
156	0	355.000	-656.250
157	0	355.000	-562.500
158	86.250	355.000	-562.500
159	-172.500	355.000	-656.250
160	-172.500	355.000	-562.500
161	-86.250	355.000	-562.500
162	-345.000	355.000	-656.250
163	-345.000	355.000	-562.500
164	-258.750	355.000	-562.500
165	172.500	355.000	-468.750
166	172.500	355.000	-375.000
167	258.750	355.000	-375.000
168	0	355.000	-468.750
169	0	355.000	-375.000
170	86.250	355.000	-375.000
171	-172.500	355.000	-468.750
172	-172.500	355.000	-375.000
173	-86.250	355.000	-375.000
174	-345.000	355.000	-468.750
175	-345.000	355.000	-375.000
176	-258.750	355.000	-375.000
177	172.500	355.000	-281.250
178	172.500	355.000	-187.500
179	258.750	355.000	-187.500
180	0	355.000	-281.250
181	0	355.000	-187.500
182	86.250	355.000	-187.500
183	-172.500	355.000	-281.250
184	-172.500	355.000	-187.500
185	-86.250	355.000	-187.500
186	-345.000	355.000	-281.250
187	-345.000	355.000	-187.500
188	-258.750	355.000	-187.500
189	172.500	355.000	-93.750
190	172.500	355.000	0
191	258.750	355.000	0
192	0	355.000	-93.750
193	0	355.000	0
194	86.250	355.000	0
195	-172.500	355.000	-93.750
196	-172.500	355.000	0
197	-86.250	355.000	0
198	-345.000	355.000	-93.750
199	-345.000	355.000	0
200	-258.750	355.000	0
201	172.500	355.000	93.750
202	172.500	355.000	187.500
203	258.750	355.000	187.500
204	0	355.000	93.750
205	0	355.000	187.500
206	86.250	355.000	187.500
207	-172.500	355.000	93.750
208	-172.500	355.000	187.500
209	-86.250	355.000	187.500
210	-345.000	355.000	93.750
211	-345.000	355.000	187.500
212	-258.750	355.000	187.500
213	172.500	355.000	281.250
214	172.500	355.000	375.000
215	258.750	355.000	375.000
216	0	355.000	281.250

Table D.1 (Continued)

Node No	x (mm)	y (mm)	z (mm)
217	0	355.000	375.000
218	86.250	355.000	375.000
219	-172.500	355.000	281.250
220	-172.500	355.000	375.000
221	-86.250	355.000	375.000
222	-345.000	355.000	281.250
223	-345.000	355.000	375.000
224	-258.750	355.000	375.000
225	172.500	355.000	468.750
226	172.500	355.000	562.500
227	258.750	355.000	562.500
228	0	355.000	468.750
229	0	355.000	562.500
230	86.250	355.000	562.500
231	-172.500	355.000	468.750
232	-172.500	355.000	562.500
233	-86.250	355.000	562.500
234	-345.000	355.000	468.750
235	-345.000	355.000	562.500
236	-258.750	355.000	562.500
237	172.500	355.000	656.250
238	172.500	355.000	750.000
239	258.750	355.000	750.000
240	0	355.000	656.250
241	0	355.000	750.000
242	86.250	355.000	750.000
243	-172.500	355.000	656.250
244	-172.500	355.000	750.000
245	-86.250	355.000	750.000
246	-345.000	355.000	656.250
247	-345.000	355.000	750.000
248	-258.750	355.000	750.000
249	172.500	355.000	843.750
250	172.500	355.000	937.500
251	258.750	355.000	937.500
252	0	355.000	843.750
253	0	355.000	937.500
254	86.250	355.000	937.500
255	-172.500	355.000	843.750
256	-172.500	355.000	937.500
257	-86.250	355.000	937.500
258	-345.000	355.000	843.750
259	-345.000	355.000	937.500
260	-258.750	355.000	937.500
261	-345.000	177.500	-843.750
262	-345.000	177.500	-750.000
263	-345.000	266.250	-750.000
264	-345.000	0	-843.750
265	-345.000	0	-750.000
266	-345.000	88.750	-750.000
267	-345.000	-177.500	-843.750
268	-345.000	-177.500	-750.000
269	-345.000	-88.750	-750.000
270	-345.000	-355.000	-843.750
271	-345.000	-355.000	-750.000
272	-345.000	-266.250	-750.000
273	-345.000	177.500	-656.250
274	-345.000	177.500	-562.500
275	-345.000	266.250	-562.500
276	-345.000	0	-656.250
277	-345.000	0	-562.500
278	-345.000	88.750	-562.500
279	-345.000	-177.500	-656.250
280	-345.000	-177.500	-562.500
281	-345.000	-88.750	-562.500
282	-345.000	-355.000	-656.250
283	-345.000	-355.000	-562.500
284	-345.000	-266.250	-562.500
285	-345.000	177.500	-468.750
286	-345.000	177.500	-375.000
287	-345.000	266.250	-375.000
288	-345.000	0	-468.750
289	-345.000	0	-375.000
290	-345.000	88.750	-375.000
291	-345.000	-177.500	-468.750
292	-345.000	-177.500	-375.000

Table D.1 (Continued)

Node No	x (mm)	y (mm)	z (mm)
293	-345.000	-88.750	-375.000
294	-345.000	-355.000	-468.750
295	-345.000	-355.000	-375.000
296	-345.000	-266.250	-375.000
297	-345.000	177.500	-281.250
298	-345.000	177.500	-187.500
299	-345.000	266.250	-187.500
300	-345.000	0	-281.250
301	-345.000	0	-187.500
302	-345.000	88.750	-187.500
303	-345.000	-177.500	-281.250
304	-345.000	-177.500	-187.500
305	-345.000	-88.750	-187.500
306	-345.000	-355.000	-281.250
307	-345.000	-355.000	-187.500
308	-345.000	-266.250	-187.500
309	-345.000	177.500	-93.750
310	-345.000	177.500	0
311	-345.000	266.250	0
312	-345.000	0	-93.750
313	-345.000	0	0
314	-345.000	88.750	0
315	-345.000	-177.500	-93.750
316	-345.000	-177.500	0
317	-345.000	-88.750	0
318	-345.000	-355.000	-93.750
319	-345.000	-355.000	0
320	-345.000	-266.250	0
321	-345.000	177.500	93.750
322	-345.000	177.500	187.500
323	-345.000	266.250	187.500
324	-345.000	0	93.750
325	-345.000	0	187.500
326	-345.000	88.750	187.500
327	-345.000	-177.500	93.750
328	-345.000	-177.500	187.500
329	-345.000	-88.750	187.500
330	-345.000	-355.000	93.750

Node No	x (mm)	y (mm)	z (mm)
331	-345.000	-355.000	187.500
332	-345.000	-266.250	187.500
333	-345.000	177.500	281.250
334	-345.000	177.500	375.000
335	-345.000	266.250	375.000
336	-345.000	0	281.250
337	-345.000	0	375.000
338	-345.000	88.750	375.000
339	-345.000	-177.500	281.250
340	-345.000	-177.500	375.000
341	-345.000	-88.750	375.000
342	-345.000	-355.000	281.250
343	-345.000	-355.000	375.000
344	-345.000	-266.250	375.000
345	-345.000	177.500	468.750
346	-345.000	177.500	562.500
347	-345.000	266.250	562.500
348	-345.000	0	468.750
349	-345.000	0	562.500
350	-345.000	88.750	562.500
351	-345.000	-177.500	468.750
352	-345.000	-177.500	562.500
353	-345.000	-88.750	562.500
354	-345.000	-355.000	468.750
355	-345.000	-355.000	562.500
356	-345.000	-266.250	562.500
357	-345.000	177.500	656.250
358	-345.000	177.500	750.000
359	-345.000	266.250	750.000
360	-345.000	0	656.250
361	-345.000	0	750.000
362	-345.000	88.750	750.000
363	-345.000	-177.500	656.250
364	-345.000	-177.500	750.000
365	-345.000	-88.750	750.000
366	-345.000	-355.000	656.250
367	-345.000	-355.000	750.000
368	-345.000	-266.250	750.000

Table D.1 (Continued)

Node No	x (mm)	y (mm)	z (mm)
369	-345.000	177.500	843.750
370	-345.000	177.500	937.500
371	-345.000	266.250	937.500
372	-345.000	0	843.750
373	-345.000	0	937.500
374	-345.000	88.750	937.500
375	-345.000	-177.500	843.750
376	-345.000	-177.500	937.500
377	-345.000	-88.750	937.500
378	-345.000	-355.000	843.750
379	-345.000	-355.000	937.500
380	-345.000	-266.250	937.500
381	-172.500	-355.000	-843.750
382	-172.500	-355.000	-750.000
383	-258.750	-355.000	-750.000
384	0	-355.000	-843.750
385	0	-355.000	-750.000
386	-86.250	-355.000	-750.000
387	172.500	-355.000	-843.750
388	172.500	-355.000	-750.000
389	86.250	-355.000	-750.000
390	258.750	-355.000	-750.000
391	-172.500	-355.000	-656.250
392	-172.500	-355.000	-562.500
393	-258.750	-355.000	-562.500
394	0	-355.000	-656.250
395	0	-355.000	-562.500
396	-86.250	-355.000	-562.500
397	172.500	-355.000	-656.250
398	172.500	-355.000	-562.500
399	86.250	-355.000	-562.500
400	258.750	-355.000	-562.500
401	-172.500	-355.000	-468.750
402	-172.500	-355.000	-375.000
403	-258.750	-355.000	-375.000
404	0	-355.000	-468.750
405	0	-355.000	-375.000
406	-86.250	-355.000	-375.000
407	172.500	-355.000	-468.750
408	172.500	-355.000	-375.000
409	86.250	-355.000	-375.000
410	258.750	-355.000	-375.000
411	-172.500	-355.000	-281.250
412	-172.500	-355.000	-187.500
413	-258.750	-355.000	-187.500
414	0	-355.000	-281.250
415	0	-355.000	-187.500
416	-86.250	-355.000	-187.500
417	172.500	-355.000	-281.250
418	172.500	-355.000	-187.500
419	86.250	-355.000	-187.500
420	258.750	-355.000	-187.500
421	-172.500	-355.000	-93.750
422	-172.500	-355.000	0
423	-258.750	-355.000	0
424	0	-355.000	-93.750
425	0	-355.000	0
426	-86.250	-355.000	0
427	172.500	-355.000	-93.750
428	172.500	-355.000	0
429	86.250	-355.000	0
430	258.750	-355.000	0
431	-172.500	-355.000	93.750
432	-172.500	-355.000	187.500
433	-258.750	-355.000	187.500
434	0	-355.000	93.750
435	0	-355.000	187.500
436	-86.250	-355.000	187.500
437	172.500	-355.000	93.750
438	172.500	-355.000	187.500
439	86.250	-355.000	187.500
440	258.750	-355.000	187.500
441	-172.500	-355.000	281.250
442	-172.500	-355.000	375.000
443	-258.750	-355.000	375.000
444	0	-355.000	281.250

Table D.1 (Continued)

Node No	x (mm)	y (mm)	z (mm)
445	0	-355.000	375.000
446	-86.250	-355.000	375.000
447	172.500	-355.000	281.250
448	172.500	-355.000	375.000
449	86.250	-355.000	375.000
450	258.750	-355.000	375.000
451	-172.500	-355.000	468.750
452	-172.500	-355.000	562.500
453	-258.750	-355.000	562.500
454	0	-355.000	468.750
455	0	-355.000	562.500
456	-86.250	-355.000	562.500
457	172.500	-355.000	468.750
458	172.500	-355.000	562.500
459	86.250	-355.000	562.500
460	258.750	-355.000	562.500
461	-172.500	-355.000	656.250
462	-172.500	-355.000	750.000
463	-258.750	-355.000	750.000
464	0	-355.000	656.250
465	0	-355.000	750.000
466	-86.250	-355.000	750.000
467	172.500	-355.000	656.250
468	172.500	-355.000	750.000
469	86.250	-355.000	750.000
470	258.750	-355.000	750.000
471	-172.500	-355.000	843.750
472	-172.500	-355.000	937.500
473	-258.750	-355.000	937.500
474	0	-355.000	843.750
475	0	-355.000	937.500
476	-86.250	-355.000	937.500
477	172.500	-355.000	843.750
478	172.500	-355.000	937.500
479	86.250	-355.000	937.500
480	258.750	-355.000	937.500
481	258.750	-177.500	937.500
482	172.500	-177.500	937.500

Node No	x (mm)	y (mm)	z (mm)
483	172.500	-266.250	937.500
484	258.750	0	937.500
485	172.500	0	937.500
486	172.500	-88.750	937.500
487	258.750	177.500	937.500
488	172.500	177.500	937.500
489	172.500	88.750	937.500
490	172.500	266.250	937.500
491	86.250	-177.500	937.500
492	0	-177.500	937.500
493	0	-266.250	937.500
494	86.250	0	937.500
495	0	0	937.500
496	0	-88.750	937.500
497	86.250	177.500	937.500
498	0	177.500	937.500
499	0	88.750	937.500
500	0	266.250	937.500
501	-86.250	-177.500	937.500
502	-172.500	-177.500	937.500
503	-172.500	-266.250	937.500
504	-86.250	0	937.500
505	-172.500	0	937.500
506	-172.500	-88.750	937.500
507	-86.250	177.500	937.500
508	-172.500	177.500	937.500
509	-172.500	88.750	937.500
510	-172.500	266.250	937.500
511	-258.750	-177.500	937.500
512	-258.750	0	937.500
513	-258.750	177.500	937.500
514	345.000	-355.000	-937.500
515	345.000	-266.250	-937.500
516	345.000	-177.500	-937.500
517	345.000	-88.750	-937.500
518	345.000	0	-937.500
519	345.000	88.750	-937.500
520	345.000	177.500	-937.500

Table D.1 (Continued)

Node No	x (mm)	y (mm)	z (mm)
521	345.000	266.250	-937.500
522	345.000	355.000	-937.500
523	258.750	355.000	-937.500
524	172.500	355.000	-937.500
525	86.250	355.000	-937.500
526	0	355.000	-937.500
527	-86.250	355.000	-937.500
528	-172.500	355.000	-937.500
529	-258.750	355.000	-937.500
530	-345.000	355.000	-937.500
531	-345.000	266.250	-937.500
532	-345.000	177.500	-937.500
533	-345.000	88.750	-937.500
534	-345.000	0	-937.500
535	-345.000	-88.750	-937.500
536	-345.000	-177.500	-937.500
537	-345.000	-266.250	-937.500
538	-345.000	-355.000	-937.500
539	-258.750	-355.000	-937.500
540	-172.500	-355.000	-937.500
541	-86.250	-355.000	-937.500
542	0	-355.000	-937.500
543	86.250	-355.000	-937.500
544	172.500	-355.000	-937.500
545	258.750	-355.000	-937.500
546	-258.750	-177.500	-937.500
547	-172.500	-177.500	-937.500
548	-172.500	-266.250	-937.500
549	-258.750	0	-937.500
550	-172.500	0	-937.500
551	-172.500	-88.750	-937.500
552	-258.750	177.500	-937.500
553	-172.500	177.500	-937.500
554	-172.500	88.750	-937.500
555	-172.500	266.250	-937.500
556	-86.250	-177.500	-937.500
557	0	-177.500	-937.500
558	0	-266.250	-937.500

Node No	x (mm)	y (mm)	z (mm)
559	-86.250	0	-937.500
560	0	0	-937.500
561	0	-88.750	-937.500
562	-86.250	177.500	-937.500
563	0	177.500	-937.500
564	0	88.750	-937.500
565	0	266.250	-937.500
566	86.250	-177.500	-937.500
567	172.500	-177.500	-937.500
568	172.500	-266.250	-937.500
569	86.250	0	-937.500
570	172.500	0	-937.500
571	172.500	-88.750	-937.500
572	86.250	177.500	-937.500
573	172.500	177.500	-937.500
574	172.500	88.750	-937.500
575	172.500	266.250	-937.500
576	258.750	-177.500	-937.500
577	258.750	0	-937.500
578	258.750	177.500	-937.500

Table D.2 Incidence Matrix of the Refrigerator

Element No	nod1	nod2	nod3	nod4	nod5	nod6	nod7	nod8
1	514	515	516	1	2	3	4	5
2	516	517	518	6	7	8	2	1
3	518	519	520	9	10	11	7	6
4	520	521	522	12	13	14	10	9
5	4	3	2	15	16	17	18	19
6	2	8	7	20	21	22	16	15
7	7	11	10	23	24	25	21	20
8	10	14	13	26	27	28	24	23
9	18	17	16	29	30	31	32	33
10	16	22	21	34	35	36	30	29
11	21	25	24	37	38	39	35	34
12	24	28	27	40	41	42	38	37
13	32	31	30	43	44	45	46	47
14	30	36	35	48	49	50	44	43
15	35	39	38	51	52	53	49	48
16	38	42	41	54	55	56	52	51
17	46	45	44	57	58	59	60	61
18	44	50	49	62	63	64	58	57
19	49	53	52	65	66	67	63	62
20	52	56	55	68	69	70	66	65
21	60	59	58	71	72	73	74	75
22	58	64	63	76	77	78	72	71
23	63	67	66	79	80	81	77	76
24	66	70	69	82	83	84	80	79
25	74	73	72	85	86	87	88	89
26	72	78	77	90	91	92	86	85
27	77	81	80	93	94	95	91	90
28	80	84	83	96	97	98	94	93
29	88	87	86	99	100	101	102	103
30	86	92	91	104	105	106	100	99
31	91	95	94	107	108	109	105	104
32	94	98	97	110	111	112	108	107
33	102	101	100	113	114	115	116	117
34	100	106	105	118	119	120	114	113
35	105	109	108	121	122	123	119	118
36	108	112	111	124	125	126	122	121
37	116	115	114	127	128	129	130	131

Table D.2 (Continued)

Element No	nod1	nod2	nod3	nod4	nod5	nod6	nod7	nod8
38	114	120	119	132	133	134	128	127
39	119	123	122	135	136	137	133	132
40	122	126	125	138	139	140	136	135
41	522	523	524	141	142	143	13	12
42	524	525	526	144	145	146	142	141
43	526	527	528	147	148	149	145	144
44	528	529	530	150	151	152	148	147
45	13	143	142	153	154	155	27	26
46	142	146	145	156	157	158	154	153
47	145	149	148	159	160	161	157	156
48	148	152	151	162	163	164	160	159
49	27	155	154	165	166	167	41	40
50	154	158	157	168	169	170	166	165
51	157	161	160	171	172	173	169	168
52	160	164	163	174	175	176	172	171
53	41	167	166	177	178	179	55	54
54	166	170	169	180	181	182	178	177
55	169	173	172	183	184	185	181	180
56	172	176	175	186	187	188	184	183
57	55	179	178	189	190	191	69	68
58	178	182	181	192	193	194	190	189
59	181	185	184	195	196	197	193	192
60	184	188	187	198	199	200	196	195
61	69	191	190	201	202	203	83	82
62	190	194	193	204	205	206	202	201
63	193	197	196	207	208	209	205	204
64	196	200	199	210	211	212	208	207
65	83	203	202	213	214	215	97	96
66	202	206	205	216	217	218	214	213
67	205	209	208	219	220	221	217	216
68	208	212	211	222	223	224	220	219
69	97	215	214	225	226	227	111	110
70	214	218	217	228	229	230	226	225
71	217	221	220	231	232	233	229	228
72	220	224	223	234	235	236	232	231
73	111	227	226	237	238	239	125	124
74	226	230	229	240	241	242	238	237
75	229	233	232	243	244	245	241	240

Table D.2 (Continued)

Element No	nod1	nod2	nod3	nod4	nod5	nod6	nod7	nod8
76	232	236	235	246	247	248	244	243
77	125	239	238	249	250	251	139	138
78	238	242	241	252	253	254	250	249
79	241	245	244	255	256	257	253	252
80	244	248	247	258	259	260	256	255
81	530	531	532	261	262	263	151	150
82	532	533	534	264	265	266	262	261
83	534	535	536	267	268	269	265	264
84	536	537	538	270	271	272	268	267
85	151	263	262	273	274	275	163	162
86	262	266	265	276	277	278	274	273
87	265	269	268	279	280	281	277	276
88	268	272	271	282	283	284	280	279
89	163	275	274	285	286	287	175	174
90	274	278	277	288	289	290	286	285
91	277	281	280	291	292	293	289	288
92	280	284	283	294	295	296	292	291
93	175	287	286	297	298	299	187	186
94	286	290	289	300	301	302	298	297
95	289	293	292	303	304	305	301	300
96	292	296	295	306	307	308	304	303
97	187	299	298	309	310	311	199	198
98	298	302	301	312	313	314	310	309
99	301	305	304	315	316	317	313	312
100	304	308	307	318	319	320	316	315
101	199	311	310	321	322	323	211	210
102	310	314	313	324	325	326	322	321
103	313	317	316	327	328	329	325	324
104	316	320	319	330	331	332	328	327
105	211	323	322	333	334	335	223	222
106	322	326	325	336	337	338	334	333
107	325	329	328	339	340	341	337	336
108	328	332	331	342	343	344	340	339
109	223	335	334	345	346	347	235	234
110	334	338	337	348	349	350	346	345
111	337	341	340	351	352	353	349	348
112	340	344	343	354	355	356	352	351
113	235	347	346	357	358	359	247	246

Table D.2 (Continued)

Element No	nod1	nod2	nod3	nod4	nod5	nod6	nod7	nod8
114	346	350	349	360	361	362	358	357
115	349	353	352	363	364	365	361	360
116	352	356	355	366	367	368	364	363
117	247	359	358	369	370	371	259	258
118	358	362	361	372	373	374	370	369
119	361	365	364	375	376	377	373	372
120	364	368	367	378	379	380	376	375
121	538	539	540	381	382	383	271	270
122	540	541	542	384	385	386	382	381
123	542	543	544	387	388	389	385	384
124	544	545	514	5	4	390	388	387
125	271	383	382	391	392	393	283	282
126	382	386	385	394	395	396	392	391
127	385	389	388	397	398	399	395	394
128	388	390	4	19	18	400	398	397
129	283	393	392	401	402	403	295	294
130	392	396	395	404	405	406	402	401
131	395	399	398	407	408	409	405	404
132	398	400	18	33	32	410	408	407
133	295	403	402	411	412	413	307	306
134	402	406	405	414	415	416	412	411
135	405	409	408	417	418	419	415	414
136	408	410	32	47	46	420	418	417
137	307	413	412	421	422	423	319	318
138	412	416	415	424	425	426	422	421
139	415	419	418	427	428	429	425	424
140	418	420	46	61	60	430	428	427
141	319	423	422	431	432	433	331	330
142	422	426	425	434	435	436	432	431
143	425	429	428	437	438	439	435	434
144	428	430	60	75	74	440	438	437
145	331	433	432	441	442	443	343	342
146	432	436	435	444	445	446	442	441
147	435	439	438	447	448	449	445	444
148	438	440	74	89	88	450	448	447
149	343	443	442	451	452	453	355	354
150	442	446	445	454	455	456	452	451
151	445	449	448	457	458	459	455	454

Table D.2 (Continued)

Element No	nod1	nod2	nod3	nod4	nod5	nod6	nod7	nod8
152	448	450	88	103	102	460	458	457
153	355	453	452	461	462	463	367	366
154	452	456	455	464	465	466	462	461
155	455	459	458	467	468	469	465	464
156	458	460	102	117	116	470	468	467
157	367	463	462	471	472	473	379	378
158	462	466	465	474	475	476	472	471
159	465	469	468	477	478	479	475	474
160	468	470	116	131	130	480	478	477
161	130	129	128	481	482	483	478	480
162	128	134	133	484	485	486	482	481
163	133	137	136	487	488	489	485	484
164	136	140	139	251	250	490	488	487
165	478	483	482	491	492	493	475	479
166	482	486	485	494	495	496	492	491
167	485	489	488	497	498	499	495	494
168	488	490	250	254	253	500	498	497
169	475	493	492	501	502	503	472	476
170	492	496	495	504	505	506	502	501
171	495	499	498	507	508	509	505	504
172	498	500	253	257	256	510	508	507
173	472	503	502	511	376	380	379	473
174	502	506	505	512	373	377	376	511
175	505	509	508	513	370	374	373	512
176	508	510	256	260	259	371	370	513
177	538	537	536	546	547	548	540	539
178	536	535	534	549	550	551	547	546
179	534	533	532	552	553	554	550	549
180	532	531	530	529	528	555	553	552
181	540	548	547	556	557	558	542	541
182	547	551	550	559	560	561	557	556
183	550	554	553	562	563	564	560	559
184	553	555	528	527	526	565	563	562
185	542	558	557	566	567	568	544	543
186	557	561	560	569	570	571	567	566
187	560	564	563	572	573	574	570	569
188	563	565	526	525	524	575	573	572
189	544	568	567	576	516	515	514	545

Table D.2 (Continued)

Element No	nod1	nod2	nod3	nod4	nod5	nod6	nod7	nod8
190	567	571	570	577	518	517	516	576
191	570	574	573	578	520	519	518	577
192	573	575	524	523	522	521	520	578

Table D.3 Nodal Velocities of the Refrigerator at 50 Hz

Node No	Velocity (mm/s)	Node No	Velocity (mm/s)	Node No	Velocity (mm/s)
1	0.00465	38	0.0135	75	0.0071
2	0.0093	39	0.0108	76	0.004
3	0.00735	40	0.01915	77	0.0032
4	0.0054	41	0.018	78	0.0033
5	0.0027	42	0.01575	79	0.00525
6	0.0065	43	0.0057	80	0.0038
7	0.013	44	0.0054	81	0.0035
8	0.01115	45	0.00745	82	0.0081
9	0.0075	46	0.0095	83	0.006
10	0.015	47	0.009	84	0.0049
11	0.014	48	0.00685	85	0.0017
12	0.00925	49	0.0056	86	0
13	0.0185	50	0.0055	87	0
14	0.01675	51	0.0114	88	0
15	0.00815	52	0.0093	89	0.003
16	0.007	53	0.00745	90	0.0016
17	0.00685	54	0.01635	91	0
18	0.0067	55	0.0147	92	0
19	0.00605	56	0.012	93	0.0019
20	0.0116	57	0.0052	94	0
21	0.0102	58	0.005	95	0
22	0.0086	59	0.0066	96	0.003
23	0.0145	60	0.0082	97	0
24	0.014	61	0.00885	98	0
25	0.0121	62	0.0052	99	0.00275
26	0.0194	63	0.0048	100	0.0055
27	0.0203	64	0.0049	101	0.0055
28	0.01715	65	0.008	102	0.0055
29	0.0065	66	0.0067	103	0.00275
30	0.006	67	0.00575	104	0.00275
31	0.00725	68	0.01245	105	0.0055
32	0.0085	69	0.0102	106	0.0055
33	0.0076	70	0.00845	107	0.0025
34	0.00915	71	0.0042	108	0.005
35	0.0081	72	0.0034	109	0.00525
36	0.00705	73	0.0047	110	0.0025
37	0.01375	74	0.006	111	0.005

Table D.3 (Continued)

Node No	Velocity (mm/s)	Node No	Velocity (mm/s)	Node No	Velocity (mm/s)
112	0.005	150	0.00275	188	0.0115
113	0.00275	151	0.0055	189	0.01375
114	0	152	0.0085	190	0.0115
115	0.00225	153	0.0154	191	0.01085
116	0.0045	154	0.016	192	0.013
117	0.005	155	0.01815	193	0.011
118	0.00385	156	0.01375	194	0.01125
119	0.0022	157	0.014	195	0.011
120	0.0011	158	0.015	196	0.009
121	0.00475	159	0.012	197	0.01
122	0.0045	160	0.0125	198	0.00875
123	0.00335	161	0.01325	199	0.0075
124	0.007	162	0.00925	200	0.00825
125	0.009	163	0.013	201	0.0089
126	0.00675	164	0.01275	202	0.0063
127	0.017	165	0.0175	203	0.00615
128	0.034	166	0.019	204	0.0085
129	0.03	167	0.0185	205	0.006
130	0.026	168	0.0155	206	0.00615
131	0.01525	169	0.017	207	0.00675
132	0.0126	170	0.018	208	0.0045
133	0.023	171	0.013	209	0.00525
134	0.0285	172	0.0135	210	0.00575
135	0.00665	173	0.01525	211	0.004
136	0.0088	174	0.01225	212	0.00425
137	0.0159	175	0.0115	213	0.00375
138	0.01075	176	0.0125	214	0.0012
139	0.0125	177	0.0175	215	0.0006
140	0.01065	178	0.016	216	0.003
141	0.0074	179	0.01535	217	0
142	0.0148	180	0.016	218	0.0006
143	0.01665	181	0.015	219	0.00225
144	0.00675	182	0.0155	220	0
145	0.0135	183	0.01325	221	0
146	0.01415	184	0.013	222	0.002
147	0.00575	185	0.014	223	0
148	0.0115	186	0.01075	224	0
149	0.0125	187	0.01	225	0.0031

Table D.3 (Continued)

Node No	Velocity (mm/s)	Node No	Velocity (mm/s)	Node No	Velocity (mm/s)
226	0.005	264	0.0265	302	0.015
227	0.005	265	0.053	303	0.0135
228	0.003	266	0.0265	304	0.011
229	0.006	267	0.0265	305	0.0145
230	0.0055	268	0.053	306	0.01025
231	0.00275	269	0.053	307	0.011
232	0.0055	270	0.0038	308	0.011
233	0.00575	271	0.0076	309	0.0095
234	0.00275	272	0.0303	310	0.007
235	0.0055	273	0.0016	311	0.00725
236	0.0055	274	0.0032	312	0.015
237	0.00825	275	0.0081	313	0.012
238	0.0115	276	0.029375	314	0.0095
239	0.01025	277	0.00575	315	0.0125
240	0.0085	278	0.004475	316	0.014
241	0.011	279	0.0285	317	0.013
242	0.01125	280	0.004	318	0.00925
243	0.007	281	0.004875	319	0.0075
244	0.0085	282	0.007675	320	0.01075
245	0.00975	283	0.00775	321	0.00825
246	0.00765	284	0.005875	322	0.0095
247	0.0098	285	0.0101	323	0.00675
248	0.00915	286	0.017	324	0.013
249	0.01125	287	0.01425	325	0.014
250	0.011	288	0.012125	326	0.01175
251	0.01175	289	0.0185	327	0.009
252	0.011	290	0.01775	328	0.004
253	0.011	291	0.01	329	0.009
254	0.011	292	0.016	330	0.00565
255	0.00785	293	0.01725	331	0.0038
256	0.0072	294	0.008625	332	0.0039
257	0.0091	295	0.0095	333	0.01
258	0.0089	296	0.01275	334	0.0105
259	0.008	297	0.0145	335	0.00525
260	0.0076	298	0.012	336	0.0095
261	0	299	0.011	337	0.005
262	0	300	0.01825	338	0.00775
263	0.00275	301	0.018	339	0.0065

Table D.3 (Continued)

Node No	Velocity (mm/s)	Node No	Velocity (mm/s)	Node No	Velocity (mm/s)
340	0.009	378	0.0077	416	0.018
341	0.007	379	0.0044	417	0.024
342	0.0035	380	0.0047	418	0.021
343	0.0032	381	0.0065	419	0.0205
344	0.0061	382	0.013	420	0.01525
345	0.01125	383	0.0103	421	0.0136
346	0.012	384	0.011	422	0.0112
347	0.00875	385	0.022	423	0.00935
348	0.006	386	0.0175	424	0.017
349	0.007	387	0.011	425	0.014
350	0.0095	388	0.022	426	0.0126
351	0.012	389	0.022	427	0.01825
352	0.015	390	0.0137	428	0.0155
353	0.011	391	0.015	429	0.01475
354	0.0047	392	0.017	430	0.01185
355	0.0062	393	0.012375	431	0.0082
356	0.0106	394	0.02225	432	0.0052
357	0.00825	395	0.0225	433	0.0045
358	0.0045	396	0.01975	434	0.0104
359	0.00715	397	0.0235	435	0.0068
360	0.00775	398	0.025	436	0.006
361	0.0085	399	0.02375	437	0.01185
362	0.0065	400	0.01585	438	0.0082
363	0.0094	401	0.026	439	0.0075
364	0.0038	402	0.035	440	0.0071
365	0.00615	403	0.02225	441	0.0036
366	0.0086	404	0.02375	442	0.002
367	0.011	405	0.025	443	0.0026
368	0.0074	406	0.03	444	0.00405
369	0.006	407	0.026	445	0.0013
370	0.0075	408	0.027	446	0.00165
371	0.00775	409	0.026	447	0.0041
372	0.007	410	0.01775	448	0
373	0.0055	411	0.0255	449	0.00065
374	0.0065	412	0.016	450	0
375	0.0044	413	0.0135	451	0.00375
376	0.005	414	0.0225	452	0.0055
377	0.00525	415	0.02	453	0.00585

Table D.3 (Continued)

Node No	Velocity (mm/s)
454	0.0029
455	0.0045
456	0.005
457	0.00215
458	0.0043
459	0.0044
460	0.0049
461	0.008
462	0.0105
463	0.01075
464	0.00735
465	0.0102
466	0.01035
467	0.0069
468	0.0095
469	0.00985
470	0.007
471	0.0074
472	0.0043
473	0.00435
474	0.0076
475	0.005
476	0.00465
477	0.00785
478	0.0062
479	0.0056
480	0.0161
481	0.0209
482	0.0078
483	0.007
484	0.0164
485	0.0098
486	0.0088
487	0.00965
488	0.0105
489	0.01015
490	0.01075
491	0.00765

Node No	Velocity (mm/s)
492	0.0075
493	0.00625
494	0.0098
495	0.0098
496	0.00865
497	0.01075
498	0.011
499	0.0104
500	0.011
501	0.0066
502	0.0057
503	0.005
504	0.00865
505	0.0075
506	0.0066
507	0.00965
508	0.0083
509	0.0079
510	0.00775
511	0.00535
512	0.0065
513	0.0079
514	0
515	0
516	0
517	0
518	0
519	0
520	0
521	0
522	0
523	0
524	0
525	0
526	0
527	0
528	0
529	0

Node No	Velocity (mm/s)
530	0
531	0
532	0
533	0
534	0
535	0
536	0
537	0
538	0
539	0
540	0
541	0
542	0
543	0
544	0
545	0

Table D.4 Nodal Velocities of the Refrigerator at 100 Hz

Node No	Velocity (mm/s)	Node No	Velocity (mm/s)	Node No	Velocity (mm/s)
1	0.00155	38	0.0045	75	0.00345
2	0.0031	39	0.0034	76	0.0014
3	0.00355	40	0.006	77	0.0012
4	0.004	41	0.0058	78	0.0016
5	0.002	42	0.00515	79	0.00215
6	0.0014	43	0.0019	80	0.0018
7	0.0028	44	0.0016	81	0.0015
8	0.00295	45	0.0024	82	0.003
9	0.00215	46	0.0032	83	0.0024
10	0.0043	47	0.00335	84	0.0021
11	0.00355	48	0.00215	85	0.001
12	0.00275	49	0.002	86	0
13	0.0055	50	0.0018	87	0
14	0.0049	51	0.00405	88	0
15	0.0028	52	0.0036	89	0.00175
16	0.0025	53	0.0028	90	0.0006
17	0.00315	54	0.0054	91	0
18	0.0038	55	0.005	92	0
19	0.0039	56	0.0043	93	0.0009
20	0.00265	57	0.00165	94	0
21	0.0025	58	0.0017	95	0
22	0.0025	59	0.00255	96	0.0012
23	0.0045	60	0.0034	97	0
24	0.0047	61	0.0033	98	0
25	0.0036	62	0.0018	99	0.00065
26	0.00585	63	0.0016	100	0.0013
27	0.0062	64	0.00165	101	0.00205
28	0.00545	65	0.00305	102	0.0028
29	0.00235	66	0.0025	103	0.0014
30	0.0022	67	0.00205	104	0.0009
31	0.00285	68	0.0043	105	0.0018
32	0.0035	69	0.0036	106	0.00155
33	0.00365	70	0.00305	107	0.0017
34	0.0024	71	0.00185	108	0.0034
35	0.0023	72	0.002	109	0.0026
36	0.00225	73	0.00275	110	0.00225
37	0.0046	74	0.0035	111	0.0045

Table D.4 (Continued)

Node No	Velocity (mm/s)	Node No	Velocity (mm/s)	Node No	Velocity (mm/s)
112	0.00395	150	0.0008	188	0.0023
113	0.00145	151	0.0016	189	0.0039
114	0.0016	152	0.0021	190	0.0038
115	0.0019	153	0.0035	191	0.0037
116	0.0022	154	0.0038	192	0.0034
117	0.0025	155	0.005	193	0.0034
118	0.0018	156	0.0031	194	0.0036
119	0.0018	157	0.0032	195	0.00245
120	0.0017	158	0.0035	196	0.0022
121	0.0037	159	0.0029	197	0.0028
122	0.004	160	0.0032	198	0.0017
123	0.0029	161	0.0032	199	0.0015
124	0.0045	162	0.002	200	0.00185
125	0.0045	163	0.0024	201	0.00295
126	0.00425	164	0.0028	202	0.0021
127	0.0033	165	0.0036	203	0.00225
128	0.005	166	0.0034	204	0.00245
129	0.00475	167	0.0046	205	0.0015
130	0.0045	168	0.0031	206	0.0018
131	0.00335	169	0.003	207	0.0011
132	0.00435	170	0.0032	208	0
133	0.0069	171	0.0029	209	0.00075
134	0.00595	172	0.0026	210	0.00145
135	0.00285	173	0.0028	211	0.0014
136	0.0017	174	0.0019	212	0.0007
137	0.0043	175	0.0014	213	0.00105
138	0.0034	176	0.002	214	0
139	0.0023	177	0.0037	215	0
140	0.002	178	0.004	216	0.00145
141	0.0016	179	0.0045	217	0.0014
142	0.0032	180	0.0032	218	0.0007
143	0.00435	181	0.0034	219	0.0007
144	0.0015	182	0.0037	220	0.0014
145	0.003	183	0.00265	221	0.0014
146	0.0031	184	0.0027	222	0.0014
147	0.0013	185	0.00305	223	0.0014
148	0.0026	186	0.00165	224	0.0014
149	0.0028	187	0.0019	225	0.001

Table D.4 (Continued)

Node No	Velocity (mm/s)	Node No	Velocity (mm/s)	Node No	Velocity (mm/s)
226	0.002	264	0.004	302	0.00275
227	0.00325	265	0.008	303	0.0038
228	0.0019	266	0.004	304	0.0045
229	0.0024	267	0.004	305	0.0035
230	0.0022	268	0.008	306	0.00195
231	0.0018	269	0.008	307	0.0022
232	0.0022	270	0.0013	308	0.00335
233	0.0023	271	0.0026	309	0.0031
234	0.0018	272	0.0053	310	0.0032
235	0.0022	273	0.001375	311	0.00235
236	0.0022	274	0.00275	312	0.00315
237	0.0026	275	0.002575	313	0.0038
238	0.0032	276	0.0058	314	0.0035
239	0.00385	277	0.0036	315	0.00375
240	0.0028	278	0.003175	316	0.003
241	0.0032	279	0.005425	317	0.0034
242	0.0032	280	0.00285	318	0.00185
243	0.0026	281	0.003225	319	0.0015
244	0.003	282	0.0021	320	0.00225
245	0.0031	283	0.0016	321	0.0032
246	0.0029	284	0.002225	322	0.0032
247	0.0036	285	0.003	323	0.0023
248	0.0033	286	0.00325	324	0.0039
249	0.00265	287	0.002325	325	0.004
250	0.0021	288	0.00355	326	0.0036
251	0.0022	289	0.0035	327	0.002625
252	0.00265	290	0.003375	328	0.00225
253	0.0021	291	0.002975	329	0.003125
254	0.0021	292	0.0031	330	0.00135
255	0.00255	293	0.0033	331	0.0012
256	0.0021	294	0.00165	332	0.001725
257	0.0021	295	0.0017	333	0.00385
258	0.0032	296	0.0024	334	0.0045
259	0.0028	297	0.003125	335	0.00295
260	0.00245	298	0.003	336	0.0039
261	0	299	0.00245	337	0.0038
262	0	300	0.003	338	0.00415
263	0.0008	301	0.0025	339	0.003125

Table D.4 (Continued)

Node No	Velocity (mm/s)	Node No	Velocity (mm/s)	Node No	Velocity (mm/s)
340	0.004	378	0.0022	416	0.00485
341	0.0039	379	0.0016	417	0.0056
342	0.0013	380	0.00185	418	0.0057
343	0.0014	381	0.00125	419	0.0057
344	0.0027	382	0.0025	420	0.00445
345	0.00475	383	0.00255	421	0.00365
346	0.005	384	0.00175	422	0.0033
347	0.0036	385	0.0035	423	0.0024
348	0.0039	386	0.003	424	0.0051
349	0.004	387	0.0019	425	0.0045
350	0.0045	388	0.0038	426	0.0039
351	0.0045	389	0.00365	427	0.00535
352	0.005	390	0.0039	428	0.005
353	0.0045	391	0.00275	429	0.00475
354	0.0017	392	0.003	430	0.0042
355	0.002	393	0.0023	431	0.00225
356	0.0035	394	0.00375	432	0.0012
357	0.006	395	0.004	433	0.0012
358	0.007	396	0.0035	434	0.00345
359	0.0053	397	0.00415	435	0.0024
360	0.0038	398	0.0045	436	0.0018
361	0.0036	399	0.00425	437	0.0041
362	0.0053	400	0.00415	438	0.0032
363	0.0042	401	0.00385	439	0.0028
364	0.0034	402	0.0047	440	0.00335
365	0.0035	403	0.0032	441	0.00135
366	0.0024	404	0.0045	442	0.0015
367	0.0028	405	0.005	443	0.00145
368	0.0031	406	0.00485	444	0.00195
369	0.00485	407	0.005	445	0.0015
370	0.0027	408	0.0055	446	0.0015
371	0.00275	409	0.00525	447	0.0021
372	0.0031	410	0.0045	448	0.001
373	0.0026	411	0.00435	449	0.00125
374	0.00265	412	0.004	450	0.0005
375	0.00275	413	0.0031	451	0.00215
376	0.0021	414	0.00535	452	0.0028
377	0.00235	415	0.0057	453	0.0024

Table D.4 (Continued)

Node No	Velocity (mm/s)
454	0.00215
455	0.0028
456	0.0028
457	0.0016
458	0.0022
459	0.0025
460	0.0025
461	0.0029
462	0.003
463	0.0029
464	0.0028
465	0.0028
466	0.0029
467	0.0025
468	0.0028
469	0.0028
470	0.0025
471	0.0022
472	0.0014
473	0.0015
474	0.0014
475	0
476	0.0007
477	0.0021
478	0.0014
479	0.0007
480	0.00295
481	0.0033
482	0.0016
483	0.0015
484	0.0044
485	0.0019
486	0.00175
487	0.0018
488	0.0019
489	0.0019
490	0.002
491	0.0016

Node No	Velocity (mm/s)
492	0.0016
493	0.0008
494	0.00195
495	0.002
496	0.0018
497	0.002
498	0.0021
499	0.00205
500	0.0021
501	0.0015
502	0.0014
503	0.0014
504	0.00215
505	0.0023
506	0.00185
507	0.00215
508	0.0022
509	0.00225
510	0.00215
511	0.00175
512	0.00245
513	0.00245
514	0
515	0
516	0
517	0
518	0
519	0
520	0
521	0
522	0
523	0
524	0
525	0
526	0
527	0
528	0
529	0

Node No	Velocity (mm/s)
530	0
531	0
532	0
533	0
534	0
535	0
536	0
537	0
538	0
539	0
540	0
541	0
542	0
543	0
544	0
545	0

APPENDIX E
COMPUTER PROGRAM

E.1 main_bem.m

```
% main_bem.m
% Definitions-------------------------------------------------------
% rho       :Fluid density
% vfs       :Speed of fluid
% z0        :Acoustical impedance of the medium
%-------------------------------------------------------------------
clc;clear;
%-------------------------------------------------------------------
rho=1.2;vfs=340;
z0=rho*vfs;
%-------------------------------------------------------------------
data_input;
%-------------------------------------------------------------------
[AH,AH1]=vel(nod,aba);
%-------------------------------------------------------------------
[AV,AA]=av_aa(1);
%-------------------------------------------------------------------
coeff;
%-------------------------------------------------------------------
Amat=4*pi*eye(2*nod);
%-------------------------------------------------------------------
surhel;
%-------------------------------------------------------------------
swrite;
%-------------------------------------------------------------------
exdata;
%-------------------------------------------------------------------
exthel;
%-------------------------------------------------------------------
extwrite;
```

E.2 data_input.m

```
% data_input.m
% Definitions-------------------------------------------------------
% kwn       :Wave number
% aba       :Dimension transformation coefficient
% nod       :Number of nodes except "dummy nodes"
% nod1      :Number of nodes which are not contact with surface
% nod2      :Total number of nodes
% AE        :Total number of elements
% ae2       :Number of elements except "dummy elements"
% AB        :Number of Gaussian points on the local horizontal and
%            vertical axes
% alfa      :Sound absorption coefficient of the surface
% Rp1       :Reflection coefficient of the surface
% alm       :The coüordinates of nodes
```

```
% AI        :Incidence matrix
% aci       :The angles between the local and global co-ordinates
% dxyzb     :The distances from global coüordinate's origin to the
%            local co-ordinate's origin in directions x, y and z
%--------------------------------------------------------------------
di=fopen('indat.txt');
    kwn=fscanf(di,'%lf',[1]);
    aba=fscanf(di,'%lf',[1]);
    nod=fscanf(di,'%d',[1]);
    nod1=fscanf(di,'%d',[1]);
    nod2=fscanf(di,'%d',[1]);
    AE=fscanf(di,'%d ',[1]);
    ae2=fscanf(di,'%d ',[1]);
    AB=fscanf(di,'%d',[1,2]);
    alfa=fscanf(di,'%lf',[1]);

Rp1=sqrt(1-alfa);

alm=zeros(nod2,12);almy=zeros(nod2,6);

for i=1:nod2
    a1=fscanf(di,'%d',[1]);
    for j=1:3
        alm(i,j)=fscanf(di,'%lf',[1]);
    end
end

for i=1:AE
    a1=fscanf(di,'%d',[1]);
    for j=1:8
        AI(i,j)=fscanf(di,'%d',[1]);
    end
end

for i=1:3
    for j=1:3
        aci(i,j)=fscanf(di,'%lf',[1]);
    end
end

for j=1:3
    dxyzb(j,1)=fscanf(di,'%lf',[1]);
end

fclose(di);
%--------------------------------------------------------------------
for i=1:3
    for j=1:3
        hhh(i,j)=cos(aci(i,j)*pi/180);
        hh2(i,j)=hhh(i,j);
    end
end

dxyz=hh2*dxyzb;
dxyz(1,1)=-dxyz(1,1);
dxyz(2,1)=-dxyz(2,1);
dxyz(3,1)=-dxyz(3,1);
```

```
for i=1:3
    hhh(i,4)=dxyz(i,1);
    hhh(4,i)=0;
end

hhh(4,4)=1;

for i=0:2
    for j=0:2
        hh3(i+1,j+1)=hh2(j+1,i+1);
    end
end

yar=zeros(4,1);
yar(4,1)=1;

for i=1:nod
    yar(1,1)=alm(i,1);
    yar(2,1)=alm(i,2);
    yar(3,1)=alm(i,3);
    yars=hhh*yar;
    yars(3,1)=-yars(3,1);
    yarts=hh3*dxyz;
    for k=1:3
        for j=1:3
            hh4(k,j)=hh3(k,j);
        end
        hh4(k,4)=-yarts(k,1);
        hh4(4,k)=0;
    end
    hh4(4,4)=1;
    yarts2=hh4*yars;
    almy(i,1)=yarts2(1,1);
    almy(i,2)=yarts2(2,1);
    almy(i,3)=yarts2(3,1);
end

for i=0:nod2-1
    for j=0:1
        alm(i+1,6*j+1)=alm(i+1,3*j+1);
        alm(i+1,6*j+2)=alm(i+1,3*j+2);
        alm(i+1,6*j+3)=alm(i+1,3*j+3);
    end
end

for i=0:nod2-1
    for j=0:1
        alm(i+1,6*j+4)=almy(i+1,3*j+1);
        alm(i+1,6*j+5)=almy(i+1,3*j+2);
        alm(i+1,6*j+6)=almy(i+1,3*j+3);
    end
end
%-----------------------------------------------------------------------
alm=aba*alm;
```

E.3 vel.m

```
% vel.m
% Definitions-------------------------------------------------------
% AH        :Nodal velocity data
% AH1       :Transpose of matrix AH
%-------------------------------------------------------------------
function [AH,AH1]=vel(nod,aba)
%-------------------------------------------------------------------
di3=fopen('inv.txt');

for hiz=1:nod
    a1=fscanf(di3,'%d',[1]);
    AH(hiz)= fscanf(di3,'%lf',[1]);
end

AH=AH*aba;
AH1=AH';

fclose(di3);
%-------------------------------------------------------------------
end
```

E.4 av_aa.m

```
% av_aa.m
% Definitions-------------------------------------------------------
% AV, AA    :Gaussian weights
%-------------------------------------------------------------------
function [AV,AA]=av_aa(d)
di2=fopen('ava.txt');
AV=fscanf(di2,'%lf', [1,136]);
AA=fscanf(di2,'%lf', [1,136]);
end
```

E.5 coeff.m

```
% coeff.m
% Definitions-------------------------------------------------------
% AU        :Gaussian weight functions
% ALtS      :Shape functions
% AJ        :Jacobian matrix
% AF        :The co-ordinates of Gaussian points
%-------------------------------------------------------------------
uba=AB(1); ubb=AB(2);
%-------------------------------------------------------------------
AK1=[0,2,1,2,1; 0,-4,0,-4,0; 0,2,-1,2,-1;
    -2,0,0,0,2; 0,2,1,-2,-1; 0,-4,0,4,0;
    0,2,-1,-2,1; 2,0,0,0,-2]/4;
```

```
BK=[0,1,2,2,1; 2,0,0,0,-2; 0,-1,2,-2,1;
    0,0,-4,4,0; 0,1,2,-2,-1; -2,0,0,0,2;
    0,-1,2,2,-1; 0,0,-4,-4,0]/4;

AK=[-1,0,0,1,1,1,1,1; 2,0,2,0,-2,0,-2,0;
    -1,0,0,-1,1,1,1,-1; 2,-2,0,0,0,-2,0,2;
    -1,0,0,1,1,1,-1,-1; 2,0,-2,0,-2,0,2,0;
    -1,0,0,-1,1,1,-1,1; 2,2,0,0,0,-2,0,-2 ]/4;

AG=uba*ubb;
%-------------------------------------------------------------------
for iz=0:uba-1;
    A(iz+1)=(uba*(uba-1)/2)+(iz);
end

for iz=0:ubb-1;
    B(iz+1)=(ubb*(ubb-1)/2)+(iz);
end

for iz=0:ubb-1;
    A1(iz+1)=AV(B(iz+1)+1);
end

for iz=0:uba-1;
    A2(iz+1)=AV(A(iz+1)+1);
end

k=0;
for iz=0:ubb-1
    for jz=0:ubb-1
        C(k+1,2)=A1(jz+1);
        k=k+1;
    end
end

for iz=0:ubb-1
    for jz=0:uba-1
        C1(iz+1,jz+1)=A2(jz+1);
    end
end
C1T=C1';

k=0;
for iz=0:ubb-1
    for jz=0:uba-1
       C(k+1,1)=C1T(iz+1,jz+1);
       k=k+1;
    end
end

for iz=0:uba-1
    A3(iz+1)=AA(A(iz+1)+1);
end

for iz=0:ubb-1
    A4(iz+1)=AA(B(iz+1)+1);
end
```

```
k=0;
for iz=0:uba-1
    for jz=0:ubb-1
        AU(k+1)=A3(iz+1)*A4(jz+1);
        k=k+1;
    end
end

for g=0:AG-1
    Lb(1,1)=1;
    Lb(2,1)=C(g+1,1);
    Lb(3,1)=C(g+1,2);
    Lb(4,1)=C(g+1,1)*C(g+1,2);
    Lb(5,1)=C(g+1,1)*C(g+1,1);
    Lb(6,1)=C(g+1,2)*C(g+1,2);
    Lb(7,1)=C(g+1,1)*C(g+1,1)*C(g+1,2);
    Lb(8,1)=C(g+1,1)*C(g+1,2)*C(g+1,2);
    LbS=AK*Lb;
    for iz=0:7
        ALtS(iz+1,g+1)=LbS(iz+1,1);
    end
end

for l=0:AE-1
    for iz=0:7
        for jz=0:2
            temp=AI(l+1,iz+1)-1;
            X(iz+1,jz+1)=alm(temp+1,jz+1);
        end
    end
    for iz=0:7
        XX1(iz+1,1)=X(iz+1,1);
        XX2(iz+1,1)=X(iz+1,2);
        XX3(iz+1,1)=X(iz+1,3);
    end
    for g=0:AG-1
        d(1)=1;
        d(2)=C(g+1,1);
        d(3)=C(g+1,2);
        d(4)=C(g+1,1)*C(g+1,2);
        d(5)=C(g+1,1)*C(g+1,1);
        d(6)=C(g+1,2)*C(g+1,2);
        DK(1,1)=d(1);DK(2,1)=d(2);DK(3,1)=d(3);
        DK(4,1)=d(4);DK(5,1)=d(6);
        DKS=AK1*DK;
        for iz=0:7
            e(1,iz+1)=DKS(iz+1,1);
        end
        DK1(1,1)=d(1);DK1(2,1)=d(2);DK1(3,1)=d(3);
        DK1(4,1)=d(4);DK1(5,1)=d(5);
        DK1S=BK*DK1;
        for iz=0:7
            f(1,iz+1)=DK1S(iz+1,1);
        end
        TE1=e*XX1;
        TE2=e*XX2;
        TE3=e*XX3;
        TF1=f*XX1;
```

```
        TF2=f*XX2;
        TF3=f*XX3;

        HJ=(TE2(1,1)*TF3(1,1))-(TE3(1,1)*TF2(1,1));
        IJ=(TE3(1,1)*TF1(1,1))-(TE1(1,1)*TF3(1,1));
        JJ=(TE1(1,1)*TF2(1,1))-(TE2(1,1)*TF1(1,1));

        DJ(1)=HJ;DJ(2)=IJ;DJ(3)=JJ;

        AJ(l+1,g+1)=sqrt(HJ*HJ+IJ*IJ+JJ*JJ);
        for i=0:2
            IO(i+1)=(g*3)+i;
            AP(l+1,IO(i+1)+1)=DJ(i+1)/AJ(l+1,g+1);
        end
        for iz=0:7
            ASMat(iz+1,1)=ALtS(iz+1,g+1);
        end

        XTrp=X';
        XTrpASMat=XTrp*ASMat;

        vec(1)=XTrpASMat(1,1);
        vec(2)=XTrpASMat(2,1);
        vec(3)=XTrpASMat(3,1);

        for iz=0:2
            AF(l+1,IO(iz+1)+1)=vec(iz+1);
        end
    end
end
```

E.6 surhel.m

```
% surhel.m
% Definitions-------------------------------------------------------
% R         :Distances between the nodes and Gaussian points
% O         :The cosines of the angles between R and n
% hh        :Real part of coefficient t given in Equation (2.52)
% iii       :Imaginary part of coefficient t given in Equation (2.52)
% jj        :Real part of coefficient v given in Equation (2.52)
% kk        :Imaginary part of coefficient v given in Equation (2.52)
% Amat      :Matrix M given in Equation (2.41)
% Bmat      :Matrix V given in Equation (2.39)
% BVc       :Vector h given in Equation (2.42)
% surf_pres:Real and imaginary sound pressures of nodes (Pa)
%-------------------------------------------------------------------
for mi=0:nod-1
    if mi>nod1-1
        Amat(mi+1,mi+1)=(1+Rp1)*2*pi;
        Amat(mi+nod+1,mi+nod+1)=Amat(mi+1,mi+1);
    end
end
Bmat=zeros(2*nod,2*nod);
for mi=0:nod-1
    for l1=0:AE-1
```

```
for p1=0:7
    iii=0;jj=0;hh=0;kk=0;
    for g1=0:AG-1

        %depar-------------------------------------------------
        say=-1;
        for i=0:1
            for d1=0:2
                say=say+1;
                W(say+1)=AF(l1+1,g1*3+d1+1)-alm(mi+1,say+1);
            end
        end
        for i=0:1;
            R(i+1)=sqrt(W(3*i+1)*W(3*i+1)...
                +W(3*i+2)*W(3*i+2)+W(3*i+3)*W(3*i+3));
        end
        say=-1;
        for i=0:1;
            for d1=0:2
                say=say+1;
                OD(say+1)=(W(say+1)/R(i+1))...
                    *AP(l1+1,g1*3+d1+1);
            end
        end
        for i=0:1;
            O(i+1)=OD(3*i+1)+OD(3*i+2)+OD(3*i+3);
        end
        %-------------------------------------------------

        %corn--------------------------------------------------
        if p1==0
           if mi<=nod1-1
              Amat(mi+1,mi+1)=Amat(mi+1,mi+1)...
                  -(AU(g1+1)*AJ(l1+1,g1+1)*O(1)...
                  /(R(1)*R(1)));
              Amat(mi+nod+1,mi+nod+1)=Amat(mi+1,mi+1);
           end
           if mi>nod1-1
              Amat(mi+1,mi+1)=Amat(mi+1,mi+1)...
                  -(1+Rp1)*(AU(g1+1)*AJ(l1+1,g1+1)*O(1)...
                  /(R(1)*R(1)));
              Amat(mi+nod+1,mi+nod+1)=Amat(mi+1,mi+1);
           end
        end
        %-------------------------------------------------
        if l1<ae2
           hg=0;ig=0;jg=0;kg=0;
           for ia=0:1
               if ia==0
                   Rp=1;
               else
                   Rp=Rp1;
               end
               hg=hg+Rp*(((cos(kwn*R(ia+1))/R(ia+1))...
                   +kwn*sin(kwn*R(ia+1)))*O(ia+1)/R(ia+1));
           end
           hg=hg*AU(g1+1)*ALtS(p1+1,g1+1)*AJ(l1+1,g1+1);
           hh=hh+hg;
```

```
            for ia=0:1
                if ia==0
                    Rp=1;
                else
                    Rp=Rp1;
                end
                ig=ig+Rp*(((sin(kwn*R(ia+1))/R(ia+1))...
                   -kwn*cos(kwn*R(ia+1)))*O(ia+1)/R(ia+1));
            end
            ig=ig*AU(g1+1)*ALtS(p1+1,g1+1)*AJ(l1+1,g1+1);
            iii=iii+ig;
            for ia=0:1
                if ia==0
                    Rp=1;
                else
                    Rp=Rp1;
                end
                jg=jg+Rp*(sin(kwn*R(ia+1))/R(ia+1));
            end
            jg=jg*AU(g1+1)*ALtS(p1+1,g1+1)...
                *AJ(l1+1,g1+1)*kwn*z0;
            jj=jj+jg;
            for ia=0:1
                if ia==0
                    Rp=1;
                else
                    Rp=Rp1;
                end
                kg=kg-Rp*(cos(kwn*R(ia+1))/R(ia+1));
            end
            kg=kg*AU(g1+1)*ALtS(p1+1,g1+1)...
                *AJ(l1+1,g1+1)*kwn*z0;
            kk=kk+kg;
        end
    end
    if l1<ae2
       CS(p1+1,1)=hh;CS(p1+1,2)=iii;
       DS(p1+1,1)=jj; DS(p1+1,2)=kk;
    end
end
if l1<ae2
   for ii=0:7
      xx(ii+1)=AI(l1+1,ii+1)-1;
      Amat(mi+1,xx(ii+1)+1)=Amat(mi+1,xx(ii+1)+1)...
          +CS(ii+1,1);
      Amat(mi+nod+1,xx(ii+1)+nod+1)=Amat(mi+1,xx(ii+1)+1);
      Amat(mi+1,xx(ii+1)+nod+1)=Amat(mi+1,xx(ii+1)+nod+1)...
          +CS((ii+1),2);
      Amat(mi+nod+1,xx(ii+1)+1)=...
          -1*Amat(mi+1,xx(ii+1)+nod+1);
   end
   for ii=0:7
      xx(ii+1)=AI(l1+1,ii+1)-1;
      Bmat(mi+1,xx(ii+1)+1)=Bmat(mi+1,xx(ii+1)+1)+...
          DS(ii+1,1);
      Bmat(mi+nod+1,xx(ii+1)+nod+1)=Bmat(mi+1,xx(ii+1)+1);
      Bmat(mi+1,xx(ii+1)+nod+1)=Bmat(mi+1,xx(ii+1)+nod+1)...
          +DS(ii+1,2);
      Bmat(mi+nod+1,xx(ii+1)+1)=...
```

```
                    -1*Bmat(mi+1,xx(ii+1)+nod+1);
            end
        end
    end
end
AH2=zeros(2*nod,1);AH2(1:nod,1)=AH1;
BVc=Bmat*AH2;
%------------------------
surf_pres=inv(Amat)*BVc;
```

E.7 swrite.m

```
% swrite.m
% Definitions-------------------------------------------------------------
% aaab      :Sound pressures of nodes (dB)
%-------------------------------------------------------------------------
dosres=fopen('surfpres.txt','wt');
for i=0:nod-1
    fprintf(dosres,'%d ',i+1);
    aaab(i+1)=20*log10(sqrt(surf_pres(i+1,1)*surf_pres(i+1,1)...
        +surf_pres(i+nod+1,1)*surf_pres(i+nod+1,1))/0.00002);
    fprintf(dosres,'%d\n',aaab(i+1));
end
fclose(dosres);
```

E.8 exdata.m

```
% exdata.m
% Definitions-------------------------------------------------------------
% T         :Number of field points
% az        :Co-ordinates of field points
%-------------------------------------------------------------------------
ddx=fopen('ext_data.txt');
T=fscanf(ddx,'%d',[1]);
for i=0:T-1
    a1=fscanf(ddx,'%d',[1]);
    for j=0:2
        az(i+1,j+1)=fscanf(ddx,'%lf',[1]);
    end
end
fclose(di);fclose(ddx);
for i=0:T-1
    yar(1,1)=az(i+1,1);
    yar(2,1)=az(i+1,2);
    yar(3,1)=az(i+1,3);
    yars=hhh*yar;
    yars(3,1)=-1*yars(3,1);
    yarts2=hh4*yars;
    az(i+1,4)=yarts2(1,1);
    az(i+1,5)=yarts2(2,1);
    az(i+1,6)=yarts2(3,1);
end
az=aba*az;
```

E.9 exthel.m

```
% exthel.m
% Definitions-------------------------------------------------------
% Rr       :Distances between field points and Gaussian points
% Oo       :The cosines of the angles between R and n
% hhe      :Real part of coefficient t given in Equation (2.43)
% iie      :Imaginary part of coefficient t given in Equation (2.43)
% jje      :Real part of coefficient v given in Equation (2.43)
% kke      :Imaginary part of coefficient v given in Equation (2.43)
% es1      :First term of right hand side of Equation (2.43)
% es2      :Second term of right hand side of Equation (2.43)
% ext_pres :Real and imaginary sound pressures of field points(Pa)
%-------------------------------------------------------------------
EA=zeros(2*T,2*nod);EB=zeros(2*T,2*nod);
for me=0:T-1
    for le=0:ae2-1
        for pe=0:7
            iie=0;jje=0;hhe=0;kke=0;
            for ge=0:AG-1

                %depar1-----------------------------------------------
                say=-1;
                for i=0:1
                    for d1=0:2
                        say=say+1;
                        Ww(say+1)=AF(le+1,ge*3+d1+1)-az(me+1,say+1);
                    end
                end
                for i=0:1
                    Rr(i+1)=sqrt(Ww(3*i+1)*Ww(3*i+1)...
                        +Ww(3*i+2)*Ww(3*i+2)+Ww(3*i+3)*Ww(3*i+3));
                end
                say=-1;
                for i=0:1
                    for d1=0:2
                        say=say+1;
                        ODd(say+1)=(Ww(say+1)/Rr(i+1))...
                            *AP(le+1,ge*3+d1+1);
                    end
                end
                for i=0:1
                    Oo(i+1)=ODd(3*i+1)+ODd(3*i+2)+ODd(3*i+3);
                end
                %-----------------------------------------------------

                hg=0;ig=0;jg=0;kg=0;
                for ia=0:1
                    if ia==0
                            Rp=1;
                       else
                            Rp=Rp1;
                    end
                    hg=hg+Rp*(((cos(kwn*Rr(ia+1))/Rr(ia+1))...
                        +kwn*sin(kwn*Rr(ia+1)))*Oo(ia+1)/Rr(ia+1));
                end
                hg=hg*AU(ge+1)*ALtS(pe+1,ge+1)*AJ(le+1,ge+1);
```

```
                    hhe=hhe+hg;
                    for ia=0:1
                        if ia==0
                                Rp=1;
                           else
                                Rp=Rp1;
                           end
                        ig=ig+Rp*(((sin(kwn*Rr(ia+1))/Rr(ia+1))...
                            -kwn*cos(kwn*Rr(ia+1)))*Oo(ia+1)/Rr(ia+1));
                    end
                    ig=ig*AU(ge+1)*ALtS(pe+1,ge+1)*AJ(le+1,ge+1);
                    iie=iie+ig;
                    for ia=0:1
                        if ia==0
                                Rp=1;
                           else
                                Rp=Rp1;
                        end
                        jg=jg+Rp*(sin(kwn*Rr(ia+1))/Rr(ia+1));
                    end
                    jg=jg*AU(ge+1)*ALtS(pe+1,ge+1)*AJ(le+1,ge+1)*kwn*z0;
                    jje=jje+jg;
                    for ia=0:1
                        if ia==0
                                Rp=1;
                           else
                                Rp=Rp1;
                           end
                        kg=kg+Rp*((-1*cos(kwn*Rr(ia+1))/Rr(ia+1)));
                    end
                    kg=kg*AU(ge+1)*ALtS(pe+1,ge+1)*AJ(le+1,ge+1)*kwn*z0;
                    kke=kke+kg;
                end
                CS(pe+1,1)=hhe;CS(pe+1,2)=iie;
                DS(pe+1,1)=jje; DS(pe+1,2)=kke;
            end
            for ii=0:7
               xx(ii+1)=AI(le+1,ii+1)-1;
               EA(me+1,xx(ii+1)+1)=EA(me+1,xx(ii+1)+1)...
                   +CS(ii+1,1);
               EA(me+T+1,xx(ii+1)+nod+1)=EA(me+1,xx(ii+1)+1);
               EA(me+1,xx(ii+1)+nod+1)=EA(me+1,xx(ii+1)+nod+1)...
                   +CS(ii+1,2);
               EA(me+T+1,xx(ii+1)+1)=-1*EA(me+1,xx(ii+1)+nod+1);
            end
            for ii=0:7
               xx(ii+1)=AI(le+1,ii+1)-1;
               EB(me+1,xx(ii+1)+1)=EB(me+1,xx(ii+1)+1)...
                   +DS(ii+1,1);
               EB(me+T+1,xx(ii+1)+nod+1)=EB(me+1,xx(ii+1)+1);
               EB(me+1,xx(ii+1)+nod+1)=EB(me+1,xx(ii+1)+nod+1)...
                   +DS(ii+1,2);
               EB(me+T+1,xx(ii+1)+1)=-1*EB(me+1,xx(ii+1)+nod+1);
            end
        end
    end
end
es1=-EA*surf_pres;
es2=EB*AH2;
for i=0:T-1
```

```
    ext_pres(i+1,1)=(es2(i+1,1)+es1(i+1,1))/(4*pi);
    ext_pres(i+T+1,1)=(es2(i+T+1,1)+es1(i+T+1,1))/(4*pi);
end
```

E.10 extwrite.m

```
% extwrite.m
% Definitions-------------------------------------------------------
% db       :Sound pressures of field points (dB)
%-------------------------------------------------------------------
exth=fopen('extpres.txt','wt');
for i1=0:T-1
    fprintf(exth,'%d ',i1+1);
    db(i1+1)=20*log10(sqrt((ext_pres(i1+1,1))*(ext_pres(i1+1,1))...
        +(ext_pres(i1+T+1,1))*(ext_pres(i1+T+1,1)))/0.00002);
    fprintf(exth,'%d\n',db(i1+1));
end
fclose(exth);
```